Selective Laser Ablation of Diseased Tissue: Investigations on a safe method of opening occluded arteries

by

Martin R. Prince

S.B., Massachusetts Institute of Technology (1980)
S.M., Massachusetts Institute of Technology (1982)
M.D., Harvard Medical School (1985)

Submitted to the Division of Health Sciences and Technology
in partial fulfillment of the
requirements for the degree of

DOCTOR OF PHILOSOPHY

at the

MASSACHUSETTS INSTITUTE OF TECHNOLOGY

June 1988

Signature of Author: _____
June 27, 1988

Certified by: _____
John A. Parrish
Thesis Supervisor

Accepted by: _____
Roger G. Mark
Chairman, Graduate Committee

SELECTIVE LASER ABLATION OF DISEASED TISSUE: INVESTIGATIONS ON A SAFE METHOD OF OPENING OCCLUDED ARTERIES

by

Martin R. Prince

Submitted to the Division of Health Sciences and Technology
on June 27, 1988 in partial fulfillment of the
requirements for the degree of
Doctor of Philosophy

ABSTRACT

To determine the optimal laser parameters for ablating plaque without damaging normal artery, an investigation was undertaken of the optical properties of normal and atherosclerotic artery and the mechanisms of laser ablation of arterial tissue. Optical studies demonstrated a waveband from 450 to 500 nm where the absorption coefficient of soft plaque was twice that of normal arterial wall. Biochemical studies demonstrated that the preferential absorption was due to carotenoid pigments present only in the plaque and that it could be significantly enhanced with beta carotene administered orally. Microsecond-long radiation pulses in this waveband of two-fold preferential absorption showed a two-fold difference in ablation thresholds. By operating the laser above the threshold fluence for ablating plaque but below the threshold fluence for ablating normal artery, it was possible to ablate plaque without ablating normal tissue. High speed photography, ablation efficiency measurements, debris analysis and histologic analysis suggested an ablative mechanism for soft plaque that involves adiabatic superheating of the irradiated tissue leading to subsurface vaporization within milliseconds of the arrival of a 1-μsec laser pulse which eventually leads to disruption of tissue due to rapid expansion of the subsurface vapor. Calcified plaque was found to be ablated by a plasma-mediated process. By using sufficiently brief laser pulses it was also possible to ablate calcified plaque with laser pulses that did not ablate normal artery in the waveband of preferential absorption. Selective ablation of atherosclerotic plaque may greatly enhance the safety and efficacy of laser endarterectomy.

Thesis Committee:
Prof. John A. Parrish
Prof. Ascher H. Shapiro
Prof. John T. Fallon
Prof. Ernest G. Cravalho

Table of Contents

LIST OF TABLES

LIST OF FIGURES

Acknowledgements

I gratefully acknowledge the many people who have made invaluable contributions over the four year course of this thesis research. John Parrish, my thesis supervisor, along with Ascher Shapiro and my other committee members encouraged me to extract the most from my doctoral research training. Rox, Franz, Myron, Tom, Irene, Tayyaba, Jay, Ken, Randy, Dan, Norm, Bill, Diane, Sharon, Chris, Margo, and the entire Wellman Laboratory staff helped with experimental details and the analysis of data.

I specifically thank Prof. Harold Edgerton for assistance with high speed photography, Micki Mathews-Roth for training in carotenoid biochemistry and assistance in analyzing specimens for carotenoid content, Glenn LaMuraglia for clinical aspects of the carotid endarterectomy study, assistance with experimental measurements and analysis and completing the pulse duration study, E.F. MacNichol for assistance in the microspectrocopic analysis of plaque, Peter Teng for collecting plasma spectroscopy data, Tom Flotte, Fritz Kerner and the MGH Pathology residents for assistance in obtaining and analyzing human specimens, Candela Laser Corp. personnel for advice, assistance and access to dye lasers not available in the Wellman Laboratory.

I give special thanks to Rayhaneh and my parents who have supported me through the difficult times and made all of the successes worthwhile.

This work was funded in part by the Arthur O. and Gullan M. Wellman Foundation, National Institute of Health grants # F32 HL07377 and R44 HL37180, the Office of Naval Research and SDIO under contract # N00014-86-K-00117, a Heede Fellowship, and the Harvard/MIT Division of Health, Science and Technology.

NOMENCLATURE

α = absorption coefficient (cm^{-1})
α_B = Beer's Law absorption coefficient (cm^{-1})
A_{km} = Kubelka-Munk absorption coefficient (cm^{-1})
bp = boiling point (^oC)
C = specific heat (J/gm^oC)
dl = deciliter
D = tissue thickness
ϵ = extinction coefficient
$E^{1\%}_{1\,cm}$ = optical density of 1 cm of a 1% solution
f = laser pulse repetition rate (Hz)
τ_R = thermal relaxation time
τ_p = laser pulse duration
F = fluence (J/cm^2)
F_{th} = threshold fluence for ablation (J/cm^2)
h = Planck's constant (6.63×10^{-34} Js)
H_v = heat of vaporization
HPLC = high pressure liquid chromatography
Hz = hertz (cycles/sec)
I = intensity (W/cm^2)
I_o = intensity at the tissue surface (W/cm^2)
I_{th} = threshold intensity for tissue ablation
J = backwards light flux in the Kubelka-Munk model
K = thermal conductivity (W/cm^oC)
KM = Kubelka-Munk model for radiation transfer in turbid materials
κ = thermal diffusivity = $K/\rho C$ (cm^2/s)
mJ = millijoule
μJ = microjoule
μl = microliter
μm = micron (micrometer)
μsec = microsecond
nm = nanometer
ρ = density (gm/cm^3)
rF = retardation factor from thin layer chromatography
R = remittance
S_{km} = Kubelka-Munk scattering coefficient (cm^{-1})
t = time
T = transmittance
T = temperature (^oC)
T_o = initial temperature - usually body temperature (37^oC)
T_v = vaporization temperature
x = depth into tissue

ablation efficiency = the ratio of tissue mass ablated per unit of energy incident on the tissue. ($\mu g/J$)

fluence = energy incident on the tissue per unit area (J/cm^2)

CHAPTER I. INTRODUCTION

Atherosclerosis occurs in near epidemic proportions in western countries. It is a disease in which fatty yellow plaques form inside arteries at a rate that depends upon diet, blood pressure, serum cholesterol, hereditary predisposition and other factors. Although there are many theories about their genesis, probably the most accepted view is that serum and some components of blood insudate through the intima (inner lining of blood vessels) particularly in regions that are injured and thus are more permeable. Fatty components, especially lipids and cholesterol then get trapped in the artery wall where they are phagocytosed by macrophage/foam cells. The deformity of the vessel wall from the extra fat renders the intima more susceptible to injury and also may increase turbulence in the local blood flow which, in turn, increases intimal injury. Injury promotes more insudation of lipids into the artery wall and a vicious cycle develops (Robbins, Cotran and Kumar, 1986).

The plaques formed by this process are highly variable and are continually changing with time. Early lesions, called fatty streaks, are small and thus have minimal hemodynamic significance. Fatty streaks are thought to evolve into the classic atheroma which can compromise blood flow and consists of a thick intimal deposit of grumous with cholesterol crystals, lipid droplets and necrotic

tissue elements often with an overlying fibrous cap. In more advanced lesions, calcium deposits form and the plaque may ulcerate, exposing grumous to the surface and stimulating thrombus formation. Generally the key distinctions between plaque and normal artery include the high lipid/cholesterol content, presence of solid calcium deposits and reduced elasticity of the plaque.

As these plaques grow, they obstruct some arteries and compromise blood flow. Since the flow across a partially occluded segment of artery varies with $(radius)^4$, these lesions tend to reach a critical point where a small increase in plaque causes a large decrease in flow (Guyton, 1986). Severe plaques may also promote blood clot formation on their surface or hemorrhage into the plaque. Because of these phenomena, a plaque may grow for years with no apparent effect and then suddenly cause a heart attack. For most arteries there are many collaterals, or alternative pathways for blood flow. Therefore, the occlusion of one or only a few of these vessels is of little consequence. But some arteries do not have collaterals; when they occlude, the tissue they supply is killed. This is the case for several arteries of the heart, brain and legs and explains the high incidence of myocardial infarction (heart attack), stroke and peripheral vascular disease.

There are many methods of treating stenotic or obstructed arteries which, in itself, reflects the fact that none of them are particularly effective, except in special circumstances. Changing diet, quitting smoking, treating high blood pressure and

eliminating other risk factors may reduce the progression of the disease. A number of drugs (Goodman and Gilman, 1987), such as nitrates or calcium channel blockers can dilate blood vessels. A small increase in vessel diameter will dramatically increase blood flow because of the $(radius)^4$ relationship with flow. Some drugs can act on the clotting system to minimize clot formation (aspirin, persantine) or dissolve existing clots ($_r$TPA, streptokinase). There are also drugs that minimize the metabolic activity of tissue supplied by a stenotic artery (beta blockers) to prevent the tissue from outrunning its restricted oxygen supply.

Surgery can be used to remove plaque or to bypass the stenosis with a vein or other graft. The surgery, however, requires general anesthesia and cutting through a lot of normal tissue to reach the lesion. Some stenoses can be expanded by inflating a balloon within the artery. This procedure has merit because it can be done without surgery or general anaesthesia. Unfortunately, it still has a significant complication and failure rate occasionally requiring immediate emergency surgery and more frequently requiring repeat balloon dilation (due to restenosis) within 6 to 12 months.

Shortly after discovery of the maser by Schawlow and Townes in 1958 and the Ruby laser by Maiman in 1960, researchers began exploring the potential use of lasers in medicine and surgery. The carbon-dioxide laser, emitting radiation at 10.6 microns which is strongly absorbed by water, was found (Hall et al, 1971) to be effective in cutting and ablating tissue presumably because of the high water content of tissue (about 70%). This laser was found to

leave a zone of coagulation in the unablated tissue so that blood vessels were sealed permitting surgery with minimal blood loss. It was also found to be useful for operating on hard to reach organs such as the vocal cords, esophagus and cervix (Dixon, 1987).

The potential of another early device, the ruby laser, was also evaluated (McGuff, 1963). It emits millisecond pulses of high intensity radiation at 694 nm where tissue does not absorb well. Its ablative effect proved to be too explosive to be useful. As laser and optical technology progressed, more medical applications were discovered.

Recently, removal of obstructing plaques in humans has been accomplished with laser radiation delivered to the obstruction via fine flexible optical fibers by Choy et al (1984), Ginsberg et al (1985), Abela et al (1986), Geschwind et al (1984) and others. This procedure has the advantage of eliminating surgery and general anesthesia because the fiber can be inserted into the circulation in an artery close to the skin and then advanced through the circulation to the point of the obstruction. It has a potential advantage over balloon angioplasty in that the diseased tissue causing the obstruction is actually removed, not just expanded. Thus, this procedure might reduce the high incidence of restenosis associated with balloon angioplasty and may also extend catheter revascularization techniques to patients in whom surgery is the only option (e.g. long stenotic lesions, multivessel disease or acute thromboses)

Early research in this area has focused primarily on evaluating the ability of existing lasers to ablate plaque. The CO_2 laser emitting 10.6 micron radiation has been favored by some researchers (Gerity et al, 1983) because of its widely accepted use as a surgical laser. In theory, the high absorption of CO_2 laser radiation in tissue can limit the depth of penetration of the energy into the tissue. But in practice, this laser is used mostly in the continuous wave mode which can cause extensive thermal damage from thermal diffusion (Walsh et al, 1988). Intraoperative ablation of coronary plaques at the time of bypass surgery has been demonstrated with CO_2 laser radiation directed into the isolated coronary artery via a metal tube by Livesay (1985). Katzir et al. (1985) has described a safe, semi-flexible, optical fiber for delivery of the CO_2 laser radiation to arteries although the high absorption of 10.6 micron radiation by water requires displacing all physiologic fluids from the space intervening between the laser catheter and the plaque.

Wolbarsht et al. (1984) has described use of Hydrogen Fluoride and Erbium:YAG lasers emitting 2.9 micron radiation which may be even more strongly absorbed in tissue and for which zirconium fluoride fibers are available. Although initially very brittle, zirconium fluoride fibers have been improving in flexibility as manufacturers develop more experience producing them. The extremely high absorption of this radiation allows the possibility of removing tissue micron by micron and leaving behind a smooth surface with virtually no thermal damage. At this point, however,

the importance of surface smoothness and thermal damage is not known.

The Nd:YAG laser, emitting at 1.06 microns has been used clinically to ablate femoral and tibial artery stenoses with a percutaneous technique. Geshwind et al. (1984) used a balloon catheter inflated proximal to the stenosis to hold an optical fiber oriented coaxially with the vessel and to partially displace blood by perfusion with saline. He reported no immediate complications on the three patients treated but has provided no long term follow-up. Since then several centers have coupled Nd:YAG lasers to sapphire-tipped fibers to ablate peripheral artery lesions (Pilger, 1988 and Cross 1988). The sapphire-tipped fibers have a large diameter sapphire ball that spreads open the artery while the laser radiation emitted at the center of the ball makes an incision in the plaque allowing the occluded artery to open (Verdaasdonk et al 1987b).

The argon ion laser emitting primarily 514 nm radiation was initially the most popular (Marcuz et al (1980), Lee et al (1981), Ginsberg et al (1985), Choy et al (1984), Abela et al (1986)). Its radiation is readily transmitted by highly flexible and rugged quartz fibers, reasonably well absorbed by tissue with a penetration depth of about 300 microns and familiar to physicians. Ginsberg treated stenoses and obstructions in leg arteries of 16 patients using a technique similar to that of Geschwind. Although successful in improving the lumen of 8 patients, there were many complications including 2 laser perforations, 1 dissection, 7

patients with severe pain, 4 with spasm, 3 occlusions and 1 acute thrombosis. In addition, the laser procedure did not make an adequate channel for blood flow and always was followed with balloon dilation to obtain an acceptable lumen. In a similar experiment, Choy used argon lasers to ablate coronary artery stenoses in 5 patients during coronary bypass surgery. None of the vessels remained open and one which was biopsied showed deep medial necrosis due to thermal injury. These early problems with confining the effect of the laser radiation to plaque have been confirmed by Gerity (1983), Lee (1984), Abela (1985) and have led to extensive analysis of argon laser ablation of tissue by Welch (1984,1985) Cothren (1987) and others. Unfortunately, the relatively low intensity radiation from the argon ion laser ablates normal artery as well as soft plaque and typically leaves a 1 mm or larger zone of histologic alteration (presumably thermal damage) in the remaining unablated tissue. Like other continuous wave lasers, it cannot ablate calcified plaque and thus, preferentially ablates normal artery when directed at a calcified lesion.

Postulating that surface heating is the main ablative effect of laser radiation on plaque, Sanborn et al. (1986) demonstrated that placing a rounded metal "hot tip" on the end of the fiber enabled recanalization of occluded peripheral arteries in humans. In this procedure the laser radiation never reaches the tissue directly but rather heats up the metal tip which in theory burns through the plaque like a hot knife through butter. Unfortunately, this device has problems with perforation, welding itself to the

vessel wall and creating excessive thermal injury. At least one death has been associated with a hot tip perforation of a coronary artery. The hot tip can make a lumen only the size of itself so this procedure must be followed by balloon angioplasty. Abela et al. (1986) have modified the hot tip by drilling a hole in the end to allow some of the radiation to pass through it and reach the tissue.

Spears et al (1986) demonstrated that hematoporphyrin derivative (HPD) is preferentially taken up by plaque as compared to normal artery. This photoactive substance has been successfully used to treat cancer. After being taken up by tumors, it can be irradiated by low intensity argon pumped dye laser radiation at 633 nm to create singlet oxygen, which can then kill tumor cells. Spears tried this technique in animals and humans but found it has significant toxicity and does not result in a change in plaque geometry.

Excimer lasers at 193, 248, 308 and 351 nm have been shown to make precise cuts in soft and calcified atheromas with little morphological damage to residual unablated tissue by Srinivasan (1987), Linsker (1984), Grundfest (1985) and Isner (1987). These ultraviolet wavelengths carry the potential and often overstated risk of mutagenesis and the short, high intensity excimer laser pulses are difficult to transmit down optical fibers. By stretching the excimer laser pulse duration, making custom optical fibers and using 308 or 351 nm radiation (which is not as highly absorbed as 193 nm, 248 nm or 2.9 micron radiation) investigators have been

able to deliver enough energy via fibers to perform laser angioplasty and clinical studies are underway.

All of the research in this area has employed lasers emitting radiation that effectively ablates the normal artery wall as well as or better than the plaque. The numerous reports of perforations, aneurysms and other forms of inadvertent damage to the normal artery that is adjacent to or underlying the plaque indicate the difficulty of confining laser radiation to the diseased tissue with present catheter techniques. To overcome this problem, many investigators are developing angioscopic (Spears 1983, Litvack 1985, Shure 1985), spectroscopic (Kitrell 1985, Sartori 1986, Deckelbaum 1987, Clarke 1988) ultrasound imaging (Sahn, 1982) and other techniques that discriminate plaque from normal artery to improve aiming. Mechanical "atherectomy" devices that take advantage of differences in tissue elasticity between plaque and normal artery to selectively remove plaque are also under development (Schwarten 1986, Kensey 1986, Hansen 1987). An ideal approach, would be one in which laser pulses completely ablated plaque while causing no damage when inadvertently directed at normal artery.

Selective destruction of tissue based on differential absorption has been described by Anderson and Parrish (1983). They took advantage of the preferential absorption by hemoglobin at 577 nm compared to nonvascular dermal tissues to selectively coagulate the anomalous micro blood vessels that cause port wine stain, an unsightly red patch of skin often occurring on the face. By using

pulses that are short compared to the thermal relaxation time for the 100 μm diseased blood vessels, the thermal damage was confined to the region of the blood vessels.

Many studies on laser ablation of materials have shown a "threshold" above which ablation occurs and below which ablation does not occur. This threshold behavior, which can depend upon optical absorption and other properties of the materials, suggests that selective ablation of plaque is possible if a waveband of differential absorption can be identified. Selective ablation of ureteral calculi and biliary stones by a plasma mediated process indicates that selective ablation of calcified plaque may be possible by a similar mechanism (Watson, 1986).

This thesis investigates the possibility of ablating plaque with laser pulses that do not ablate normal artery.

HYPOTHESIS: It is possible to ablate arterial plaque with laser pulses that do not ablate normal artery.

CHAPTER II. RATIONALE FOR SELECTIVE ABLATION

Selective ablation requires capitalizing on the optical, thermal and mechanical differences between normal and diseased tissue to remove unwanted tissue with a minimal effect on normal. Thermal properties of atheromas and normal artery are known to be similar because of the high water content ($\approx$ 70%). There are, however, obvious mechanical and optical differences between atheromas and normal artery. Atheromas are generally yellow while normal artery is pink. Atheromas are weakly held together, inelastic and sometimes hard and brittle while normal artery is strong, tough, elastic and soft. The idea behind this work is to take advantage of the optical differences to preferentially deposit radiation energy in atheromas. How this selective deposition of laser energy affects ablation would obviously depend on the precise mechanism of ablation. Analysis of the complex processes by which laser radiation incident on tissue causes ablation has recently been reviewed from many perspectives (Regan and Parrish 1982, Ready 1971 and 1982, Welch 1984, Boulois 1987, Wolbarsht 1984, Hillenkamp 1980, Weber and Zweig 1987, Letokhov 1985, Partovi et al 1987, Yoon et al 1987) and will be described in greater detail in Chapter VI.

To see how selective deposition of laser energy may lead to selective ablation, assume for the moment that ablation is nothing more than evaporation of water (as will be discussed later, this is

far too simple a model). If we further assume homogeneous material, Beer's law absorption, and apply the one-dimensional heat equation (which is justified if the laser beam diameter is greater than $1/\alpha$), then the temperature distribution during irradiation with an intensity, I_o, would be given by

$$\frac{\partial^2 T}{\partial x^2} - \frac{\rho C}{K}\cdot\frac{\partial T}{\partial t} = \frac{I o \alpha e^{-\alpha x}}{K} \qquad \text{II.1}$$

where x = depth into the tissue
K = thermal conductivity
C = specific heat
ρ = density
α = absorption coefficient
I_o = intensity of incident radiation
T = temperature
t = time

To maximize selectivity, the energy should not have time to diffuse to adjacent tissue once it is selectively absorbed. This restricts the laser pulse duration to times much shorter than the thermal relaxation time, τ_R, where

$$\tau_R = 1/4\alpha^2\kappa \qquad \text{II.2}$$

$\kappa = K/\rho C$ = thermal diffusivity

as described by Anderson and Parrish (1983). This allows simplification of equation I.1 to

$$\frac{\partial T}{\partial t} = \frac{I_o \alpha e^{-\alpha x}}{\rho C} \qquad \text{II.3}$$

for the period of irradiation, which can be integrated to yield:

$$T = \frac{I_o t \alpha}{\rho C} e^{-\alpha x} + T_o \qquad \text{II.4}$$

where T_o = initial temperature.

Now assume that vaporization will begin as soon as the surface reaches a vaporization temperature, T_v. Then, the threshold intensity, I_{th}, for ablation can be calculated by solving for the intensity at which the surface temperature $T_{(x=0)}$ exceeds T_v, i.e.

$$I_{th} = \frac{\rho C(T_v - T_o)}{\alpha t} \qquad \text{II.5.}$$

This threshold intensity can be rewritten in terms of a threshold energy per area (fluence) to give

$$F_{th} = \frac{E_{th}}{\text{Area}} = I_{th} t = \frac{\rho C(T_v - T_o)}{\alpha} \qquad \text{II.6.}$$

Selectivity in this ablative regime will occur when the threshold fluence, F_{th}, is higher for normal tissue than for plaque

and when one is operating above the threshold for plaque and below the threshold for normal tissue. The thermal properties, ρ, C and (T_v-T_o) have been measured and found to be comparable for plaque, normal artery and water (Welch 1984). This is presumably because water is the dominant thermodynamic material in tissue accounting for 70% - 90% of its mass. This leaves the absorption coefficient, α, as the only parameter in this model system available for differentiating the ablation thresholds between plaque and normal artery. Since in theory, the threshold fluence scales inversely with α, selective ablation would be predicted to occur at wavelengths where the plaque absorption coefficient is significantly greater than the normal artery absorption coefficient (sssuming all plaque has the same absorption coefficient and all normal tissue has the same absorption coefficient).

In the region of the electromagnetic spectrum from 1.3 μm to mm, absorption in all tissue is dominated by water. Since water is the dominant component of both plaque and normal artery no selectivity based upon preferential absorption would be expected in that part of the spectrum. At ultraviolet wavelengths below 300 nm, the strong absorption by DNA and proteins in cellular tissues like normal artery also make selectivity for plaque unlikely. These higher energy photons (greater than 3-4 electron-volts) also can initiate a variety of undesirable photochemical reactions. However, in between these regions there may be differential absorption as evidenced by the obvious difference in color between

plaque and normal artery.

Thus, selective ablation may be possible if one could identify a wavelength between 300 to 1300 nm where there is preferential absorption and a laser emitting sufficiently short pulses at that wavelength. This laser then, should be operated above the threshold for ablating plaque and below the threshold for ablating normal artery.

Chapters 3 and 4 will discuss the studies undertaken to identify a waveband of preferential absorption and to demonstrate that preferentially absorbed radiation can selectively ablate atherosclerotic plaque.

CHAPTER III. EXPERIMENTAL METHODS

This chapter describes the experiments used to

a. identify a waveband of preferential absorption,

b. measure ablation thresholds,

c. demonstrate selective ablation,

d. evaluate the mechanisms of ablation,

e. identify carotenoids as the chromophores responsible for selective ablation, and

f. demonstrate that selectivity is enhanced by feeding carotenoids to patients.

These experiments are summarized in Table III.1 and described in detail below.

III.1 Optical Studies

Two techniques were used to evaluate tissue absorption. First, diffuse spectral remittance and transmittance were measured on a spectrophotometer fitted with an integrating sphere and the Kubelka-Munk (1931, 1948, 1954) model for light propagation in scattering media was used to calculate absorption coefficients. The integrating sphere measurements showed reduced precision in regions of high absorbance, which were the most relevant to this study. Accordingly, a tunable-dye-laser-based-spectrophotometer

was constructed which could measure transmittance with a precision of 10^{-5} percent over areas as small as 1 mm^2.

III.1.1 **Specimens.** Specimens of human aorta were obtained less than 48 hours post mortem from 10 cadavers. Optical measurements with the integrating sphere were made on 6 soft, yellow, raised plaques from which the outer portion of the media and adventitia had been stripped by blunt dissection. Each plaque came from a different cadaver and was measured once. A total of 7 normal aorta specimens were prepared from 3 of those cadavers. One was studied as an intact, full thickness specimen and measured 3 times. A second was studied intact and then roughly divided into adventitia, media and intima by blunt dissection, and the integral parts examined separately. A third was divided into an intimal and a medial specimen before measurement. Laser spectrophotometer measurements were made on specimens from 4 cadavers. In each specimen, 3 atheromatous regions and 3 adjacent normal spots were studied, for a total of 12 pairs of measurements.

III.1.2 **Integrating Sphere Measurements.** Specimens of .2 to 2 mm thickness were mounted in a holder with polished quartz windows; the holder was filled with normal saline to minimize optical artifacts from tissue surface irregularities. The air-quartz interfaces of the holder had a consistent and predictable remittance that was measured and subtracted from the tissue remittance measurement. The mounted tissue was placed on a 7.5-cm-diameter, barium sulfate-coated integrating sphere connected by 2-

mm-internal-diameter fiber optic bundles to a Beckman 5270 double beam spectrophotometer as shown in Figure III.1 and described previously by Anderson (1981) and Wan (1981). This spectrophotometer was interfaced to a Hewlett Packard 9825A computer for digital data acquisition and analysis. The apparatus used a collimated light beam to illuminate a 5-mm-diameter region of the sample tissue. Diffuse illumination was not used because it would have required illumination of a substantially larger diameter spot to achieve the same level of precision, making it difficult to study individual, discrete atheromas. The illumination wavelength was scanned from 1330 to 250 nm. Freshly coated barium sulfate plates were used as 100% remittance standards. Thickness of the tissue, positioned between the two quartz windows, was measured with a micrometer. To examine the effect of denaturation on tissue optics, some mounted specimens were heated with a hot air gun to 100°C and reexamined.

Immediately following measurement of remittance and transmittance, the area examined was marked with india ink, fixed in 10% buffered formalin, processed through xylene and graded alcohols and paraffin embedded. Sections were stained with hemotoxylin and eosin for light microscopy. Silver stains were used on selected sections to better visualize elastic fibers.

III.1.3 **Laser-based Spectrophotometer Measurements.** Because the integrating sphere measurements were limited to a minimum of a 5-mm-diameter region on the sample and a transmittance of > 0.5

percent, a tunable-dye-laser-based spectrophotometer was constructed which could measure transmittances as low as 10^{-5} in 1-mm-diameter spots (see Figure III.2).

A nitrogen-laser-pumped dye laser (Laser Sciences Inc.) was used to provide light from 400 to 605 nm using DPS, coumarin 440, coumarin 480, coumarin 540A and rhodamin 6G dyes. All transmitted light was detected with a 1 cm^2 UV-IR enhanced silicon photodiode (Hamamatsu #1337-1010BQ). An RC integrating circuit was used to average over 100 laser pulses. A reference beam with an identical detection circuit was employed to compensate for pulse to pulse variations in laser output. Another identical detection circuit was submerged in the saline bath on top of the specimen to measure remittance. Remittance was calibrated using a 1.5 mm thick piece of teflon. The specimens were immersed in a normal saline bath during measurements to minimize the effects of irregular surface contours and to simulate the in vivo optical environment. The small spot size permitted translating the tissue through the beam to directly compare optical properties at normal and atheromatous regions on the same specimen. Following measurements, the spots studied were marked and processed as previously described.

III.1.4 Calculation of Absorption and Scattering Coefficients based on Kubelka-Munk Theory. Absorption and scattering coefficients were calculated with the Kubelka-Munk (KM) model for light propagation in turbid and absorbing media (Kubelka, 1948, 1954). In this model, light in the tissue is separated into two

diffuse fluxes, the first, I, propagating forward into the tissue, the second, J, propagating backwards towards the source (Figure III.3). The model defines absorption and back scattering coefficients, A_{km} and S_{km}, and describes light propagation by two first order differential equations,

$$\frac{dI}{dx} = -S_{km}I - A_{km}I + S_{km}J \qquad \text{III.1}$$

and

$$\frac{dJ}{dx} = S_{km}J + A_{km}J - S_{km}I \qquad \text{III.2.}$$

These equations have been solved for the boundary conditions illustrated in Figure III.3 to give the A_{km} and S_{km} coefficients in terms of the measurable quantities remittance, R, transmittance, T and thickness, D, where

$$S_{km} = \frac{1}{D}\left[\left(\frac{1+R^2-T^2}{2R}\right)^2 - 1\right]^{-\frac{1}{2}} \coth^{-1}\left[\frac{\frac{1-R^2+T^2}{2R}}{\left[\left(\frac{1+R^2-T^2}{2R}\right)^2 - 1\right]^{\frac{1}{2}}}\right] \qquad \text{III.3}$$

$$A_{km} = S_{km}([(1 + R^2 - T^2)/2R] - 1) \qquad \text{III.4.}$$

When T is small, equation III.4 can be approximated as

$$A_{km} = S_{km}[(1 - R)2/2R] \qquad \text{III.5.}$$

For very small values of T, such as in a thick specimen or

in a region of high absorption, the value of S_{km} in equation III.3 is very sensitive to errors in the measurement of T. Because scattering usually varies slowly with wavelength (32), it is possible to calculate A_{km} using the measured R, and the S_{km} from an adjacent spectral region with higher T. In regions of T < 0.5%, A_{km} was calculated this way.

III.1.5 Calculation of Absorption Coefficients based on Beer's Law. In the waveband of preferential absorption in atheromas an additional method was used to evaluate absorption. Beer's law absorption coefficients, α_b, were calculated using equation III.6

$$\alpha_b = -\ln(\text{Transmittance})/\text{thickness} \qquad \text{III.6}$$

and the ratio of atheroma α_b to normal aorta α_b was plotted to locate the wavelength of maximum preferential absorption in atheromas. This simplified analysis ignores the effect of light scattering within the tissue. In cases where scattering is small compared to absorption as well as wavelength and sample-independent, α_b will be similar to A_{km}.

III.1.6 Statistical Analysis. A t test for dependent measures was used to evaluate the significance of the observed difference in absorption between atheromatous and normal aorta at the wavelength

of maximal preferential absorption in atheromas (470 nm). The laser spectrophotometer measurements were treated as paired data, since both atheroma and normal aorta were compared within the same individual. The three measurements on the atheromatous and on the normal regions of each of the specimens were averaged, and the average atheroma and normal absorption coefficient for each individual were treated as two separate observations. For the integrating sphere measurements, determinations of atheroma or normal absorbance on multiple specimens from the same individual were also averaged. The averaged data were treated as independent observations.

III.2 Ablation Studies

III.2.1 Radiation Source. All laser radiation was provided by flashlamp-excited dye lasers (Candela Laser Corp. Wayland, MA). Initially a coaxial flashlamp-excited dye laser was used that generated 1-μsec-long pulses (full width at half maximum) at a repetition rate of 1 Hz with energies up to 1.5 joules per pulse. This laser could be frequency doubled using a ammonium dihydrogen phosphate crystal and provided up to 30 mJ/pulse of 290 nm radiation at a pulse duration of 500 ns. A repetition rate of only 1 Hz made it difficult to quantitate the ablative effect because of

the need to average over many pulses. Accordingly, a linear flashlamp-excited dye laser was obtained which operated at up to 10 Hz with up to 500 mJ/pulse with a pulse duration of 1 μsec. To study the effect of pulse duration, additional lasers were constructed with 8 and 50 μsec pulse durations. Fundamental mode radiation at 465, 480, 504, 540, 658 and 690 nm was produced using various laser dyes (Exciton Chemical Co. Dayton, OH) in the 1 μsec lasers. The longer pulse duration lasers were operated only at 480 nm. Laser wavelength was measured with a grating monochromator (Bausch Lomb #33-86-76). Pulse width was measured with a reverse biased silicon photodiode (EG&G FND 100Q). The laser mirrors were adjusted prior to each experiment until output burn patterns on exposed polaroid film were circular and uniform. Spot size was determined by measuring burn patterns on polaroid film placed just in front of specimens. The energy per pulse was measured with an energy meter (Scientech #36-5002 & 38-0101) or power meter (Coherent #CT-210). Pulse-to-pulse energy variation was $\pm$ 5%.

III.2.2 Specimens. Specimens of atherosclerotic human aortas, heart, inferior vena cava, pulmonary artery and pulmonary embolus were obtained from the Massachusetts General Hospital morgue and used within 5 days of death. All specimens were reviewed by a pathologist (or pathology resident), rinsed with normal saline to wash off blood and post-mortem clot, tightly wrapped in plastic and

placed in refrigerated storage; they were allowed to equilibrate to room temperature just before irradiation. Normal-appearing regions of aorta were categorized as normal intima. The underlying media and adventitia were made avaliable for study by blunt dissection. Atherosclerotic regions were categorized into fatty streaks, fibro-fatty plaque or calcified plaque. Post-mortem thrombus was discarded. Organized thrombus adherent to plaque was labelled thrombus. Organized thrombus in pulmonary arteries was labelled pulmonary emboli.

III.2.3 Ablation Thresholds. The threshold energy for ablation was defined as that energy delivered through the fiber that caused visible removal of tissue from the specimen. Any visible change in the surface of the tissue including just roughening of the tissue surface was considered to be ablation. Typically it was accompanied by a characteristic snapping sound and fiber recoil. It was measured as shown in Figure III.4. Initially the coaxial flashlamp-excited dye laser was employed and the laser beam was made uniform by focusing into a step-index, multimode, quartz optical fiber with a 1 mm or 650 micron core, approximately 1 meter long (Math Associates QSF 1000 or QSF 650). The output end of this fiber was placed flush against aortic specimens submerged in saline. The laser energy was increased at increments of 5-10 mJ until the ablation threshold was reached. This energy was then

measured by aiming the fiber into the energy meter. Threshold fluence was calculated by dividing this energy by the area of the fiber core.

When the linear, high repetition rate, laser became available, the recorded threshold energy for ablation of each specimen was determined as the energy at which 50% of 20 separate exposures showed signs of ablation. Threshold fluence was calculated as described previously. This technique was fast and permitted averaging over a large volume of tissue. For each pulse duration, specimens of each tissue type from at least 5 different cadavers were studied and averaged. Statistical comparisons were made with a t test for independent measures.

III.2.4 Histology of Preferential Ablation. To examine the selective ablative effect of this laser histologically, large areas of plaque were ablated as shown in Figure III.5. Atheromatous and adjacent normal regions of 20 specimens were irradiated with multiple pulses at a rate of 1 Hz and a fluence of 18 J/cm^2/pulse either in air or submerged under 1 cm of saline. Following irradiation, the irradiated areas were marked with india ink, fixed in formalin, processed routinely and stained with hematoxylin and eosin. Calcified plaques were first decalcified in nitric acid and then processed routinely.

III.2.5 Measuring Mass Ablated. Two techniques were used to quantify the mass of tissue ablated per laser pulse (ablation

efficiency). In the first technique, specimens were mounted vertically at the edge of an analytic balance (Mettler AE163) such that ablation debris landed off the balance as shown in Figure III.6. A humidified chamber surrounding the specimen minimized interference from air currents and weight loss from evaporation. Specimen mass was recorded automatically at 2 Hz by a computer (IBM PC) interfaced to the balance (Mettler Interface Option 011). All specimens were cut from human aortas using a 6 mm biopsy punch to provide the same surface area for water evaporation. A 2.5-mm-diameter spot on each specimen was irradiated with 10 pulses, each at 0.9 J (18 J/cm^2/pulse) delivered at 1 second intervals. This was repeated for 7-10 normal and atheromatous aortic specimens from each of 4 aortas for a total of 66 measurements. Balance readings were also taken before and after laser irradiation to correct for drift due to water evaporation.

When a linear flashlamp laser with a repetition rate of 10 Hz became available it was possible to deliver many more laser pulses in between balance readings. This greatly enhanced the signal-to-noise ratio of the measurement. It was then possible to weigh a small specimen before and after irradiation under saline with 100 to 200 pulses. A total energy of 0.8 or 8 J was delivered to each specimen under saline between mass measurements depending on the tissue's susceptibility to ablation. This was repeated at 2 different pulse energies including subthreshold (control) and twice the threshold for plaque tissue. This measurement was repeated 10 times for each specimen. Normal intima, fibro-fatty plaque and

calcified plaque were all studied in this manner. Specimens of each tissue type from at least 5 different humans were studied at each pulse duration.

III.2.6 High Speed Photography. The ablation process was photographed using a method developed in collaboration with Edgerton (1979). A 35 mm camera with the shutter open was aimed perpendicular to the laser beam. A yellow filter (Corning #3-370) excluded the 465 nm laser radiation from exposing the film. The room was darkened sufficiently to allow exposure of the film (Kodak Plus-X) only by a 1-μsec-long electronic flash pulse. A delay circuit permitted triggering the flash at times ranging from 10 to 2500 μsec, as measured with a photodiode (Centronics BPX65), after the laser pulse. Specimens from the two atheromatous aortas were ablated at 25 J/cm^2/pulse over 2.5-mm-diameter spots. A luminescent plume associated with ablation of calcified plaque ablation was photographed in a similar manner but without the electronic flash.

III.2.7 Ablation plume spectral analysis. To determine if the luminescent plume associated with calcified plaque ablation represented a plasma, as opposed to incandescent or fluorescent emissions, the spectral distribution of the luminescent plume, in the spectral range from 300 to 600 nm, was measured using a method described in detail by Teng et al (1987a). A grating spectrometer with a gated multichannel analyzer detection system (OMA-3 Princeton Applied Research Princeton, NJ) was used to obtain

emission spectra at various times after the beginning of the laser pulse.

III.2.8 Analysis of Ablation Products. Ablation debris was collected by placing a microscope slide in the path of the laser radiation, 2 cm away from the specimen. The debris on the slide was examined while fresh, and again after being fixed and stained with hemotoxylin and eosin. Debris was also collected by placing a saline filled petri dish just in front of the specimen (oriented vertically) being ablated; it was collected on 5 micron filter paper (Millipore SM 5.0 um), fixed in 95% ethanol and stained with hematoxylin, orange-green and eosin to evaluate particle size. Calcified plaque debris was collected by irradiationg the plaque under prefiltered saline. Following irradiation, the saline was examined under a dissecting microscope.

III.3 Chromophore Studies

III.3.1 Chromophore Identification. After identifying a spectral region of preferential absorption in atheromas (see chapter IV), it was possible to partially characterize the responsible chromophores. Lipophilic pigments were extracted by shaking 1.2 gm of atheroma or normal aorta in 10 ml common xylenes (Fisher X-5 SK) for 12 hour at 5^{o}C. After filtration (Whatman #42 ashless filter paper), absorption spectra of the filtrate were determined in 1-cm-path cuvettes using a Beckman 5270 UV-VIS spectrophotometer. The

xylene extracts were then evaporated to 0.2 ml, chromatographed on Eastman Kodak silica gel thin layer sheets and developed with petroleum ether (bp 30-60°C, Fisher E139). The spots were cut out and eluted with ethanol. The absorption spectra were measured from 300 to 600 nm on a Cary model 14 spectrophotometer.

III.3.2 Chromophore Enhancement.

Patients Ten patients scheduled for carotid endarterectomy volunteered (with the informed consent process) to take 180 mg of beta carotene (Solatene, Hoffmann-LaRoche, Nutley, NJ) per day in 3 divided doses for periods varying from 8 to 41 days prior to their surgery. On the day of surgery, blood was taken for serum beta carotene determination and the pills remaining from the bottle provided to the patient were counted to evaluate compliance. Following surgery each endarterectomy specimen was examined by a pathologist, washed in normal saline and frozen at -70°C. Three of the patients had a prior carotid endarterectomy on the contralateral side without having taken beta carotene and their specimens were saved (in an identical manner) to use as controls. An additional 16 patients underwent carotid endarterectomy without taking beta carotene and their specimens and serum were also saved at -70°C for use as controls. For all patients in the study, data on risk factors for atherosclerosis including age, sex, tobacco use, diabetes, hypertension, serum cholesterol and serum triglycerides were obtained by chart review. The study was not randomized or blinded. Specimens of normal vascular tissue were

not obtained because, in the carotid endarterectomy procedure, only abnormal tissue is removed.

Carotenoid and Lipid Extraction Lipids and carotenoids were extracted from all specimens using a method described by Blankenhorn (1957). Endarterectomy specimens were first weighed and homogenized. Canthaxanthin, a carotenoid not normally found in human tissues, was added to 5 specimens as an internal control for evaluating the extraction yield. The homogenate was then saponified by adding 1 ml of 6% potassium hydroxide (KOH) in absolute methanol and shaking in a 60°C water bath for 60 minutes. After saponification, the mixture was cooled to room temperature and extracted twice with 2 ml of petroleum ether (b.p. 30-60°C; No. E-139, Fischer Scientific Co.). The methanol and petroleum ether layers were allowed to separate (centrifuging when necessary). When necessary, a third ether extraction was performed. The petroleum ether extracts for each specimen were pooled. Serum was extracted by adding the 1 ml 6% KOH directly to 0.5 ml serum and then proceeding as with the plaque.

Beta Carotene Determination The extracted carotenoids were further separated by a high pressure liquid chromatograph (HPLC) method described by Bieri et al (1985). For each specimen, the ether was evaporated under nitrogen and the residual pigment was resuspended in 1 ml of methanol. After centrifuging at 2000 rpm for ten minutes to eliminate any particulate contaminants, 220 μl of each specimen was injected (Hewlet Packard HPLC model# 1090)

onto a C-18, 5 micron, reverse-phase column (LC18, Supelco Inc., Bellefonte, PA) with an isocratic solvent (acetonitrile:methylene-chloride:methanol, 70:20:10) flowing at 1.7 ml/min. The absolute amount of beta carotene was determined by integrating the area under the curve of absorbance at 450 nm versus time and comparing to the area obtained for a known amount of purified beta carotene. Extraction yield was determined as the ratio of canthaxanthin mass in the extract to the mass of canthaxanthin added to the specimen.

Statistical Analysis Comparisons were made by a t-test for dependent measures in the group of 3 patients who had two endarterectomy specimens, one with and one without beta carotene pretreatment. These data were then pooled with the unpaired data of the appropriate type and means of these data sets were compared with the t-test for independent measures.

Microscopy In order to evaluate where the beta carotene accumulated within the plaque, 6 specimens were examined microscopically. These included specimens from 2 patients who were studied both before and after beta carotene treatment and specimens from 2 patients who were studied only after beta carotene treatment. All specimens were prepared for histologic analysis by embedding in optimal cutting temperature medium (OCT), sectioning by cryostat and mounting without staining between coverslips with a single drop of aqueous mounting medium. They were then examined by conventional light microscopy and also by microspectrophotometry. On some specimens, additional sections were made with

hematoxylin/eosin and pentachrome stains to examine the histological architecture in detail.

Microspectrophotometry Absorption spectra were determined for all 6 sectioned specimens by a microspectrophotometry technique described by MacNichol (1978). A beam of radiation that scanned from 375 to 750 nm transilluminated specimens sandwiched between coverslips on the stage of a microscope. By adjusting slits that defined the beam, illumination could be confined to spots as small as 2 by 2 microns. Light from this measuring beam was collected by a 100x glycerol immersion, UVF objective that focused the slit image in the specimen plane onto an eyepiece or a photomultiplier tube. An additional broadfield illumination source could be turned on to permit precise alignment of the measuring beam with the tissue structure of interest. The monochromator and photomultiplier tube with photon counting electronics were interfaced to a computer for data collection and analysis. Data was collected by first scanning a blank area for calibration and then scanning the structure of interest.

CHAPTER IV. EXPERIMENTAL RESULTS

IV.1 Optical Studies

Figure IV.1A shows the integrating sphere measurement of remittance and transmittance for a typical specimen of endothelium and intima (310 microns thick) from normal aorta. The absorption and scattering coefficients calculated from the data of Figure IV.1A using Kubelka-Munk theory are given in Figure IV.1B. Comparable data for a typical atheroma (1.5 mm thick) are shown in Figures IV.1C and IV.1D. The greater thickness of this sample gives lower transmittance and higher remittance compared to the sample of normal aorta. The effect of thickness is accounted for in the calculation of absorption and scattering coefficients. When these measurements were repeated three times for one of the specimens, there was only a few percent variation in measured remittance and transmittance and even less in the calculated absorption and scattering coefficients. Another specimen, the full thickness normal aorta, was subdivided and showed no difference in the shape of the absorption and scattering spectra amoung its three parts.

Figure IV.2A shows the average Kubelka-Munk absorption coefficient for integrating sphere measurements on 6 atheromas compared to that of the 7 normal specimens. The results for the

normal aorta are generally similar to those described by Kaminow (1984), Anderson (1981), Wan (1981) and Van Gemert (1985), and display peaks characteristic of known tissue chromophores including hemoglobin (alpha band at 550-570 nm, beta band at 530-550 nm, Soret band at 390-420), aromatic amino acids and DNA (both having absorption bands at 250-290 nm). The atheroma and normal data do not differ significantly for most of the spectral range covered by the two curves. However, in the region of 420 to 530 nm the atheromas clearly absorb more than the normal tissues. At 470 nm, the average Kubelka-Munk absorption coefficient for the six atheromas was 50 ± 7 cm^{-1}, while that of the normal specimens was 24 ± 4 cm^{-1} (Table IV.1). Using a Beer's law analysis which accounts only for the transmitted radiation, the average absorption coefficient was 63 ± 7 cm^{-1} for atheroma, compared to 36 ± 7 cm^{-1} for normal tissue.

The laser spectrophotometer data taken in the range of 400-605 nm were similar to the integrating sphere results for all 24 samples from the 4 cadavers. Figure IV.2B shows the calculated KM absorption coefficients for three, 1-mm-diameter normal and atheroma measurements on a typical specimen. All of the atheromatous spots studied had greater absorption from 430-500 nm than all of the normal spots. For the laser spectrophotometer measurements, the average Kubelka-Munk absorption coefficient at 470 nm for the twelve measurements on atheromas from four individuals was 61 ± 16 cm^{-1} while the average absorption of the uninvolved areas in the same specimins was 27 ± 14 cm^{-1} (Table

IV.1). Beer's law analysis gave 48 $\pm$ 9 cm^{-1} and 25 $\pm$ 4 cm^{-1}, respectively (Table IV.1).

Figure IV.3 shows the ratio of atheroma to normal aorta absorption from 300-600 nm, for both integrating sphere and laser spectrophotometer measurements. This ratio is largest near 470 nm, with a value of 2.2 or 2.3.

For the laser spectrophotometer data, using a t test for dependent measures and comparing average absorbance within the same individual (see Methods), the differences were statistically significant with $p < 0.05$ for both the Kubelka-Munk and Beer's law analyses (Table IV.1). For the integrating sphere data, comparing the average absorbance of atheroma or normal from different individuals and using a t test for independent measures gave $p < 0.001$. Thus the differences between atheroma and normal were highly significant.

Scattering coefficients (Figures IV.1B &)D increased 2 to 3 fold with decreasing wavelength over the spectral range, varying slowly and smoothly. In general, scattering was slightly higher in atheromas but always similar in shape to the normal aorta. For thin specimens, where T was large enough to use equation III.4, as in Figure IV.1B, the scattering coefficient (S_{km}) was essentially constant at 8 cm^{-1} from 450-550 nm. The flat behavior of S_{km} in this region justifies the approximation used for thick samples with small T (see Methods). In thicker specimens (Figures IV.1C and IV.1D) transmittance was < 0.5% in some regions requiring use of

equation III.5. The minima seen in Figure IV.1B at 260 and 400 nm are probably artifacts due to errors in transmittance and remittance measurements at regions of high absorbance.

Following thermal denaturation there was a slight increase in both absorption and scattering over the entire measured spectrum except near 410 nm (Soret band) where absorption was diminished. These changes were small compared to the preferential absorption in atheromas.

Histologic analysis confirmed that the areas of specimens chosen to be "normal" had normal morphology. A typical atheroma is shown in Figure IV.4. In the atheromas the intima was thickened with dense, hyalinized collagen bundles and diminished amounts of elastic tissue and smooth muscle cells. In the centers of the atheromas there were variable amounts of irregularly deposited grumous material that appeared to consist of extracellular lipids and cellular debris. In some of the specimens there were scattered, dystrophic calcifications. There was no evidence of ulceration or direct exposure of the grumous material to the luminal surface, although in two specimens there were scattered acute and chronic inflammatory cells in the superficial portion of the atheroma.

IV.2 ABLATION STUDIES

IV.2.1 Threshold Fluence. For each specimen there was a threshold

fluence above which ablation occurred and below which the tissue appeared to the eye to be unaffected. Near the threshold, the ablative effect was a slight roughening of the surface, but at 2 to 3 times the threshold value, craters were formed which were of the same diameter as the laser beam and up to several hundred microns deep. When the fiber was in contact with tissue, laser pulses at or above the threshold fluence were always associated with a "recoil" force which could be felt while holding the fiber and which increased with increasing fluence.

With calcified lesions, laser pulses above threshold were associated with a loud popping noise. There was also a flash of white light, like an electrical spark, at the site of irradiation (easily seen through goggles that excluded the laser radiation).

Figure IV.5 shows the threshold fluence at 465 nm (with a 1 mm fiber) for normal and atheromatous aorta from seven individuals. In each case the threshold fluence for ablating normal tissue was higher than for atheromatous tissue. The average threshold for ablating atheromatous tissue was 6.8 + 2.0 J/cm^2 compared to 15.9 $\pm$ 2.2 J/cm^2 for normal. Ablation threshold for all types of cardiovascular tissues are shown in Figure IV.6 and Table IV.2. These data indicate that at 482 nm (with a 320 micron fiber), the diseased tissues (including fresh thrombus, pulmonary embolus, calcified plaque and fibro-fatty plaque) all have a lower ablation threshold than the normal tissues (including adventitia, media, normal intima, inferior vena cava and pulmonary artery).

The effect of wavelength on the ablation threshold is indicated in Tables IV.3 & IV.4 and in Figure IV.7. In the ultraviolet, at 290 nm, there is no selectivity for the plaque. At 482 nm, where there is 2-fold preferential absorption in yellow plaque, there is about 2-fold selectivity for fibro-fatty plaque, calcified plaque and fatty streaks. Also at 482 nm there is enormous selectivity for thrombus (>10-fold). At 658 nm where there is no preferential absorption, there is no selectivity for fatty streaks or fibro-fatty plaque, but, interestingly, there is still significant selectivity for calcified plaque and thrombus. This suggests that the selectivity for yellow plaque is based upon absorption differences but the selectivity for calcified plaque and thrombus may be due to a different mechanism.

The effect of pulse duration on the ablation threshold is shown in Figure IV.8 and Table IV.5. In general, as the pulse duration increased, the threshold fluence also increased. Despite the increase in threshold, the relative magnitudes of the thresholds for plaque and normal artery were roughly preserved with only a slight decrease in the ratio of the ablation threshold for normal tissue to the ablation threshold for plaque. This suggests the introduction of some inefficiency in the ablation process at the longer pulse durations which affects plaque and normal artery equally. A more extensive study covering a wider range of pulse durations would be useful to better characterize this effect but was not done in this thesis due to technical and financial constraints.

Table IV.6 and Figure IV.9 indicate the effect of fiber diameter on the ablation threshold fluence. The threshold fluence increases with decreasing fiber diameter presumably due to scattering and beam divergence which becomes significant with small diameter fibers. This makes the beam spot size different from the fiber diameter and hence, results in uncertainty in calculating fluences.

IV.2.2 Histology. Figure IV.10 presents a cross section of 2 atheromatous and 2 adjacent normal regions of human aorta. Each region was irradiated with 10, 1 μsec pulses of 465nm laser radiation at a fluence of 18 J/cm^2/pulse; a level that is well above the threshold for ablating atheromas but near the threshold for ablating normal aorta. As expected, there was substantial removal of atheroma forming craters greater than 1 mm deep, while the normal tissue showed only a slightly roughened surface. This selective ablation occurred both in air and under saline with radiation direct from the laser or delivered via a quartz optical fiber. All soft yellow atheromas as well as red, brown/black or green thrombus were readily ablated at this fluence. Pipe stem-like yellow calcific plaques were also ablated in saline; in air they were usually ablated to a depth of about 1/2 mm, exposing bright white material which could not be ablated. Normal tissue, irradiated at 18 J/cm^2/pulse, was slightly roughened and in some regions turned slightly brown at the surface. No char was seen grossly on any of the specimens.

Figure IV.11 shows the histology for a typical ablation crater made by 10 pulses of 465 nm radiation at 18 J/cm^2/pulse. The edges are irregular but show only traces of coagulation (the black material is the india ink used to mark the site of irradiation). Specimens ablated in air showed a zone of coagulation about 100 microns thick lining the ablation crater; this coagulation was also present in some regions that were not irradiated, but rarely seen in specimens ablated under saline. Histology on older specimens (greater than 24 hours post-mortem) showed some autolysis in the media but no other differences from the fresher specimens. When specimens were irradiated with 20 to 50 pulses, ablation virtually stopped at the media or fibrous/sclerotic material underlying the more fatty or grumous part of the plaque. Irradiation of normal aorta, in air with 10 pulses at 18 J/cm^2/pulse, produced ablation up to a maximum depth of 200 microns with the formation of irregular crater edges and a similar zone of thermal damage. Normal tissue irradiated under saline often could not be distinguished from adjacent unirradiated normal aorta.

IV.2.3 Ablation Efficiency. Measurements of the mass of tissue ablated per laser pulse were undertaken to learn more about the nature of the ablative process (see Figure III.6). Measurements of the mass ablated by ten pulses of 465 nm radiation at 18 J/cm^2/pulse showed that for the four aortas studied, every atheroma was ablated more than every specimen of normal tissue. Figure IV.12A shows how mass varies with time during ablation for atheromatous and normal aorta. Ablation efficiencies (see Table

IV.7) ranged from 161 to 370 μg/J for atheromas and from 50 to 74 μg/J for normal aorta. These averaged ablation efficiencies are comparable to the efficiency of water vaporization (≈400 μg/J). However, some of the specimens had efficiencies as high as 900 μg/J which indicates that simple water vaporization may not be able to account for this ablation process. In many atheromatous specimens, when the atheroma was completely removed down to the underlying normal tissue, the ablation efficiency diminished considerably (Figure IV.12C) due to the lower ablation efficiency of normal artery at this fluence.

To evaluate the ablation efficiency under conditions closer to those one might expect in vivo, a highly reproducible technique for evaluating ablation efficiencies under saline was developed (see section III.2.5). By ablating with a large number of pulses in between each mass measurement, it was possible to keep the variability in the mass measurement (from variable water content) to substantially less than 10% of the mass change. It was also possible to ablate with an optical fiber of a small enough diameter to be sufficiently flexible for clinical use and to use lasers at 3 different pulse durations.

The data on ablation efficiency under saline at the maximally selective fluence are summarized in Table IV.8 and illustrated in Figure IV.13 for three different pulse durations. It is difficult to compare these measurements directly with those made in air, because of the different fluences, wavelength and spot size. Nevertheless, the ablation efficiencies under saline are even

higher than those in air and significantly higher than water vaporization. Thus, water vaporization alone cannot account for the tissue ablation observed here.

The ablation efficiency for normal artery and fibrofatty plaque are relatively unaffected by pulse duration for these pulses which are all short compared to the thermal relaxation time ($\tau_R \approx$ 40 msec). But for calcified plaque, the ablation efficiency drops off considerably at 50 μsec and it cannot be ablated by continuous wave lasers (at much longer pulse durations). This suggests that the optimal pulse duration for selective ablation of plaque is less than 50 μsec.

IV.2.4 high speed photography. Figure IV.14 shows high-speed flash photographs of the ablation process at 10, 150, 500 and 2500 μsec after exposure to a single pulse of laser radiation. At 10 μsec, a mist of fine particles emanates from the ablation site at a velocity of at least 300 meters/second. At 150 microseconds, some larger droplets and a large plume are visible. At 550 microseconds, the plume is gone but there is a jet-like stream of apparently fluid or semisolid material emanating from the ablation site. At 2.5 msec, debris is still apparent in front of the specimen. This pattern of explosive ablation on a time scale much longer than the 1 μsec duration of the laser pulse was consistently photographed on all specimens of atheroma studied.

High speed photography of calcified plaque ablation, shown in Figure IV.15A, revealed a luminescent plume that obscured details

of the ablation process. This plume was always present when calcified plaque was ablated at any of the wavelengths tested. Spectroscopic characterization of this plume is shown Figure IV.15B (In this Figure the irradiation was at 690 nm to avoid interference with the interesting part of the spectra around 450 nm). The spectra revealed emission lines for ionized and neutral calcium superimposed upon a continuum centered around 400 nm. This indicates the presence of a plasma.

IV.2.5 ablation debris. Ablation debris are shown in Figure IV.16. They consist of whole and fragmented cholesterol crystals, small pieces of calcific material and fibers that appear shredded and occasionally hypereosinophilic. No smooth muscle or elastin was apparent. The particles collected on the filter paper were mostly under 100 microns in maximum diameter, although there were a few as large as 300 microns.

IV.3 Chromophore Studies

IV.3.1 Chromophore Identification. During extraction with xylenes, the atheroma turned from yellow to white and the xylenes turned from clear to yellow; the xylenes used to extract normal aorta remained clear. This result indicated the presence of yellow pigments in plaque that were not present in normal aorta. The similiarity of the absorbance of the atheroma extract before thin layer chromatography and that of beta-carotene can be seen in

Figure IV.17. The absorption at 400 nm and the large peak below 350 nm are probably due to other components. Thin layer chromatography of the atheroma extract yielded 6 bands with rF (retardation factor) values of 0.25, 0.13, 0.12, 0.11, 0.01-0.10 and 0.0, respectively. Bands 1 and 2 had absorption peaks at 420, 440, and 470 nm (consistent with 2 isomers of beta-carotene), band 4 had absorption peaks at 442, 470 and 500 nm (consistent with lycopene) and band 5 had absorption peaks at 440, 465 and 495 nm. The pigment in band 6 had 4 peaks at 400, 422, 445 and 470 nm suggesting that it might be a mixture of carotenoids. Band 3 had no significant absorption between 400-550 nm. The yellow color of these pigments, their characteristic 3-peak absorption spectra and the characteristics of separation by thin layer chromatography definitively identify these pigments as carotenoids

IV.3.2 Chromophore Enhancement. All ten patients treated with beta carotene tolerated it well and did not report any adverse affects. Compliance was good with one patient averaging only 3.7 pills per day and the rest averaging 5-6 pills per day (see Table IV.9 for a tabulation of the data). All patients on beta carotene had a serum beta carotene level that was more than 15 times the mean serum beta carotene level of the controls. The control group (consisting of 16 patients who did not take beta carotene pooled with 3 patients who were studied both before and after beta carotene treatment) was well matched to the study group (consisting of 7 patients studied only after taking beta carotene pooled with the 3 patients who were studied before and after beta carotene

treatment) with similar age, sex distribution, smoking history, incidence of diabetes and hypertension, serum creatinine, serum cholesterol and serum triglycerides (Table IV.10).

At the time of surgery, the normal arterial tissue did not appear different in color in patients taking beta carotene. Some of the endarterectomy specimens from patients on beta carotene, however, did have a deeper yellow tone. Conventional light microscopy revealed faint, yellow, 0.1 to 10 micron diameter drops and streaks which were present diffusely throughout both of the control specimens that were examined microscopically. All 4 post beta carotene treatment specimens that were examined microscopically had deeper yellow and yellow-orange coloring to fat drops in the atheroma. Many specimens from patients on beta carotene had orange crystalline objects suggesting that the beta carotene had come out of solution in the fat during freezing. Three of the post beta carotene treatment specimens had a few layers of normal appearing smooth muscle interspersed with elastic tissue and collagen at the outermost edge. This normal tissue did not contain any noticeble yellow pigment.

Microspectrophotometry (Figure IV.18) of the normal smooth muscle on the 3 specimens where it could be identified, always revealed spectra consistent with myoglobin with peaks at 410 nm and 530-600 nm. Spectra of plaque were more variable. In both control patients studied microscopically, the plaque spectra consisted of a broad peak at 410 nm with a shoulder at 430 to 530 nm consistent with absorption by endogenous carotenoids. The magnitude of this

shoulder varied from one location to another but was always greatest in fat droplets and least in regions of plaque in between fat droplets. Spectra from the yellow fat drops in post beta carotene treatment specimens were dominated by beta carotene absorption with a peak at 450 nm.

Determination of beta carotene levels by HPLC was performed on all specimens of plaque and serum. A representative HPLC chromatogram is shown in Figure IV.19. For all specimens, the HPLC separated the carotenoids into multiple components each having the characteristic three peaked absorption spectra of carotenoids. These major carotenoid components varied in peak area from one individual to the next but always eluted at the same times. These differences in peak areas presumably reflect variations in diet among the subjects. Beta carotene eluted at 12-13 minutes as a single distinct peak. The average of the beta carotene levels in plaque and serum, calculated from the areas of the beta carotene peaks, are shown in Table IV.9. For plaque, the average beta carotene levels in control and post beta carotene treatment specimens were .066 $\pm$ .07 μg/g of plaque and 3.3 $\pm$ .07 μg/g of plaque respectively. This 50-fold increase in beta carotene content was highly significant with a p value of less than 0.001. If just the group of 3 patients studied before and after beta carotene treatment is considered, there was an average increase in the plaque beta carotene content by a factor of 31 ($p = 0.011$). Extraction yield was 35%.

CHAPTER V. ANALYSIS

The main objective of this research is to identify the characteristics of a pulse of radiation that will ablate atherosclerotic plaque but not normal artery. In chapter II, a simple first order theory suggested that selective ablation of plaque would be possible if a waveband of preferential absorption to the plaque could be identified. Chapters III & IV describe studies that

1) identify the waveband of preferential absorption,
2) demonstrate that selective ablation is indeed possible with short pulses in the waveband of preferential absorption
3) identify the chromophore responsible for preferential absorption and demonstrate that oral administration of carotenoids can enhance this preferential absorption.

This demonstration of selective ablation due to differential absorption is consistent with the simple theory of Chapter II which assumed ablation was simply evaporation of the water contained in the tissue. A careful review of the data gathered in this study, however, suggests that the model of chapter II is far too simplistic and that a number of additional (perhaps second order) effects are present. These effects will be described in the following analysis of the data in order to lay the foundation for a proposed model of ablation.

V.1 Absorption

This study employed two different measurement techniques to demonstrate a significant two-fold preferential absorption in plaque relative to normal artery in the 430 to 520 nm waveband (see Figure IV.2). This absorption accounts for the yellow color of plaque compared to the reddish-pink color of normal artery. The ability of nonpolar solvents to extract the yellow color from plaque but not from normal artery indicates that the preferential absorption is due to lipohpylic yellow pigments found only in the plaque. The nature of these pigments will be discussed in greater detail in V.4.

Aside from the preferential absorption from 420 to 530 nm, atherosclerotic and normal artery had similar absorption spectra with several absorption peaks corresponding to known tissue chromophores including DNA and aromatic amino acids (250-290 nm), and hemoglobin (Soret band 390-420 nm, alpha band 530-550 nm and beta band 550-570 nm). There was also light scattering occurring which was small compared the magnitude of the larger absorbance peaks but significant in spectral regions where absorption was low (500-1300 nm).

It is the scattering which has made characterization of the optical properties of vascular tissue difficult in the past. Light scattering complicates the measurement of tissue absorption by requiring a spectrophotometer that can collect the scattered light and an optical model that takes scattering into account. One

popular model is the Kubelka-Munk (KM) formulation (described in detail in Chapter III.1.4) which ignores reflection and refraction of light at sample boundaries and assumes that inhomogeneities within the sample are small compared with thickness, that illumination is diffuse and the scattering is isotropic. Although these assumptions are not entirely met by tissue, the KM model has been useful for studying skin (Anderson, 1981), arteries (van Gemert, 1985), plants (Kazarinova, 1985) and other biological materials.

An attempt was made to meet some of the assumptions of the KM model in this study. To minimize surface effects, the measurement device was index matched to the tissue. To minimize the effect of inhomogeneities, relatively thick specimens were used. Diffuse illumination, however, was impractical since it would have reduced precision to an unacceptable level. The error from using collimated illumination is at most a factor of two and should be of the same order for both atheroma and normal tissue (Kortum, 1969). Although scattering may not have been isotropic, this possibility primarily affects the interpretation of the scattering coefficient. Any errors from inadequate modeling of scattering are likely to be small in the region of preferential absorption because absorption is greater than scattering for both atheroma and normal aorta in that waveband. There is also close agreement between the KM absorption coefficient A_{km} at 470 nm (equations III.1 - III.5) and the Beer's law absorption coefficient α_b at 470 nm (equation III.6) which ignores scattering (see Table IV.1) and these results are

similar to those of Kaminow (1984), Anderson (1981), Wan (1981), and van Gemert (1985). A more detailed description of how these KM coefficients relate to actual radiation transport is provided by Star et al (1988).

Although only fibrofatty lesions were studied, preferential absorption would be expected in any yellow plaque. Some arterial obstructions, however, are not yellow and therefore cannot be expected to preferentially absorb blue laser radiation. It is not known if these lesions will accumulate exogenous yellow pigment. Thrombotic lesions might preferentially absorb visible laser radiation in this waveband because of their high hemoglobin concentration compared to the myoglobin concentration in smooth muscle and the overlap of heme and carotenoid spectra.

Optical properties of calcified lesions could not be studied because their rigid curved shape would not readily flex to accommodate the measurement apparatus. However, as discussed in Chapter VI, linear absorption may not be as important in analyzing ablation of calcified plaque because it is ablated by a non-thermal, plasma-mediated mechanism in which absorption is nonlinear.

V.2 Ablation Threshold

If ablation was by simple evaporation, the two-fold difference in absorption should have resulted in a two-fold difference in ablation thresholds as predicted by,

$$\text{Threshold fluence, } F_{th} = \frac{\rho C(T_v - T_o)}{\alpha} \qquad \text{II.6.}$$

Table IV.4 shows that for soft plaque, in the waveband of preferential absorption, there is approximately a two-fold difference in ablation threshold and that at wavelengths outside the waveband of preferential absorption there is no difference in ablation thresholds. Although this may seem to validate the theory used to derive equation II.5, the fact that the ratio of ablation thresholds is 2.6 (slightly greater than two-fold) suggests that there may be other factors such as inhomogeneities or differential mechanical properties which confer additional selectivity beyond that expected on the basis of optical absorption.

Table IV.4 also shows that calcified plaque can be selectively ablated both in the waveband of preferential absorption and at a longer visible wavelength outside the waveband of preferential absorption. We shall see in chapter VI that this may be because the mechanism for ablating calcified plaque is fundamentally different from the mechanism of ablating soft tissue and thus equation II.6 could not be expected to apply to calcified plaque.

V.2.1 Surface temperature. Assuming that the ablation threshold represents the point at which the tissue surface is just beginning to be ablated, it is possible to determine the temperatures at

which ablation occurs from equation II.4. The surface temperatures achieved by plaque, normal artery and thrombus at their respective fluences are shown in Table V.1. For all three types of tissues, the surface temperatures at the ablation threshold are just greater than 120-140^{o}C which is consistent with both a thermal ablative mechanism and that water evaporation accompanies the ablative process.

V.2.2 Fiber diameter effect. For small (< 1mm) fiber diameters, the threshold fluence, calculated based on a spotsize equal to the fiber core diameter, was increased as shown in Figure IV.8. A number of phenomena may account for this discrepancy. First, the effective spot size in the tissue is larger than the fiber core diameter. This is because light emanating from the fiber is divergent by an amount that depends upon the index of the fiber and tissue as well as the extent of mode mixing in the fiber. Tissue scattering also expands the beam. These effects cause a larger percentage increase in the spot size of radiation from a small fiber than from a large fiber. Secondly, ablation thresholds vary significantly from one area to another so a small diameter fiber irradiating a small sample of the tissue will have a lower probability of irradiating an area of low threshold as compared to a larger diameter. This may cause a statistical bias toward recording higher thresholds when irradiating tissue with small diameter fibers. In order to correct the 320 micron core diameter fiber threshold data to agree with the 1 mm diameter fiber data it was necessary to assume an effective spot size of approximately 600

microns. Another way to view this effect is that fibers smaller than ≈ 300-400 μm in diameter are the equivalent of a point source because for these small diameter fibers, tissue scattering, beam divergence and the other effects are the primary determinate of the effective spot size, not the fiber diameter.

V.2.3 Pulse duration effect. The effect of laser pulse duration on selective ablation was difficult to study because in the μsec domain it required development of a new laser for each pulse duration of interest. With the current laser technology it was also impossible to generate 480 nm radiation at ablative intensities at pulse durations in the region from 50 μsec to 100 msec. Ablation of plaque by Argon ion laser radiation (primarily at 488 and 514 nm) at pulse durations of 100 msec and longer has already been extensively studied by Cothren (1987) and others and no selectivity at those pulse durations has been reported. (This is not surprising since 100 msec is longer than the time required for thermal diffusion in tissue (see Table V.2) and thus, these long pulses would allow thermal diffusion to negate the selective effect of preferential absorption.) At pulse durations shorter than 1 μsec one may get nonlinear absorption and have difficulties transmitting sufficient energy down an optical fiber to ablate tissue. Consequently, in this thesis, ablation thresholds for 480 nm radiation were measured only at 1, 8 and 50 μsec.

Since 1, 8 and 50 μsec are all more than an order of magnitude shorter than the thermal relaxation time for plaque (calculated

based upon a characteristic dimension equal to the depth of penetration of light, $1/\alpha$), the model for ablation by pulsed radiation predicts that the threshold should be related only to the total energy delivered and not vary with pulse duration. The data (Figure IV.8), however, shows about a two-fold increase in the ablation threshold fluence associated with the 50-fold increase in pulse duration. The fact that this threshold does vary with pulse duration suggests that there are phenomena occurring which affect the ablation threshold, in addition to thermal diffusion over the scale of $1/\alpha$.

One possible explanation for the variation in threshold with pulse duration on the μsec time scale is that the appropriate thermal diffusion distances are on the scale of tissue inhomogeneities ($\approx$ 1 μm) rather than the depth of penetration of light into the tissue. Another possibility is that the laser beam may be attenuated by surface deformities and/or debris that is created by the initial part of the laser pulse. If these processes require at least several μsec to begin occurring as is suggested by the high speed photography, then a 1 μsec pulse would be totally absorbed but 8 and 50 μsec pulses would be increasingly interfered with by surface changes and debris. Another effect may be related to a mechanical/shearing ablative process. The pressure waves and shear forces associated with delivering energy over 1 μsec might be considerably greater than if the energy was delivered over longer pulse durations. One might then expect to generate an ablative response with less total energy at the shorter pulse durations.

All of these effects are discussed in greater detail in Chapter VI.

V.3 Selective Ablation

The idea behind selective ablation is to operate above the ablation threshold for plaque but just at or below the ablation threshold for normal artery. The primary parameters to be optimized to make this possible are wavelength, fluence and pulse duration.

V.3.1 Wavelength. For non-calcified plaque, the importance of preferential absorption for selective ablation is apparent from the absence of selective ablation at wavelengths outside the waveband of preferential absorption as shown in Figure IV.7. For calcified plaque, however, the low ablation threshold at both 482 and 658 nm, indicates that selective ablation of calcified plaque is not due to preferential absorption but is probably a plasma mediated process. As a result, ablation of calcified tissue does not follow the thermal model of chapter II and is governed by a different mechanism (discussed in chapter VI).

V.3.2 Fluence. The optimal fluence is one that is above threshold for ablating plaque but just at or below the threshold for ablating normal artery. This would maximize the rate of plaque ablation while minimizing the chance of ablating normal artery.

V.3.3 Pulse duration. Determining the optimal pulse duration for

selective ablation was difficult for several reasons. As discussed in V.2, a thorough study of pulse duration in the submillisecond domain would require development of new lasers. However, a cursory study of the effect of pulse duration has been made in this thesis by comparing the ablation efficiencies for removal of calcified plaque, fibrofatty plaque and normal artery at three different pulse durations, 1, 8 and 50 μsec with three different lasers. In making this comparison, each laser was operated at the threshold fluence for ablating normal artery for that laser.

The ablation efficiency for fibrous plaque and normal artery changed only marginally over this range of pulse durations which was expected since these pulse durations are all significantly shorter than the thermal relaxation time, τ_R, for these tissues. The significant drop in ablation efficiency for calcified plaque at 50 μsec is consistent with its intensity dependent plasma-mediated ablative mechanism (which will be discussed in Chapter VI). Thus, the optimal pulse duration for maximizing selective ablation of both soft and calcified plaque is less than 50 μsec.

Pulse duration may also affect other important factors such as the size of debris, vasoreactivity, shockwave damage, fiber damage etc. that would be important for clinical implementation. These factors deserve further investigation.

V.3.4 Summary. These data indicate that the optimal parameters for selective ablation are as follows:

wavelength: 450 - 500 nm

pulse duration: < 50 μsec

fluence: between the plaque and normal artery ablation thresholds

In theory, a difference in ablation thresholds should provide infinite selectivity in ablation. In practice, however, the tissue variability allows some ablation of normal artery at fluences that are required to ablate all plaque. Thus, enhancing the magnitude of preferential absorption in plaque is worth investigating.

V.4 Carotenoid Chromophores

To explore how to enhance the magnitude of preferential absorption in plaque, several studies were undertaken to understand the nature of the existing two-fold preferential absorption of plaque. In the first study, nonpolar solvents were used to extract yellow pigment from the plaque. The same solvents failed to extract detectable amounts of yellow pigment from normal artery. This yellow pigment had absorption peaks from 400 to 550 nm (see Figure IV.17) and was identified by two chromatographic techniques to consist of a mixture of carotenoids as shown in Figure IV.19.

The identification of the yellow atheroma chromophores as carotenoids in this thesis is in agreement with the work of Blankenhorn (1957,1960), who demonstrated carotenoids within atheromas more than 20 years ago and showed that the amount of

carotenoid in atheromas increases with the severity of the lesion.

Carotenoids are ubiquitous in nature giving the red and yellow coloring of many vegetables (tomatoes, carrots, squash) animal products (egg yolk, butter, chicken fat) and exotic animals (parrots, canaries) (Baurenfeind, 1981). Their structures, shown in Figure V.1, are characterized by a long sequence of conjugated carbon-carbon bonds. This creates a single electron cloud running the length of the molecule which binds the carbon atoms together with shared pi orbitals. This large electron cloud is responsible for the the absorption of 400 to 550 nm radiation. Although absorption is by electronic excitation (exciting electrons to more energetic orbitals), this long electron cloud allows the energy to be rapidly redistributed throughout the molecule and thermalized by exciting vibrational and rotational modes in the carotenoid molecule. Thus, carotenoids do not readily exhibit phenomena associated with electronic excitation that compete with thermalization, i.e. fluorescence, phosphorescence, photochemistry, photodecomposition, etc. Also for this reason, carotenoids are excellent quenchers, very photo-stabile and unlikely to have saturable absorption within the range of intensities used in this study.

In nature, carotenoids are synthesized by plants to protect cells from the highly reactive species generated during photosynthesis (Krinsky, 1971). Epidemological data indicates that cultures with diets rich in carotenoids (i.e. high in vegetables) have a low incidence of some cancers. It is thus speculated that

carotenoids may also protect humans from the mutagenic effects of reactive species.

Blankenhorn found, in one patient, that the carotenoid content in xanthomas can be increased about 30% by administration of low dose beta-carotene orally (17 mg/day for 5 weeks). Patients with erythropoietic protoporphyria treated with oral doses of beta-carotene (30-300 mg/day) often develop yellow coloration on the palms and soles from cutaneous accumulation of carotenoids within a few weeks. It was thus, postulated that oral beta carotene might also increase the carotenoid content of atheromas.

To evaluate the possibility of enhancing the carotenoid content of plaque, ten carotid endarterectomy patients were treated with oral beta carotene (180 mg/day in three divided doses for 8 to 41 days). HPLC analysis of the specimens demonstrated a 50-fold increase in the plaque beta carotene content as shown in Table IV.9 and Figure IV.19. Microscopic examination of the plaque revealed that the additional beta carotene was confined to the plaque and not present in the underlying more normal media. This level of increased carotenoid in the plaque should significantly enhance the selective ablative effect of 450 - 500 nm laser radiation.

Since beta carotene is not the only carotenoid present in plaque and carotenoids are not the only absorbers of 450 to 500 nm radiation in plaque, increasing beta carotene by a factor of fifty does not generate a factor of 50 increase in plaque absorption. If beta carotene is estimated to account for about 6% of plaque

carotenoid absorption at 480 nm, its 50-fold increase translates into about a two-fold increase in plaque absorption to give about 4 to 1 preferential absorption to plaque.

The 50-fold increase in plaque beta carotene, achieved here with low dose oral beta carotene for a limited period of time, underestimates the degree of carotenoid loading that could be achieved if the treatment were optimized. The beta carotene content of lipid-rich stratum corneum in erythropoietic protoporphyria patients being treated with similar or higher doses of beta carotene reaches a peak only after a minimum of six weeks of treatment. The 180 mg/day used here is very safe and could be increased considerably. Intravenous administration may enhance both the speed and magnitude of beta carotene partitioning into plaque particularly if the main limitation is intestinal or serum transport. There may also be other carotenoids (although beta carotene is the only one with US Food and Drug Administration approval) that can accumulate in plaque more quickly, in larger amounts, or with greater extinction coefficients. Furthermore, using other carotenoids (see Table V.2) that absorb at different wavelengths may permit manipulation of the peak absorption wavelength in plaque so as to match a laser emission line.

The beta carotene appears to accumulate in the plaque over the course of days to weeks. Determining the optimal dose and time for maximizing plaque beta carotene content will require a much larger patient population. The 57-fold increase in serum beta carotene compared to the somewhat smaller 50-fold increase in plaque beta

carotene suggests that not all patients had time for the plaque beta carotene to equilibrate with the serum. The rapid accumulation of beta carotene compared to the time course of plaque formation, however, suggests that atheromas do evolve. The mechanism of beta carotene accumulation in plaque may be simple partitioning into lipids. This process is probably governed by the rate of transport of carotenoids in blood within micelles and diffusion constants once the lipids contact the plaque.

Increasing the absorption coefficient of plaque also decreases the penetration depth of laser radiation into the plaque. This enables the laser pulse to remove plaque in smaller increments and may result in a smoother surface for the remaining unablated tissue. Since the laser energy is distributed over a smaller volume, less intensity would be required, reducing the potential for damage to normal artery and delivery system optics. It may also reduce the maximum size of debris.

CHAPTER VI. ABLATION MECHANISMS

Analysis of the ablation process observed in this research is difficult because ablation involves a complex interplay between optical, thermal and mechanical effects, which is not well understood. Some investigators have speculated about possible mechanisms for tissue ablation by other types of lasers and this has been the subject of many recent reviews (Regan and Parrish 1982, Ready 1971, Welch 1984, Boulois 1987, Wolbarsht 1984, Hillenkamp 1980, Weber and Zweig 1987, Furzikov 1987, Partovi et al. 1987 and Walsh 1988), but today there is no single compelling explanation for this process. This chapter will explore how the hypothesized mechanisms fit with the data of Chapter IV on pulsed dye laser ablation of plaque.

VI.1 Overview of Tissue Ablation

VI.1.1 Definition of Tissue Ablation Although tissue is mostly water (about 70%), it is mechanically much different from water because the water is confined within a matrix of organic molecules. This matrix includes elements that are strong in tension such as collagen, elements that are highly elastic, such as elastin, and may include elements that are strong primarily in compression, such as calcium salts. This complex composite structure resists mechanical forces like a viscoelastic solid despite being mostly

water. If laser radiation removes only the water, the tissue is dessicated but not ablated. Tissue removal occurs only when the solid elements are removed. In surgery, a scalpel is used to cut the tensile elements so that unwanted tissue can be removed in large chunks. The goal of laser surgery is to convert unwanted tissue into harmless vapors or small fragments that can be convected away. Preferably, debris should be of cellular dimensions (10 μm) or smaller to minimize the chance of occluding distal vessels.

VI.1.2 Types of Ablative Mechanisms. Processes by which laser energy can convert the tissue matrix into small particles involve photochemical, thermal and mechanical mechanisms. The photochemical processes include photodecomposition and ionization. Thermal refers to vaporization and pyrolysis. Mechanical mechanisms involve breaking the solid, structural elements of the tissue by rapid/explosive expansion of the subsurface tissue fluid. For a given tissue, wavelength and spot size, the ablation mechanisms occur in different domains on an intensity versus pulse duration plot as shown in Figure VI.1. There are also characteristic length, time and wavelength scales to these ablative processes which determine when each mechanism is important (see Tables VI.1, VI.2 and VI.3). Figure VI.1 and Tables VI.1-VI.3 will be useful to refer to as these mechanisms are described in detail below.

VI.2 Photochemical Ablation Mechanisms

VI.2.1 Photodecomposition. Photodecomposition refers to the direct breaking of molecular bonds by the absorbed photons. This can occur when the energy per photon, $h\nu$, where h is Plank's constant and $\nu = c/(\lambda)$, exceeds the bond energies in organic molecules. These bond energies are typically 3-4 eV or larger which corresponds to the amount of energy carried by ultraviolet and shorter wavelength photons. Srinivasan (1987) has elegantly demonstrated that during excimer laser (an ultraviolet laser) ablation of polymers, high energy photons may be absorbed by the shared electrons in pi orbitals, causing the molecule to split apart, forming smaller molecules. How this process ultimately results in ablation of polymers is unknown. The molecular products created may be gaseous; cleaving bonds may change the mechanical properties of the material making ablation by a thermal mechanism occur more efficiently; cleaving bonds may allow increased conjugation of the molecular products (i.e. the process could be exothermic) giving the products enough energy to vaporize; or other phenomena may occur which influence ablation.

Srinivasan and others have also shown that excimer laser ablation of tissue has some features to suggest that photodecomposition of tissue can also occur. These features include:

1) ablation products consisting of small molecular fragments (different from those associated with pyrolysis) indicating

molecular bonds may have been broken photochemically,

2) highly efficient ablation greater than the efficiency one would expect if the tissue-water were vaporized, and
3) negligible histologic evidence of thermal damage to the residual, unablated tissue (suggesting a non-thermal ablation mechanism).

A theoretical explanation for these findings is that the high energy photons break enough bonds in the structural matrix of the tissue to convert the tissue into a slurry of water and small organic molecular fragments that readily washes away. Since the optical energy is converted into potential energy, in the form of a new chemical structure, there may be negligible heating of the tissue. In this way, thermal damage to the remaining unablated tissue is minimized. Since water vaporization is not necessary for this process to occur, the efficiency for tissue removal can be much higher than if vaporization of the tissue-water was required.

These three features are also characteristic of the atheroma ablation achieved here with the pulsed dye laser at 465 to 490 nm. But the photon energy at 490 nm is only 2.5 eV, not enough to overcome most organic bond energies. Bond dissociation could still occur if a molecule absorbed 2 photons (multiphoton absorption) in a sufficiently short period of time that they acted as a single photon of twice the energy. Since optical absorption takes approximately 10^{-15} seconds, multiphoton absorption can occur only at very high intensities (empirically found to be about 10^8 W/cm^2 or greater in most materials). If this were occurring, the

efficiency should vary with the square of the intensity. But in these experiments at 465 to 490 nm, the intensities were usually less than 10^8 W/cm^2 and the ablation threshold decreased only slightly and linearly with increasing intensity. In addition, the primary absorbers are known to be carotenoid molecules which are noted for their photostability (or resistance to photodecomposition) and rapid conversion of absorbed optical energy to thermal energy. Since carotenoid pigments are not the structural elements of the tissue, even if photodecomposition of carotenoids did occur, it would not necessarily result in tissue ablation. Thus, photodecomposition is unlikely to play a significant role in the selective plaque ablation process seen here.

The advantages of direct photodecomposition of tissue, however, when it occurs, are significant. It might be appropriate to combine ultraviolet radiation with the preferentially absorbed 450 to 500 nm radiation in order to enhance the ablation efficiency, reduce particle size and further reduce thermal damage.

VI.2.2. Plasma Ablation. Plasmas are collections of charged particles with approximately equal numbers of electrons and positive ions and mechanical behavior that is similar to vapor. The ionized particles are highly energetic with temperatures typically of the order of 1000's of degrees centigrade or higher. This high-temperature cloud of ions usually has a blackbody emission peak in the visible or ultraviolet spectrum and thus, is

seen as a bright white or blue light. The plasma can also have an enormous pressure, typically of the order of kilobars.

Initiation of plasmas by laser radiation was discovered shortly after the invention of the laser (Ready, 1971) and found to occur by several mechanisms including:

1) direct ionization of molecules by ionizing single-photon absorption,
2) ionization by multiphoton absorption,
3) avalanche breakdown when the existing free electrons within a material are sufficiently excited by the electric field of incident radiation that their collisions with molecules liberate/ionize more electrons. (This is thought to occur when the electric field strength of the laser radiation is comparable to or greater than the strength of the coulomb interaction between electrons and their nuclei.)
4) thermionic initiation in which the number of free electrons available for the avalanche process is increased by heating the material.

For all of these mechanisms, the actual initiation occurs when the rate of ion formation greatly exceeds the rate at which the ions recombine into neutral species. Once initiated, the cloud of ions constituting the plasma interacts with light so strongly that all subsequent photons are absorbed by the plasma. This continued accumulation of energy by the strongly absorbing plasma (inverse Bremsstrahlung) promotes a rapid expansion of the plasma. The plasma continues to accumulate energy until either the laser

radiation stops or the density of free electrons becomes so large that the plasma frequency approaches the frequency of the incident radiation. When the plasma frequency approaches the radiation frequency, the interaction of light with the plasma changes from absorption to scattering preventing further accumulation of energy.

Plasmas can cause ablation of materials by several mechanisms. Those molecules constituting the plasma are ablated by definition. Adjacent material may be vaporized or pyrolyzed (discussed in detail below under thermal ablation mechanisms) by the high temperature. The rapid expansion and collapse of a plasma may mechanically disrupt the material (also discussed in detail below).

Since mechanical ablation or shattering of calcified material by plasmas does not require evaporation of the tissue fluid, the plasma ablation process can be much more efficient than a mechanism that does require water vaporization. Plasmas may also interfere with efficient laser ablation of materials by forming at the surface of the material and not allowing the laser radiation to penetrate into the material. This is referred to as plasma shielding.

Laser-induced plasmas are used in ophthalmology to cut membranes inside the eye without having to cut the eye open. This is based on the concept that a convergent laser beam will be harmless where it enters the eye at low intensity but at the focal point where the intensity is high, plasma initiation will occur even if the focal point is at a transparent part of the eye. This

process has been studied extensively by Steinert and Puliafito (1985). The plasma is formed by avalanche breakdown under the intense electric field at the focus of a Q-switched Nd:YAG laser pulse. As the plasma expands it disrupts undesirable membranes or other tissues and shields (by inverse Bremsstrahlung) the retina from excessive exposure to laser radiation.

The use of laser-induced plasmas to ablate ureteral calculi and biliary stones has been extensively analyzed by Teng et al (1987). The proposed mechanism involves first heating and evaporation or desorption of surface material. This material is then ionized (thermionically) to initiate the plasma. In the case of flashlamp-excited dye laser fragmentation of stones (1 μsec pulses of 504 nm radiation), the plasma expands at $\approx$ 30 m/sec to a diameter of $\approx$ 0.5-1 cm with peak electron densities of the order of $10^{18}/cm^3$. When the laser energy stops, the plasma collapses at a rate of $\approx$ 12 m/sec. The expansion and collapse of the plasma is thought to create stress waves in the material with calculated pressures of the order of .2 to 35 kbar. These stress waves are believed to be responsible for mechanical fracture of the stone. The magnitude of the stress waves was measured qualitatively and found to be 10-fold higher under saline than in air (Teng et al, 1987). The ablation process has also been found to be significantly more efficient under saline as well indicating that stress waves are a primary part of the plasma ablation process. More detailed studies of this process are on going (Rosen et al, 1988)

Ablation of soft plaque, in this thesis, by microsecond pulses of visible radiation was not associated with emission of white light and therefore, there was probably no plasma. Ablation of soft tissue by ultraviolet radiation at 290 nm was associated with a faint blue emission that was attributed to fluorescence.

Hard, calcified plaque ablation by visible radiation, however, produced an obvious bright white light at the site of ablation, that was not excluded by goggles that excluded the laser radiation. Spectral characterization of this emission demonstrated a broad continuum peaked at 400 nm with superimposed emission lines due to ionized and neutral calcium. These features indicate the presence of a plasma. The obligatory presence of the plasma for ablation to occur indicates that the plasma is probably involved in the ablation process for calcified plaque.

Ablation of calcified plaque was also associated with a sharp report, particulate debris and a very high ablation efficiency, up to 9.5 mg/J. This is 25 times more efficient than water vaporization. These features suggest that the plasma ablation mechanism is independent of water vaporization. The size of the plume estimated photographically (see Figure IV.15A) was .5 to 1 cm which is comparable to the plume produced by similar laser pulses incident on kidney and gall stones. Consequently, the calcified plaque plasmas are probably similar to the plasmas formed on stones (Teng et al, 1987) which have peak pressures of the order of .2 to 35 Kbar. These pressures explain the acoustic report. Pressure waves could also drive a mechanical process that shatters plaque,

thus accounting for the particulate debris and high ablation efficiency.

The mechanism of plasma initiation on stones is thought to be thermionic because there is an energy threshold (all other plasma initiation mechanisms are intensity dependent). Similarly, plasma initiation on calcified plaque was found to have an energy threshold that varied only weakly with intensity. This threshold increased by only a factor of 2 as the pulse duration was increased by a factor of 50 (see Figure IV.8). Interestingly, however, at the longest pulse duration studied, 50 μsec, (where the intensity is the least) the ablation efficiency was significantly less than for shorter pulse durations (where the intensity is higher) (see Figure IV.13). One possible explanation for this is that the intensity determines the rate and maximum extent of plasma expansion, which in turn may determine the magnitude of stress exerted by the plasma on the calcific material. Greater stress waves may produce more ablation.

Why plasmas are observed for calcified plaque and not for soft plaque and normal artery is not obvious. With a sufficient intensity and fluence, radiation can form plasma from any material; it is not clear why the calcified plaque has a significantly lower plasma initiation threshold than soft tissue. The spectroscopic data of Figure IV.15B show emission lines that are attributable to ionized and neutral calcium suggesting that calcium is the primary species involved in this ionization process. This is not surprising since calcium is a metal with 2 valence electrons that

that are easily ionized to form a stable electron cloud in the form of Ca^{2+}. But calcium is present in all tissues. Thus, it is not clear whether the difference in plasma susceptibility between calcified and soft tissue is due to a calcium concentration effect or the solid form that precipitated calcium salts have in the hard tissues but which is not present in soft tissues.

VI.3 Thermal Ablation Mechanisms

The historically most popular description of how tissue is ablated by laser radiation is that it is vaporized or burned. This mechanism is particularly compelling when one casually observes tissue ablation by the conventional CO_2, Nd:YAG or argon ion lasers (which are continuous wave and typically operate at relatively low intensities for durations of the order of seconds to minutes). When continuous wave laser energy is directed at tissue, for a moment nothing happens, then the spot being irradiated erupts into a plume of smoke and vapor that continues for as long as the laser is turned on. The irradiated surface turns black as it slowly recedes into the tissue (forming an ablation crater) and a foul aroma of burning tissue permeates the room.

This thermal process has two parts, first tissue desiccation by evaporation of the water and second, decomposition of the desiccated solid elements by pyrolysis.

Tissue desiccation by continuous wave laser radiation has been extensively characterized and modeled (with the heat equation) and

is the subject of many recent reviews by Ready (1971), Welch (1984), Boulois (1987), Wolbarsht (1984), Hillenkamp (1980), Weber and Zweig (1987), Furzikov (1987), Partovi et al. (1987). Evaporation is a surface phenomenon and the models generally address this process as occurring in an infinitely thin plane that separates the solid tissue from air. Since the water must be vaporized, the best possible efficiency that may be achieved is 1/(heat of vaporization of water) or $\approx$ 0.4 mg/J. In general, the efficiency will be considerably less than that because of thermal diffusion losses and energy required for pyrolysis.

Pyrolysis, the lysis of organic bonds by heat, has not been studied as extensively in relation to laser ablation of tissue. It is known to require temperatures in excess of 100^{o}C and begins to occur rapidly at temperatures in excess of 400^{o}C. Temperatures of this magnitude have been measured by Welch (1984) during argon ion laser ablation of tissue.

The black residue this process forms, which is primarily carbon, undoubtedly changes the tissue optical properties significantly. Indeed, if the laser radiation is primarily absorbed by water, such as with the Holmium laser at 2.1 μm (Alves 1988), as the water evaporates, tissue absorption decreases and laser radiation ceases to have any effect on the tissue. If the absorber is a solid element (as is the case for visible radiation), then as water is evaporated the tissue absorption is increased and the ablative effect of the laser radiation is enhanced. The black color of char indicates its strong absorption of visible radiation.

Accordingly, tissue ablation by visible radiation may accelerate due to formation of char.

Plaque ablation by 488 and 514 nm radiation from the continuous wave argon ion lasers (pulse duration of > .1 sec) always leaves some char. But the plaque ablation by 465 to 490 nm radiation observed in this thesis (pulse duration $\leq 50\mu$sec) was never associated with char. The radiation here was different in that the intensities were of the order of 10^6 W/cm^2 or greater compared to argon ion laser intensities of 10^4 W/cm^2 and that the pulse duration was of the order of microseconds as compared to seconds for the argon ion laser. The ablation process was also different in that the ablation efficiency was frequently higher than 1/(heat of vaporization of water). Thermal ablation is also inconsistent with the particulate debris and the negligible evidence of thermal damage observed with the pulsed dye laser. Thus, simple water evaporation cannot, by itself, explain the ablation process observed in this thesis.

VI.4 Mechanical Ablation Mechanisms

If tissue is being heated by laser radiation rapidly or inhomogeneously, vaporization may occur not only at the surface but also below the surface. Expanding subsurface vapor bubbles may mechanically tear apart the tissue and carry away tissue fragments. To heat the tissue sufficiently rapidly for this to occur requires high intensity radiation.

VI.4.1 Lane model. One simple approach to modeling this process was proposed by Lane et al (1987). The model assumes instantaneous heating (i.e. infinite intensity) with a delta function. The energy of the delta function is considered to be distributed uniformly throughout the tissue to a depth of $1/\alpha$. This heated volume is then assumed to undergo an adiabatic, isentropic expansion which disrupts the solid tissue elements, ejects the ablation products and rapidly cools the irradiated tissue to minimize thermal damage. Unfortunately, this model only provides a qualitative picture of a possible process without allowing calculation of ablation thresholds or efficiencies. Thus it does not permit detailed analysis of the data in this thesis.

VI.4.2 Dabby, Gagliano and Paek model. Dabby and Paek (1972) and later Gagliano and Paek (1974) address the issue of the intensity at which the ablation mechanism converts from thermal evaporation to explosive subsurface vaporization. The premise of this model is that as the surface temperature exceeds the vaporization temperature for the material, some molecules have enough energy to leave the surface as vapor. This surface evaporation cools the material's surface. As more energy is absorbed deep in the material, deeper regions may reach temperatures slightly in excess of the vaporization temperature. This establishes a temperature gradient which conducts the internally absorbed energy to the surface, promoting further surface vaporization.

Dabby and Paek have modeled this process by assuming that the surface temperature is locked at the vaporization temperature, the material is homogeneous with temperature independent optical and thermal properties, there is no optical absorption by vaporized material, and negligible radial heat conduction, scattering, blackbody radiation or convective losses. They further assume a one-dimensional coordinate system where x is depth in tissue with respect to the original surface and Z is the depth of the crater formed by ablation with a bottom surface receding into the tissue at a rate $\dot{Z}$.

At the surface, the rate at which energy leaves in the form of vaporized material is equal to the rate at which energy is conducted to the surface by thermal diffusion. This energy balance shows that

$$\rho H_V \dot{Z} = K \left.\frac{\partial T}{\partial x}\right|_{(x=Z)} \qquad \text{VI.1}$$

where $\dot{Z}$ = the phase front velocity

H_V = the heat of vaporization of tissue fluid.

Within the tissue, diffusion of thermal energy is described by the one-dimensional heat equation with an exponential source term for the laser radiation as

$$\rho C \frac{\partial T}{\partial t} = \alpha I_o e^{-\alpha(x-Z)} + K \frac{\partial^2 T}{\partial x^2} \qquad \text{VI.2.}$$

Dabby and Paek introduced the non-dimensional parameters:

$$\theta = \frac{(T - T_o)}{(T_v - T_o)} \qquad \text{temperature}$$

$$s = \frac{IC}{KH_v}(x - Z) \qquad \text{depth into tissue}$$

$$u = \frac{\rho H_v}{I}\dot{Z} \qquad \text{velocity of ablation front}$$

$$\lambda = \frac{C(T_v - T_o)}{H_v} \qquad \text{heating parameter}$$

$$B = \frac{K\alpha H_v}{IC} \qquad \text{absorption parameter}$$

$$\tau = \frac{I^2 C}{\rho K H_v^2} t \qquad \text{time}$$

and solved these equations for the case of gradual heating and ablation of metals. The temperature distribution prior to ablation is obtained from equation VI.2 (equation VI.1 is irrelevant since Z=0 prior to ablation) Once ablation starts, however, it is necessary to simultaneously solve both equations VI.1 and VI.2

since Z would be nonzero at that point. To simplify solving these two equations, Dabby and Paek assume that the temperature distribution at the moment ablation begins has the form

$$T = T_v(1 + qx)e^{-qs} + T_o \qquad \text{VI.3}$$

where q is a fitted parameter.

They then select a value for q which best approximates the exact solution of equation VI.2 at the moment the surface reaches the vaporization temperature. With an additional initial condition:

$$Z = 0 \text{ at } t = 0$$

the appropriate boundary conditions:

$$T = T_{vap} \text{ at } x = Z$$

$$T = T_o \text{ at } x = \infty$$

and equations VI.1 and VI.2 in the normalized form:

$$\frac{\partial\theta}{\partial\tau} - u\frac{\partial\theta}{\partial s} - \frac{\partial^2\theta}{\partial s^2} = -\frac{B}{\lambda}e^{-Bs} \qquad \text{VI.4}$$

$$u = \lambda \frac{\partial\theta}{\partial s}\Big|_{s=0} \qquad \text{VI.5}$$

it is possible to calculate temperature distributions during ablation of metals.

As expected, the model demonstrates a subsurface temperature peak exceeding the material vaporization temperature. The magnitude of this peak is inversely related to the normalized absorption parameter, B. Using high speed photography and examining ablation craters, Gagliano and Paek were able to experimentally identify when the ablation was explosive or simple surface evaporation. Explosive ablation correlated well with small values of B (< 1) although the precise transition level depended upon the specific material. This material variation may reflect mechanical properties of the material that are not accounted for in the model but which may influence the magnitude of a subsurface temperature peak required for explosion.

For tissue, the vaporization temperature is small and the heat of vaporization is large compared to metals. Thus, radiation capable of ablating tissue will rapidly heat the tissue surface to the vaporization temperature before there is time for much thermal diffusion. This is especially true for the high intensity radiation pulses used to achieve selective ablation in this thesis. Accordingly, the temperature at the moment the surface reached the vaporization temperature is best approximated by an exponential of the form

$$T = (T_v - T_o)\, e^{-\alpha x} \qquad \text{VI.6}$$

There is no appropriate value of the fitted parameter, q, for this temperature distribution. Thus, to apply the Dabby and Paek model to the flashlamp-excited dye laser ablation described in Chapter III, it is necessary to solve equations VI.4 and VI.5 with the initial condition of equation VI.6.

Solution strategy:

The steady state temperature distribution, θ_{ss} is found in terms of the steady state ablation front velocity, v, by setting $\partial\theta/\partial\tau = 0$ in equation VI.5 to give

$$\theta_{ss} = e^{-vs} + \frac{1}{\lambda(v - B)} [e^{-Bs} - e^{-vs}] \qquad \text{VI.7.}$$

where $v = u_{(t \rightarrow \infty)}$

Equations VI.6 and VI.7 can be combined and solved for

$$v = \frac{1}{(1 + \lambda)} \qquad \text{VI.8.}$$

By substituting the steady state ablation front velocity, v, for u it is possible to solve equation VI.4 for large values of τ to give

$$\theta = \left[1 - \frac{(B/\lambda)}{vB - B^2} \right] \frac{1}{2} \left(e^{-vs} \operatorname{erfc}\left[\frac{s - v\tau}{2\sqrt{\tau}} \right] + \operatorname{erfc}\left[\frac{s + v\tau}{2\sqrt{\tau}} \right] \right)$$

$$- \left[1 - \frac{(B/\ )}{vB - B^2} \right] \frac{e^{B(B-v)\tau}}{2} \left(e^{s(B-v)} \operatorname{erfc}\left[\frac{s + |v-2B|\tau}{2\sqrt{\tau}} \right] \right.$$

$$\left. + e^{-sB} \operatorname{erfc}\left[\frac{s - |v-2B|\tau}{2\sqrt{\tau}} \right] \right)$$

$$+ e^{-Bs} \left[1 - \frac{B}{\lambda(vB-B^2)} \right] e^{B(B-v)\tau}$$

$$+ e^{-Bs} \frac{B}{\lambda(vB-B^2)} \qquad \text{VI.9.}$$

Knowing θ, one can calculate a better approximation for u from equations VI.5 and VI.9 for the time of interest. With this new u the temperature distribution can be recalculated to obtain greater accuracy. By iterating many times any degree of solution accuracy can be obtained.

The calculated temperature distribution in tissue using this model is plotted in Figure VI.2 for radiation which is characteristic of the argon ion class of lasers. These lasers ablate tissue by a thermal process (Welch, 1984).

The thermally long pulse durations typical of argon irradiation of tissue allow significant thermal diffusion during the period of the laser pulse and thus, the subsurface temperature peak is insufficient to cause explosive ablation. For radiation typical of pulsed dye laser ablation of plaque the calculated temperature distribution shows an enormous subsurface temperature peak as seen in Figure VI.3. These high subsurface temperatures suggest the possibility of an explosive, mechanical ablation process due to subsurface vaporization of a fraction of the tissue fluid.

The intensity at which the ablative mechanism shifts from being evaporative to explosive can be calculated from the definition of B assuming (as Gagliano and Paek empirically demonstrated) that explosive ablation occurs when $B \ll 1$. Explosive ablation occurs when

$$I >> \frac{K\alpha H_v}{C} \qquad \text{VI.10}$$

For 482 nm radiation this intensity would be ≈ 200 W/cm^2.

VI.4.3 Inhomogeneous absorption. Microscopic examination of plaque shows yellow fat droplets (which are absorbing foci) distributed throughout a weakly absorbing tissue matrix. This suggests that blue laser radiation is absorbed

inhomogeneously. The result would be heating of fat droplets, which in turn, would heat surrounding water to its vaporization temperature. If the intensity is low, there will be time for thermal diffusion to evenly redistribute the energy before abla ion occurs. In that case no explosive or mechanical effects based upon inhomogeneous absorption would occur. But if the intensity is sufficiently high, enough energy to cause ablation would accumulate at the absorbing centers before it could diffuse away and mechanical/explosive ablation could occur.

To determine the intensity necessary to achieve a mechanical effect from inhomogeneous absorption, consider a medium with absorbers of diameter, d and absorption coefficient, α, separated by a distance, D, within an otherwise transparent medium. Thermal, thermodynamic and mechanical properties of the absorbing and transparent media will be assumed to be identical or irrelevant. If $D \ll d$, then there is not really inhomogeneous absorption but rather a uniform absorber with a few bits of transparent material here and there. If $D \gg d$, then the absorbing centers can be treated (for an order of magnitude calculation) to act as isolated drops in an infinite medium with a thermal relaxation time,

$$\tau_R = d^2/4\kappa \qquad \text{VI.11.}$$

For absorbers near the surface, energy will be absorbed as a function of time by an amount,

$$\Delta H = I_o \alpha t/\rho \qquad \text{VI.12}$$

where I_o is the incident laser intensity. For explosive ablation to occur, the time required to deposit energy in the droplets must be less than the thermal relaxation time, or,

$$\Delta H \rho / I_o \alpha < d^2/4\kappa \qquad \text{VI.13.}$$

Solving equation VI.13 for intensity yields,

$$I_o > 4\kappa\rho\Delta H/\alpha d^2 \qquad \text{VI.14.}$$

For the case of pulsed dye laser ablation of plaque with 465-490 nm radiation the absorbers are known to be carotenoid molecules concentrated in the lipid parts of the tissue. The histologic sections show yellow fat drops ranging from .1 to 10 μm in diameter and separated by about distance slightly larger than the droplet diameters. Although this appearance (on oil red o stains of frozen sections) may have some preparation artifact and reflect an irreversible phase transition from the cooling below body temperature, one might let d = 1 micron for purposes of order of magnitude calculation. If the volume fraction of

fat is estimated to be 20% then the fat absorption coefficient is about 100 to 300 cm^{-1} depending upon the extent of carotenoid loading. Fat does not vaporize, but surrounding water will vaporize with a heat of vaporization = 2000 to 3000 J/gm. Using these number and a density of 1 gm/cm^3 and thermal diffusivity, κ = 0.0013, the threshold intensity required for explosive ablation can be calculated from equation VI.14 as 6 MW/cm^2. This is in the range of intensities used in this thesis.

This intensity (6 MW/cm^2) is substantially lower than the observed thresholds for 1μsec pulses, comparable to the observed thresholds for 8 μsec pulses and higher than the observed thresholds for 50 μsec pulses. The effect of inhomogeneous absorption would be to increase the ablation efficiency and lower the ablation threshold fluence. Indeed, from Figures IV.8 and IV.13 it is apparent that at the shorter pulse durations, the ablation efficiency increases and the ablation threshold decreases. This suggests that inhomogeneous absorption probably is important for the plaque ablation observed in this thesis.

VI.5 Pulse Repetition Rate Effects

Thus far, this analysis of ablation mechanisms has considered only the effect of a single, isolated laser pulse which can remove only a small amount of tissue corresponding

approximately to the penetration depth of that light into the tissue, $1/\alpha$. But in the clinical setting, one would like to deliver a sequence of pulses as rapidly as possible in order to remove a large amount of plaque with the least "surgical" or "anesthesia" time. If the pulses of radiation are delivered sufficiently rapidly there may be cumulative heating of the tissue and perhaps a different ablative mechanism more like that of continuous wave lasers. The magnitude of cumulative heating can be estimated from the average intensity which is equal to the intensity during irradiation, I_o, times the duration of each laser pulse, τ_p, times the pulse repetition rate, f. For ablative pulses, some of the energy will be carried away with the debris and some will be left behind, heating the residual tissue. If the residual heated tissue is ablated with the next pulse, then there will be no cumulative heating. However, if one is operating just at threshold, then the residual tissue will receive the maximum irradiance and still be present for irradiation by successive pulses. Thus, the maximum cumulative heating will occur when operating near the ablation threshold where $I_o\tau_p$ = the threshold fluence, F_{th}, and the

$$\text{Maximum Average Intensity} = I_a = F_{th}f.$$

The steady state temperature rise in the tissue associated with a given I_a has been shown by Furzikov (1987) to depend

upon the relative magnitudes of the light penetration depth, $1/\alpha$, and laser beam diameter, d. For the data in this thesis, the penetration depth is short, about 200 μm, and the beam diameter is large, 2-3 mm, which creates a flat disk of irradiated tissue. The steady state temperature in the disk can be calculated by an energy balance analysis for the flat disk where:

$$\text{incoming energy} = F_{th} f \pi d^2/4 \qquad \text{VI.15,}$$

$$\text{thermal diffusion} = k \times \text{Area} \times \frac{\Delta T}{\Delta x} \qquad \text{VI.16}$$

where K = thermal conductivity = .005 J/cmsec^{o}C

Area = $4\pi d^2/4$

Δx = laser beam radius = d/2, and

$$\text{radiative loss} = \text{Area}\,\epsilon\sigma(T_{tissue}^{4} - T_{background4}) \qquad \text{VI.17}$$

where Area = $4\pi d^2/4$

ϵ = emissivity = 1

σ = Stephan Boltzman constant = 6×10^{-8} W/m^{2o}K^{4}.

For a steady state temperature rise as high as 400^{o}K, the radiative heat loss is only .1 W/cm^2 and can be neglected. Convective loss will be considered below. Equating the rate

of incoming energy with the rate of thermal diffusion loss and solving for ΔT gives

$$\Delta T = F_{th} f \frac{d}{8K} \qquad \text{VI.18}$$

For the mass-balance experiments of section IV.2.3, a laser beam diameter of 2 mm and a repetition rate of 1 Hz, plaque ablation would produce a maximum steady state temperature rise of 34°C. This is bordering on being significant, although it is still less than the temperature rise needed to achieve continuous water vaporization. The measured ablation rate under these conditions did not accelerate with time. Indeed, the only consistently observed change in ablation rate was a decrease in ablation rate which occurred as the ablation front reached the level of normal tissue. Nevertheless, it is unlikely that one could increase the pulse repetition rate, f, much beyond 1 Hz under these conditions without encountering some deleterious effect of cumulative heating.

One way to minimize cumulative heating would be to introduce convection by vigorous perfusion of the irradiated tissue with saline. This would reduce the distance (Δx in equation VI.16) over which heat diffuses and thus increase the temperature gradient driving this cooling process. If

this distance is reduced to cellular dimensions or ≈ 10 μm (.001 cm) then equation VI.18 can be rewritten as

$$\Delta T = \frac{F_{th} f}{1000K} \qquad \text{VI.19}$$

which is no longer spot size dependent. For the F_{th} in this this thesis, a repetition rate of 1 Hz produces cumulative heating of only 1.4 ^{o}C. If one can tolerate a 30^{o}C temperature rise, than the calculated allowable repetition rate would be 20 Hz. If tissue is removed to a depth, $1/\alpha$, with each pulse, then rate of ablation achieved at a 20 Hz repetition rate could be as high as 1-4 mm/sec depending upon the extent of carotenoid loading. In addition, the saline could be pre-cooled to 5-10^{o}C, which would allow even higher repetition rates.

VI.6 A Proposed Ablation Mechanism for Soft Plaque

The discussion of the previous sections suggest an ablation scenario that is much more complex than the simple vaporization of tissue fluid. In what follows, one possible sequence of events that may explain the data is proposed. This scenario is schematically illustrated in Figure VI.4

VI.6.1 Instantaneous heating of fat droplets. Since the laser energy is delivered over a microsecond but the ablation occurs over milliseconds, one can initially consider the energy to be deposited instantaneously and later consider the effect of less than instantaneous heating. The initial distribution of absorbed energy will reflect the distribution of the carotenoid chromophores which are located in small (.1-10μm diameter) fat droplets dispersed throughout the tissue. These fat droplets will be heated to very high temperatures. If plaque is 20% fat with the same heat capacity as water then the temperature of the fat would be expected to be raised 5 times the amount predicted by equation II.4. Thus, at threshold, the fat droplet would be heated by $\approx 500^{o}C$ and even higher at suprathreshold fluences.

VI.6.2 Superheating surrounding water. These hot oil drops would immediately begin heating adjacent tissue fluid. At the tissue surface, water would be expected to vaporize and leave the tissue at an appropriate Boltzman velocity. Below the surface, however, the hot water would be constrained by inertial confinement and the tensile strength of surrounding tissue. Thus, below the surface, water would be superheated and generate large pressures (Steam tables show that

isovolumic heating of water from 37 to 150°C increases the pressure in excess of 1000 atmospheres). Since the thermal relaxation time of 1 μm fat droplets is of the order of 1 μsec, the pressure increase would occur rapidly, on the same time scale as the tissue heating.

VI.6.3 Propagation of acoustic or shock waves. The rapidly created, superheated water with an initially complex, highly variable pressure distribution would initiate propagation of stress waves throughout the tissue. The propagation of these waves would be further complicated by the multiple surfaces of impedance-mismatching present in the inhomogeneous tissue. The presence of these complex stress waves has been observed by Dyer and Srinivasan (1986) as a ringing response of pressure transducers connected to tissue during ablation by 14 nsec pulses of the excimer laser. If traveling at the speed of sound they could propagate the 200 μm characteristic depth of irradiation in about 2×10^{-7} seconds. These stress waves might contribute to shearing and liquefaction of the irradiated tissue. If strong enough, they could damage tissue beyond the zone which is irradiated.

VI.6.4 expansion of pressurized tissue fluid. The expansion

of the pressurized tissue will be toward the air which offers the least impedance and inertial confinement. The edges of the zone of irradiation may act like a nozzle causing the expansion of debris to resemble initially the expansion of pressurized gas through a nozzle as suggested by the high speed photography in Figure IV.14. The surrounding unirradiated tissue may be transiently stressed elastically when the irradiated volume expands. When the surrounding tissue later collapses as the pressure diminishes it may create the jet-like train of fluid seen at around 500 μsec in Figure VI.14C. This stress on surrounding tissue may also explain the fissures seen histologically.

VI.6.6 disruption and ejection of solid tissue elements by the expanding vapor. Expansion of the superheated fluid and vapor would create additional shear forces that further disrupt the tissue. The expanding vapor would carry the disrupted solid elements of the tissue along with it.

VI.6.7 post ablation events.

- convection effects. In the in vivo setting of flowing blood or saline, the ejected debris would be washed downstream and the residual unablated tissue would be

rapidly cooled as described in section VI.5.

- thermal damage. Residual heat may remain long enough to cause some thermal denaturation at the edges of the ablation crater.

- biological response. Although the immediate and long term biological responses of this process are not known, preliminary, informal reports of the initial clinical trials in the superficial femoral artery indicate that there is minimal pain, vasospasm or thrombosis occurring immediately and the healing process is not causing re-occlusion (Geschwind et al, 1988 and Bonner, personal communication) .

VI.6.8 Effect of increasing laser pulse duration. As the pulse duration is increased, there is more time to deliver energy and consequently, the threshold intensity is decreased. However, the effects which drive explosive/mechanical ablation are intensity dependent so decreasing the intensity also decreases the explosiveness of the ablative process. The relationship between pulse duration, threshold intensity and ablation mechanism can be more easily analyzed in terms of the times-scales of various energy transport phenomena occurring in the tissue. These time scales are shown in Table VI.2

At pulse durations less than 10^{-12} seconds, there will

be multiphoton absorption effects with ionization and photodecomposition. As the pulse duration exceeds the time-scale for propagation of stress waves, shock and stress wave effects will become less important. As the pulse duration exceeds the time-scale for thermal relaxation of the fat drops, the effect of inhomogeneous absorption will become less important. As the pulse duration exceeds the time-scale for thermal relaxation over the depth of penetration of radiation into the tissue, the mechanism would be expected to shift from primarily subsurface vaporization to primarily thermal ablation.

VI.6.9 effect of pulse repetition rate. At low repetition rates (< 1Hz if there is no convective cooling and < 20 Hz if there is vigorous convective cooling), each pulse will be an independent ablation event. As the repetition rate increases, the residual unablated tissue, will not have time to cool in between laser pulses and there will be some cumulative steady state heating of the tissue. When the steady state heating is sufficient to keep the tissue continuously near or above the water vaporization temperature, then thermal ablation will occur.

VI.6.10 Effect of hard plaque. If calcified tissue is encountered, then it will be ablated by a plasma mediated process described in VI.2.2.

VII. SUMMARY

Investigations on laser ablation of arterial plaque have demonstrated the feasibility of opening stenotic or obstructed arteries with laser radiation delivered into the body via fine optical fibers. This research is promising because it may lead to methods of removing the life-threatening arterial plaques without requiring surgery or general anaesthesia.

In these studies, a major limitation is the absence of confinement of the laser effects to the diseased tissue (plaque); there are many reports of perforations, aneurysms, spasm and other forms of injury to adjacent and underlying normal tissue. Attempts to develop a method of selectively ablating only the plaque have been prevented by the lack of information on optical properties of these tissues and uncertainty about the mechanisms for laser ablation of plaque. This thesis critically analyzes these factors and evaluates the potential for selective ablation of arterial plaque.

Spectrophotometers, optimized for studying vascular tissue, were constructed and used to assess the optical properties of atheromatous and normal aorta over the ultraviolet, visible and near-infrared spectrum. Remittance, transmittance and thickness were measured and the Kubelka-Munk model for light propagation in

scattering media was used to determine absorption and scattering coefficients. Two-fold preferential absorption in plaque was found from 450 to 500 nm.

Chemical analysis of the plaque led to identification of a mixture of yellow carotenoid pigments as responsible for the preferential absorption and the yellow color of plaque. Patients scheduled for carotid endarterectomy were given low-dose, oral beta carotene and achieved a 50-fold increase in the beta carotene content of their carotid plaques. This should significantly enhance the level of preferential absorption due to endogenous carotenoids.

Several techniques were developed to study the physics of plaque ablation and to determine how to take advantage of preferential absorption to achieve selective ablation of the plaque. These techniques included a method of measuring ablation thresholds, a method of measuring ablation efficiency and high speed photography of the ablation process. Using these techniques, a regime of selective ablation was identified using thermally short pulses of laser radiation that was preferentially absorbed by the plaque. Using 1 μsec pulses of 465 nm radiation from a flashlamp-excited dye laser delivered via a 1 mm diameter fiber, the threshold fluence for ablation was 6.8 ± 2.0 J/cm^2 for atheromas and 15.9 ± 2.2 J/cm^2 for normal aorta. Selective ablation was obtained by setting the laser radiation to be above threshold for ablating plaque but below threshold for ablating normal artery.

Ablation efficiencies as high as 6000 μg/J indicated that ablation was occurring with less energy then would be required to vaporize all of the ablated material (400 μg/J). High speed photography of soft plaque ablation showed an explosive process ejecting incompletely vaporized debris. Histology of the debris and the ablation crater revealed minimal thermal injury. Ablation products consisted of cholesterol crystals, shredded collagen fibers and small bits of calcific material. These findings are consistent with models for short-pulse laser ablation of materials which predict subsurface vaporization, mechanical disruption and ejection of incompletely vaporized material. This process is rapid and more efficient than pure vaporization, which explains the minimal evidence of thermal injury.

Ablation of calcified plaque was associated with a snapping sound and a flash of white light like a spark. Spectral analysis of this spark showed emission lines of hot ionized calcium superimposed upon a continuum (Bremsstrahlung emission), consistent with a plasma. Formation of this plasma with pulses that do not ablate normal aorta makes selective ablation of calcific plaque possible even though the energy required to vaporize calcium is much greater than the latent heat of vaporization of water.

The implications of this work are: (a) laser angioplasty may become safer and more effective by taking advantage of laser pulses that selectively ablate only plaque; (b) several techniques for studying laser tissue interactions have been developed including specialized spectrophotometers, high speed photography and a method

of measuring tissue mass ablated; (c) tissue ablation, as with engineering materials, is not necessarily surface vaporization but may also involve subsurface vaporization with pressure waves that disrupt and eject incompletely vaporized tissue; (d) selective ablation of calcific plaque is associated with ionization of the calcium and plasma formation.

The optimal conditions for selective ablation of plaque are as follows:

wavelength: 450 - 520 nm

pulse duration: < 50 μsec

fluence: between plaque and normal artery ablation thresholds

pulse repetition rate: < 20 Hz

beta carotene pretreatment: 60 mg tid for > 1 week

References

Abela GS, Normann SJ, Cohen DM, Franzini D, Feldman RL, Crea F, French A, Pepine CJ, Conti RC, "Laser recanalization of occluded atherosclerotic arteries in vivo and in vitro," Circulation 71:403-411, 1985.

Abela GS, Seeger JM, Barbieri E, Franzini D, French A, Pepine CJ, Conti CR: Laser angioplasty with angioscopic guidance. J. Am. Coll. Cardiol. 8:184-192, 1986.

Albright LF, Crynes BL, Corcoran WH, editors: Pyrolysis Theory and Industrial Practice, Academic Press, New York, 1983.

Anderson RR, Hu RJ, Parrish JA, "Optical radiation transfer in the human skin and application in in vivo remittance spectroscopy," Proc. Symp. Bioengineering Skin 245-257, 1981.

Anderson RR, Parrish JA, "The optics of human skin," J. Invest. Derm. 77:13-19, 1981.

Anderson RR, Parrish JA, Selective photothermolysis: precise microsurgery by selective absorption of pulsed radiation, Science 220:524-527, 1983.

Anisimov SI, Bonch-Bruevich AM, El'yashevich MA, Imas YA, Pavlenko NA, Romanov GS, Effect of powerful light fluxes on metals, Soviet Physics - Technical Physics 11:945-952, 1967.

Baurenfeind JC: Carotenoids as colorants and vitamin A precursors. New York, Academic Press, 1981.

Bell CE, Landt JA, Laser-induced high-pressure shock waves in water, Appl. Phys. Lett. 10:46-48, 1967.

Bieri JG, Brown ED, Smith JC: Determination of individual carotenoids in human plasma by high performance liquid chromatography. J. Liquid Chromatography 8:473-484, 1985.

Blankenhorn DH: Carotenoids in man, II. Fractions obtained from atherosclerotic and normal aortas, serum and depot fat by separation on alumina. J. Biol. Chem. 227:963-973, 1957.

Blankenhorn DH: The infiltration of carotenoids into human atheromas and xanthomas. J. Clin. Invest. 53:944-954, 1960.

Boulnois J, Photophysical processes in recent medical laser

developments: a review, Lasers in Medical Science 1:47-66, 1986.

Bowman HF, Cravalho EG, Woods M, Theory, measurement and application of thermal properties of biomaterials, Annual review of biophysics and bioengineering 4:43-80, 1975.

Brauwnwald E, Isselbacher KJ, Petersdorf RJ, Wilson JD, Martin JB, Fauci AS editors: Harrison's Principles of Internal Medicine, McGraw Hill Inc. New York, 1987.

Byer RL, "Diode laser-pumped solid state lasers," Science 239:742-747, 1988.

Carslaw HS, Jaeger JC, Conduction of Heat in Solids, Clarendon Press, Oxford, 1986.

Choy DSJ, S.H. Stertzer, R.D. Myler, J. Marco and G. Fournay, "Human coranaory laser recanalization," Clin Cardiol vol. 7, pp. 377-381, 1984.

Clarke RH, Isner JM, Gauthier T, Nakagawa K, Cerio F, Hanlon E, Gaffney E, Rouse E, DeJesus S: Spectroscopic characterization of cardiovascular tissue. J. Lasers Surg. Med. 8:45-59, 1988.

Cole RH, Underwater Explosions, Princeton University Press, Princeton, 1948.

Cothren RM, Hayes GB, Kramer JR, Sacks B, Kittrell C, Feld MS, A multifiber catheter with an optical shield for laser angiosurgery, Lasers in the Life Sciences 1:1-12, 1986

Cothren RM, "Design and development of a multifiber shielded laser catheter system for removal of atherosclerotic plaque," MIT Archives, Cambridge, 1987.

Dabby FW, Paek U, High-intensity laser-induced vaporization and explosion of solid material, IEEE J. Quantum Elec. QE-8:106-111, 1972.

Deckelbaum LI, Isner JM, Donaldson RF, Laliberte SM, Clarke RH, Salem DM, Use of pulsed energy deliverry to minimize tissue injury resulting from carbon dioxide laser irradiation of cardiovascular tissues, J. Am Coll. Cardiol. 7:898-908, 1986.

Deckelbaum LI, Lam JK, Cabin HS, Clubb KS, Long MB, Discrimination of normal and atherosclerotic aorta by laser-induced fluorescence, Lasers in Surgery and Medicine, 7:330-5, 1987.

Dixon J, Surgical Applications of Lasers, Yearbook Medical Publishers, Chicago, 1987.

Edgerton HE, Electronic Flash, Strobe, MIT Press, Cambridge, MA, 1979.

Esterowitz L, et. al. SPIE Proceedings 712, (1986) in press.

Fair HD, Medical Instrumentation vol. 12, pp. 100-105, 1978.

Fields CD, Slovenkai GA, Halaburka KR, Clarke RH, Isner JM, "Pulsed laser ablation at microsecond pulse durations does not produce thermal injury during fiber-mediated irradiation of cardiovascular tissues," (abstract) Lasers Surg. Med. 8:152, 1988.

Furui S, Yamauchi T, Ohtomo K, Tsuchiya K, Makita K, Takenaka E, "Hepatic inferior vena cava obstructions:Clinical results of treatment with percutaneous transluminal laser-assisted angioplasty," Radiology 166:673-677, 1988.

Furzikov NP, Different lasers for angioplasty: thermooptical comparison, IEEE J. Quantum Electronics QE-23:1751-5, 1987.

Gagliano FP, Paek UC, Observation of laser-induced explosion of solid materials and correlation with theory, Applied Optics 13:274-279, 1974.

Gerrity RG, F.D. Loop, L.A.R. Golding, L.A. Ehrhart and Z.B. Argenyi, "Arterial response to laser operation for removal of atherosclerotic plaques," J. Thorac. Cardiovasc. Surg. vol. 85, pp. 409-421, 1983.

Geschwind HJ, G. Boussignac, B. Teisseire, N. Benhaiem, R. Bittoun and D. Laurent, "Conditions for effective Nd-YAG laser angioplasty," Br. Heart J. vol. 52, pp. 484-9, 1984.

Geschwind HJ, Dubois-Rande JL, Bonner RF, Boussignac G, Prevosti LG, Leon MB: Percutaneous pulsed laser angioplasty with atheroma detection in humans (abstract). J. Am. Coll. Cardiol. 11:107A, 1988.

Ginsberg R, L. Wexler, R.S. Mitchell and D. Profitt, "Percutaneous transluminal laser angioplasty for treatment of peripheral vascular disease, clinical expereince with 16 patients," Radiology vol. 156, pp. 619-624, 1985.

Gilman AG, Goodman LS, Rall TW, Murad F, Goodman and Gilman's The pharmacologic basis of therapeutics, MacMillan Publishing Co.,

New York, 1985.

Grundfest WS, I.F. Litvack, T. Goldenberg, T Sherman, L Morgenstern, R. Carroll, M. Fishbein, J. Forrester, J. Margitan, S. McDermid, T.J. Pacala, D.M. Rider and J.B. Laudenslager, "Pulsed ultraviolet lasers and the potential for safe laser angioplasty," Am. J. Surg. vol. 150, pp. 220-226, 1985.

Guyton AC, Medical Physiology, W.B. Saunders Co. Philadelphia, 1986.

Hall RR, Beach AD, Baker E, Morison PCA, Incision of tissue by carbon dioxide laser, Nature 232:131-2, 1971.

Hansen DD, Intlekofer MJ, Hall M, Ritchie JI., "In vivo rotational endarterectomy in canine coronary arteries," Lasers Surg. Med. (Abstract) 7:124, 1987.

Hillenkamp F, Pratesi R, Sacchi CA, Lasers in Biology and Medicine, New York, Plenum Press, 1980.

Isner JM, Steg PG, Clarke RH, "Current status of cardiovascular laser therapy, 1987," IEEE J. Quantum Electronics QE-23:1756-1771, 1987.

Kaminow IP, Weisenfeld JM, Choy DSJ, "Argon laser disintegration of thrombus and atherosclerotic plaque," Appl. Optics 23:1301-1302, 1984.

Katzir A, Arieli R, "Long infrared optical fibers," J. Non. Cryst. Solids 47:149, 1982.

Katzir A, "Optical fibers for medicine," Scientific American, 1985.

Kazarinova-Fukshansky N, Seyfried M, Schofer E, "Distortion of action s[ectra in photomorphogenesis by light gradients within the plant tissue, Photobiology Photochemistry, 1985.

Kensey K, Nash J, Abrahams C, Lake K, Zarins CK, "Recanalization of obstructed arteries using a flexible rotating tip catheter," Circulation (abstract) 74:supple II:457, 1986.

Kitrell C, Willett RL, Santos-Pecheo C, Ratliff NB, Kramer JR, Malk EG, Feld MS: Diagnosis of fibrous arterial atherosclerosis using fluorescence. Applied Optics 24:2280-1, 1985.

Kortum G, Reflectance Spectroscopy, Springer-Verlag Inc., New York, 1969 p 15-87.

Krinsky NI. In: Isler O (ed) Functions of Carotenoids, Birkhauser, Basel, 1971.

Kubelka P, Munk F, "Ein Beitrag zur optik der farbanstriche," Z. Technichse. 12:593-601, 1931.

Kubelka P, "New contributions to the optics of intensely light-scattering materials. Part I," J. Opt. Soc. Am. 38:448-457, 1948.

Kubelka P, "New contributions to the optics of intensely lignt-scattering materials. Part II: nonhomogeneous layers," J. Opt. Soc. Am. 44:330-335, 1954.

Lane RJ, Wynne JJ, Geronemus RG, "Ultraviolet laser ablation of skin: Healing studies and a thermal model," Lasers Surg. Med., 6:504-513, 1987.

Lee G, Ikeda RM, Dwyer RM, Hussein H, Dietrich P, Mason DT, "Feasibility of intravascular laser irradiation for in vivo visualization and therapy of cardiocirculatory diseases," Am Heart J. 103:1076-1077, 1982.

Lee G, Ikeda RM, Theis JH Chan MC, Stobbe D, Ogata C, Kumagai A, Mason DT, " Acute and chronic complications of laser angioplasty: vascular wall damage and formation or aneurysms in the atherosclerotic rabbit," Am. H. Cardiol 53:290-293, 1984.

Letokhov VS, "Laser biology and medicine," Nature 316:325-330, 1985.

Linde RK, Crewdson RC, "Shock waves in solids," Scientific American, 220:83-91, May, 1969.

Linsker R, Srinivasan R, Wynne JJ, Alonso DR, "Far-ultraviolet laser ablation of atherosclerotic lesions," Lasers Surg. Med. 4:201-6, 1984.

Litvack F, Grundfest WS, Lee ME, Carroll RM, Foran R, Chaux A, Berci G, Rose HB, Matloff JM, Forrester JS: Angioscopic visualization of blood vessel interior in animals and humans. Clin. Cardiol. 8:65-70, 1985.

Livesay JJ, Leachman DR, Hagan PJ, "Preliminary report of laser coronary endarterectomy in patients," (abstract), Circulation (suppl. III) 72:302, 1985.

MacNichol EF, A photon counting microspectrophotometer for the study of single vertebrate photoreceptor cells. In Cool SJ,

Smith EL editors: Frontiers in Visual Science, New York, 1978, Springer, pp. 194-208.

Maiman TH, "Stimulated Emission in Ruby," Nature 187:493, 1960.

Marcuz R, J.R.M. Martins, A. Tupinamba, E.A. Lopes, H. Vargas, A.F. Pena, V.B. Cravalho and L.V. Decourt, "Possibilidades terapeuticas do raio laser em ateromas," Arq Bras Cardiol. vol. 34, pp. 9-12, 1980.

McGuff PE, Bushnell D, Soroff HS, Deterling RA: Studies of the surgical applications of laser (light amplification by stimulated emission of radiation). Surgical Forum, 14:143, 1963.

Mnitentag J, Marques EF, Ribeiro MP, Braga GA, Navarro MR, Veratti AB, Armelin E, Marcruz R, Jatene AD, Thermographic study of laser on arteries, Lasers in Surgery and Medicine 7:307-329, 1987.

Murray A, Crocker PR, Wood RFM, "The pulsed dye laser and atherosclerotic vascular disease," Br. J. Surg. 75:349-351, 1988.

Nishioka NS, Teng P, Deutsch TF, Anderson RR, "Mechanism of laser-induced fragmentation of urinary and biliary calculi," Lasers Life Sciences 1:231-245, 1987.

Nordstrom LA, Castenada-Zuniga WR, Lindeke CC, Rasmussen TM, Burnside DK, "Laser angioplasty: controled delivery of argon laser energy," Radiology 167:463-465, 1988.

Partovi F, Izatt JA, Cothren RM, Kittrell C, Thomas JE, Strikwerda S, Kramer JR, Feld MS, "A model for thermal ablation of biological tissue using laser radiation," Lasers Surg. Med. 7:141-154, 1987.

Paek UC, Gagliano FP, Thermal analysis of laser drilling processes, IEEE J. Quantum Electron. QE8:112-119, 1972.

Paek UC, Kestenbaum A, Thermal analysis of thin-film micromaching with lasers, J. Appl Phys. 44:2260-2268, 1973.

Paek UC, Zaleckas VJ, Scribing of alumina material by YAG and CO_2 lasers, Ceramic Bulletin 54:585-588, 1975.

Parrish JA, Deutsch TF, "Laser Photomedicine," IEEE J. Quantum Electronics QE-20:1386-1396, 1984.

Pilger E, Lammer J, Kleinert R, Ascher J, Bertuch H, "Laser angioplasty with a contact probe for the treatment of peripheral vascular disease," Cardiovascular Research 22:149-153, 1988.

Ready J.F. Development of plume of material vaporized by giant pulse laser, Appl. Phys. Lett. 3:11-13, 1963.

Ready JF, Effects of high-power laser radiation, Academic Press, Inc. New York, 1971.

Ready JF, "Material processing - an overview," Proc. IEEE 70:533-544, 1982.

Regan JD, Parrish JA editors: The science of photomedicine, Plenum Press, New York, 1982.

Robbins SL, Cotran RS, Kumar V, editors: The Pathologic Basis for Disease, W.B. Saunders Co. Philadelphia, 1986.

Rosen D, Weyl G, Simons G, Petcshek H, Popper L, "Modeling of the laser-induced thermal response, ablation, and fragmentation of biological tissue," Annual report, Physical Sciences, Inc. Research Park, P.O. box 3100, Andover, MA 01810.

Sahn DJ, Barratt-Boyes BG, Kerr GK, "Ultrasonic imaging of the coronary arteries in open-chest humans: evaluation of coronary atherosclerotic lesions during cardiac surgery," Circulation 66:1034-1044, 1982.

Sanborn Ta, Faxon DP, Kellett MA, Ryan TJ, "Percutaneous coronary laser thermal angioplasty," J. Am. Coll. Cardiol. 8:1437-1440, 1986.

Sartori M, Henry PD, Sauerbrey R, Tittel FK, Weilbaecher D, Roberts R, Tissue interactions and measurement of ablation rates with ultraviolet and visible lasers in canine and human arteries, Lasers in Surgery and Medicine, 7:300-306, 1987.

Schawlow AL, Townes CH, Phys. Rev. 112:1940-1949, 1958.

Schwarten DE, Katzen BT, Simpson JB, Cutcliff WB, "Simpson catheter for percutaneous transluminal removal of atheroma," Am. J. Roentgenology 150:799-801, 1988.

Shure D, Gregoratos G, Moser KM: Fiberoptic angioscopy: role in the diagnosis of chronic pulmonary arterial obstruction. Ann. Int. Med. 103:844, 1985.

Simpson JB, Johnson DE, Braden IJ, "transluminal coronary atherectomy (TCA): Results in 21 human cadaver vascular segments," Circulation (abstract) 74:Suppl.II:202, 1986.

Singleton DL, Paraskevopoulos G, Taylor RS, Higginson LAJ, Excimer laser angioplasty: Tissue ablation, arterial response, and fiber optic delivery, IEEE J. Quantum Electronics QE-23:1772-82, 1987.

Spears JR, Serur J, Shropshire D, Paulin S, "Fluorescence of experimental atheromatous plaques with hematoporphyrin derivative," J. Clin. Invest. 71:395-9, 1983.

Spears JR, Marais HJ, Serur J, Pomerantzeff O, Geyer RP, Sipzener RS, Weintraub R, Thurer R, Paulin S, Gerstin R, Grossman W: In vivo coronary angioscopy. J. Am. Coll. Cardiol. 5:1311-4, 1983.

Star WM, Marijnissen JPA, van Gemert MJC, "Light dosimetry in optical phantoms and in tissues: I. Multiple flux and transport theory," Phys. Med. Biol. 33:437-454, 1988.

Steinert RF, Puliafito CA, The Nd-YAG Laser in Ophthalmology, W.B. Saunders Co., Philadelphia, 1985.

Srinivasan R, "Ablation of polymers and biological tissue by ultraviolet lasers," Science 234:559-565, 1986.

Teng P, Nishioka NS, Anderson RR, Deutsch TF, "Optical studies of pulsed-laser fragmentation of biliary calculi," Appl. Phys. B 42:73-78, 1987.

Teng P, Nishioka NS, Anderson RR, Deutsch TF, Acoustic studies of the role of immersion in plasma-mediated laser ablation, IEEE J. Quantum Electronics QE-23:1845-1852, 1987.

Ursu I, Apostol I, Dinescu M, Hening A,Mihailescu IN, Prokhorov AM, Chapliev, Threshold conditions for the air plasma initiation near solid surfaces under the action of powerful pulsed CO^2 laser radiation, J. Appl. Physics 58:1765-1771, 1985.

Van Gemert MJC, Shets GACM, Stassen EG, Gijsbers GHM, Bonnier JJ, "Optical properties of human blood vessel wall and plaque," Lasers Surg. Med. 5:235-238, 1985.

Verdaasdonk RM, Borst C, Boulanger L, vanGemert MJC, "Laser angioplasty with a metal laser probe ('hot tip'): probe temperature in blood," Lasers Med. Sci. 2:153-158, 1987a.

Verdaasdonk RM, Cross FW, Borst C, "Physical properties of sapphire

fibretips for laser angioplasty," Lasers Med. Sci. 2:183-188,1987b.

Walsh JT, Flotte TJ, Anderson RR, Deutsch TF, "Pulsed Co_2 laser tissue ablation: effect of tissue type and pulse duration on thermal damage, Lasers Surg. Med. 8:108-118, 1988.

Walsh JT, Deutsch TF, "Pulsed CO_2 laser tissue ablation: measurement of the ablation rate," Lasers Surg. Med. 8:264, 1988.

Wan S, Anderson RR, Parrish JA, "Analytical modeling for the optical properties of the skin with in vitro and in vivo applications," Photochem. Photobiol. 34:493-499, 1981.

Welch AJ, "The thermal response of laser irradiated tissue," IEEE J. Quantum Electronics vol. QE-20, pp. 1471-81, 1984.

Welch AJ, Valvano JW, Pearce JA, Hayes LJ, Motamedi M, Effect of laser radiation on tissue during laser angioplasty, Lasers Surg. Med. 5:251-264, 1985.

Welch AJ, Bradley AB, Torres JH, Motamedi M, Ghidoni JJ, Pearce JA, Hussein H, O'Rourke RA, Laser probe ablation of normal and atherosclerotic human aorta in vitro: a first thermographic and histologic analysis, Circulation 76:1353-1363, 1987.

Wolbarsht ML, "Laser surgery: CO_2 or HF," IEEE J. Quantum Electronics QE-20:1427-1432, 1984.

Yoon G, Welch AJ, Motamedi M, van Gemert MCJ, "Development and application of three-dimensional light distribution model for laser irradiated tissue," IEEE J. Quantum Electronics, QE-23:1721-1733, 1987.

Zweig AD, Weber HP, "Mechanical and thermal parameters in pulsed laser cutting of tissue," IEEE J. Quantum Electronics QE-23:1787-1793, 1987.

PRIOR PUBLICATIONS

Prince MR, Deutsch TF, Mathews-Roth MM, Margolis R, Parrish JA, Oseroff AR. Preferential absorption in atheromas in vitro; implications for laser angioplasty. Journal of Clinical Investigation, 78:295-302, 1986.

Prince MR, Deutsch TF, Shapiro AH, Margolis RJ, Oseroff AR, Fallon JT, Parrish JA, Anderson RR, Selective laser ablation of atheromas using a flashlamp-excited dye laser at 465 nm. Proc. Nat. Acad. Sci. USA 83:7064-8, 1986.

Prince MR, LaMuraglia GM, Teng P, Deutsch TF, Anderson RR, Selective Ablation of Calcified Arterial Plaque with Laser-Induced Plasmas. IEEE J. Quantum Electronics QE23:1783-6, 1987.

LaMuraglia GM, Murray S, Anderson RR, Prince MR, Effect of pulse duration on selective ablation of atherosclerotic plaque by 480-490 nm radiation. Lasers Surg. Med. January, 8:18-21, 1988.

Prince MR, LaMuraglia GM, MacNichol EF, Increased preferential absorption in atherosclerotic plaque with oral beta carotene: Implications for laser endarterectomy. (Circulation, in press, August, 1988).

Table III.1

Summary of Experiments

Experiment	Purpose	Major Findings	Methods page #	Results page #
OPTICAL STUDIES			24	41
Integrating Sphere Measurement of R & T	Identify waveband of Pref. abs.	pref. abs. exists from 420-530 nm	25	41
Laser Spectrophotometer measurement of R & T	Verify waveband of pref. abs.	pref. abs. exists from 430-500 nm	26	42
ABLATION STUDIES			30	44
Ablation threshold measurements	Identify a fluence above plaque threshold & below the normal threshold	Selective ablation is possible in the waveband of pref. abs.	32	44
Histology	Investigate extent of thermal injury	Thermal injury is less than 100 microns	33	47
High speed photography	Investigate ablation mechanism	Soft plaque is ablated explosively	34	47
Ablation efficiency measurements	Investigate ablation mechanism	Ablation can be more efficient than boiling water	35	48
Plume spectroscopy	Characterize emission during calcified plaque ablation	Calcified plaque ablation is associated with a plasma	35	51
Ablation debris analysis	Investigate ablation mechanism and risks	Most debris is < 10 μm and not denatured	36	51
CHROMOPHORE STUDIES			36	51
Extraction and thin layer chromotography	Identify chromophores confering pref. abs.	Carotenoids confer pref. abs.	36	51
Treat patients with beta carotene	Enhance plaque absorption	Carotenoids enhance plaque absorption	37	52
HPLC	Measure beta carotene enhancement in plaque	50-fold increase found in plaque beta carotene	38	54
Microscopy and Microspectrophotometry	Identify where beta carotene accumulates	Beta carotene localizes to plaque fat drops	40	53

Table IV.1

Absorption coefficients (α) at 470nm
for atheroma and normal aorta

Measurement method Analysis method	α Atheroma (cm^{-1})	α Normal (cm^{-1})	Significance (p value)	Ratio
Integrating Sphere				
Kubelka-Munk Analysis	50±7[a] $(6,6)_b$	24±4[a] $(3,7)_b$	5.8x10-4[c]	2.1[d]
Beer's Law Analysis	63±7 (6,6)	36±7 (3,7)	1.1x10-3	1.8
Laser Spectrophotometer				
Kubelka-Munk Analysis	61±16 (4,12)	27±14 (4,12)	.043	2.2 (1.5-3.8)[e]
Beer's Law Analysis	48±9 (4,12)	25±4 (4,12)	.042	1.9 (1.4-3.1)e
Combined Data				
Kubelka-Munk Analysis	54±12 (10,18)	26±4 (7,19)	2.4x10-5	2.2
Beer's Law Analysis	57±11 (10,18)	30±8 (7,19)	4.5x10-5	1.9

a mean ± standard deviation

b parameters denote (# of individuals, # of measurement sites).

c p value is calculated by first calculating the average absorbance at all measurement sites for each tissue type in each individual and then treating each of those averages as a separate observation.

d mean atheroma absorbance/mean normal aorta absorbance.

e range of ratios over the 4 individuals studied.

Table IV.2

Comparison of ablation thresholds with 482 nm radiation for all types of vascular tissue

(320 micron core diameter fiber, 1 μsec pulse duration)

Tissue Type	Threshold	
	(mJ)	(J/cm2)
thrombus	1.5 ± 0.01	1.8
pulmonary embolus	5.1 ± 1.2	6.3
calcified plaque	35 ± 5.8	43.5
fibro-fatty plaque	37 ± 5.1	46.0
fatty streak	35 ± 9.5	43.5
adventitia	68 ± 23	85
media	69 ± 15	86
intima	80 ± 14	99
inferior vena cava	120 ± 36	149
pulmonary artery	124 ± 30	154

Table IV.3

Effect of wavelength on ablation threshold fluence

(1 μsec pulse duration, 320 μm diameter fiber)

Wavelength (nm)	Ablation Threshold (mJ)						
	Normal intima	Deep media	Adventitia	Fibrous plaque	Calcific plaque	Fatty streak	Thrombus
290	3.2±.65			3.0±.4	3.6±.56		
482	80±14	69±15	68±23	37±5	35±6	35±10	5±.5
658	250±5	240±16	240±19	220±24	102±15	227±18	17

Table IV.4

Effect of wavelength on the selective ablation

(1 μsec pulse duration, 320 μm diameter fiber)

Wavelength (nm)	ratio of threshold fluences	
	(Normal Aorta)/(fibrous plaque)	(Normal Aorta)/(calcified plaque)
290	.94	1.1
465 (1 mm fiber)	2.6	
482	2.2	2.3
658	1.1	2.5

Table IV.5

Effect of pulse duration on ablation thresholds

(482 nm radiation, 320 μm core diameter fiber)

Pulse Duration (μsec)	Ablation Threshold (mJ)				
	Normal Intima	Media	Adventitia	Fibrous Plaque	Calcified Plaque
1	80±14	69±15	68±23	37±5.1	35±5.8
8	113±20	86±10	69±12	45±9.7	50±11
50	160±11	169±8.5	131±9.3	79±8.0	90±8.7

Table IV.6

Effect of fiber size on ablation threshold fluence

(465-482 nm radiation, 1 μsec pulse duration)

Fiber diameter (microns)	Plaque threshold fluence (J/cm^2)	Normal threshold fluence (J/cm^2)
1000 (465nm)	6.8	15.9
650 (465nm)	8.7	26.5
320 (482nm)	46	99.5

Table IV.7

Ablation efficiency in air

(465 nm radiation, 18 J/cm2, 1 μsec pulse duration, 2.5 mm spot size)

Aorta #	Atheroma (μg/J)	Normal Intima (μg/J)	Significance (p value)	Ratio
1	161±37	74±11	$8x10^{-6}$	2.2
2	196±37	53± 9	$4x10^{-4}$	3.7
3	370±126	73±17	$5x10^{-5}$	5.0
4	288±122	50±20	1x10-5	5.7
average	253	62		4.0

Table IV.8

Ablation Efficiency under saline

(480 nm radiation at twice plaque threshold, 320 μm diameter fiber)

Pulse Duration (μsec)	Energy per pulse (mJ)	Ablation Efficiency (μg/J)		
		Normal Artery	Fibrous Plaque	Calcified Plaque
1	80	50±50	1200±470	4100±2400
8	100	60±100	850±250	6100±3500
50	170	130±120	800±160	500±100

Table IV.9

Tabulation of serum and plaque beta carotene levels

patient #	days on βc	pills per day	plaque βc (μg/g plaque)	serum βc (μg/dl)
beta carotene	treated patients			
1*	8	5.9	2.08	281
2*	10	6	2.65	611
3	14	6	8.21	561
4	18	5.7	2.10	310
5*	20	5.4	2.52	257
6	20	5.8	5.20	710
7	23	6	0.93	389
8*	28	3.7	1.78	185
9	32	5.9	4.52	607
10	41	5.7	2.92	924
average	21		3.3 ± 2.0	483 ± 224
control patients				
2*$	0	0	0.18	21.7
5$	0	0	0.022	2.92
8*$	0	0	0.023	9.16
11	0	0	0.012	10.4
12	0	0	0.051	6.36
13	0	0	0.023	0.31
14	0	0	0.084	2.05
15	0	0	0.023	5.24
16	0	0	0.015	5.52
17	0	0	0.027	1.77
18	0	0	0.287	10.1
19	0	0	0.018	5.91
20	0	0	0.123	9.05
21	0	0	0.016	6.19
22	0	0	0.114	25.0
23	0	0	0.014	6.41
24	0	0	0.037	9.76
25	0	0	0.054	---¶
26	0	0	0.110	14.2
average			0.07 ± 0.07	8.4 ± 6.3

βc beta carotene

* light microscopy and microspectrophotometry performed on these specimens

$ these patients had bilateral carotid endarterectomies; the first served as an internal control.

¶ serum was hemolyzed

Table IV.10

Statistical comparisons of control
and
post beta carotene treatment specimens

parameter	controls	patients on beta carotene	significance (p value)
subjects:			
number*	19	10	
age	65 (49-78)	67 (53-80)	NS**
sex	14M 5F	6M 4F	NS
tobacco use	89%	80%	NS
diabetes	21%	30%	NS
hypertension	58%	60%	NS
serum:			
creatinine (mg/dl)	1.42	1.25	NS
cholesterol (mg/dl)	218	207	NS
triglycerides (mg/dl)	180	185	NS
beta carotene (μg/dl)	8.4 ± 6.3	483 ± 224	<.001
plaque:			
beta carotene (μg/gm plaque)	.066 ± .07	3.3 ± 2.0	<.001

* 3 patients were studied before and after beta carotene treatment, 7 patients were studied only after beta carotene treatment, 16 patients were studied without beta carotene treatment.

** NS = not significant

dl = deciliters

Table V.1

Predicted tissue surface temperature
at the ablation threshold for
465-480 nm radiation

tissue type	threshold energy (J/cm2)	absorption coefficient (cm-1)	predicted surface temp. at threshold (^{o}C)
plaque	6.8	54	117
normal aorta	15.9	26	128
thrombus	1.5	300	138

Table V.2

Carotenoids known to exist in humans

carotenoid	wavelengths of absorption maxima in light petroleum (nm)	extinction coefficient ($E^{1\%}_{1cm}$)*
lycopene	446,472,505	3450
beta-carotene	425,451,480	2592
canthaxanthin	466	2200
alpha carotene	422,444,480	2800
zeta carotene	378,400,425	2555
lutein	420,447,477	2550
cryptoxanthin	425,451,483	2386
zeaxanthin	423,451,483	2348
capsanthin	474-475,504	2072
capsorubin	444,474,506	2200

* the optical density of a 1 cm pathlength of a 1% (by mass) solution of the carotenoid in an organic solvent (Bauernfeind, 1981).

Table VI.1

Length scales of energy transport during tissue ablation

Subjective Dimension	Physical Dimension
typical thickness of plaque	1-2 mm
penetration depth of 480 nm radiation ($1/\alpha$)	200 μm
diameter of fat drops	0.1-10 μm
optical fiber diameter	320-1000 μm

Table VI.2

Time scales of energy transport during tissue ablation

Event	Time Required
absorption of a single photon	10^{-15} s
thermal relaxation of an excited molecule	10^{-12} s
stress wave to propagate .1-10 μm*	3×10^{-10}-3×10^{-8} s
stress wave to propagate 200 μm*	7×10^{-7} s
thermal diffusion over .1 μm**	10^{-8} s
thermal diffusion over 10 μm**	10^{-4} s
thermal diffusion over 200 μm**	0.04 s

* assume stress waves propagate at the speed of sound in water ($\approx$300 m/s).

** calculated from equation II.2

Table VI.3

Wavelength scales for tissue ablation

Wavelength	Absorption Depth	Primary Chromophore	Primary Effects
X-rays			
.01-1 nm	minimal absorption	calcium	minimal effect
Ultraviolet			
193 nm	1 μm	organic bonds	photochemistry
250 nm	5-10 μm	DNA & aromatics	photochemistry
Visible-NIR			
410 nm	5 μm	hemoglobin	heating/ablation
450-500 nm	200 μm	carotenoids	heating/ablation
600-1300 nm	2 mm	none	heating
Infrared			
2.9 μm	1 μm	H_2O	heating/ablation
10.6 μm	30 μm	H_2O	heating/ablation

Table VI.4

LASER TISSUE REMOVAL MECHANISMS

	TIME (sec)	LOW INTENSITIES (continuous wave lasers)	HIGH INTENSITIES (pulsed lasers)		HIGH ENERGY PHOTONS (eV > 3-4)	
ELECTRONIC EVENTS	10^{-15}	Electronic or Vibrational Excitation	Electronic or Vibrational Excitation		Electronic Excitation	
	10^{-12}	thermalization	thermalization	ionization	photochemistry	
		tissue temperature increases	rapid adiabatic heating pressure rise with sub-surface vaporization tissue expansion shear stress liquefaction ejection of debris	plasma initiation plasma expansion/collapse stress waves disruption and fragmentation	bond dissociation tissue removal by an unknown mechanism (photodecomposition)	toxic molecules created including free radicals and singlet oxygen
MECHANICAL EVENTS	10^{-6}					
	10^{-3}	thermal diffusion begins coagulation begins surface evaporation and pyrolysis begins	coagulation of small zone from residual heat	coagulation of small zone from residual heat		
	1	pain / vasospasm				death of unwanted cells inflammation
BIOLOGICAL EVENTS		inflammation of large coagulation zone	inflammation of small coagulation zone	inflammation		
	10^{6}	healing	healing	healing		healing process removes unwanted tissue
disadvantages for plaque ablation		calcified plaque not ablated	high intensity radiation is difficult to transmit via optical fibers except from 300 - 1300 nm		?	tried with HPD no beneficial effect

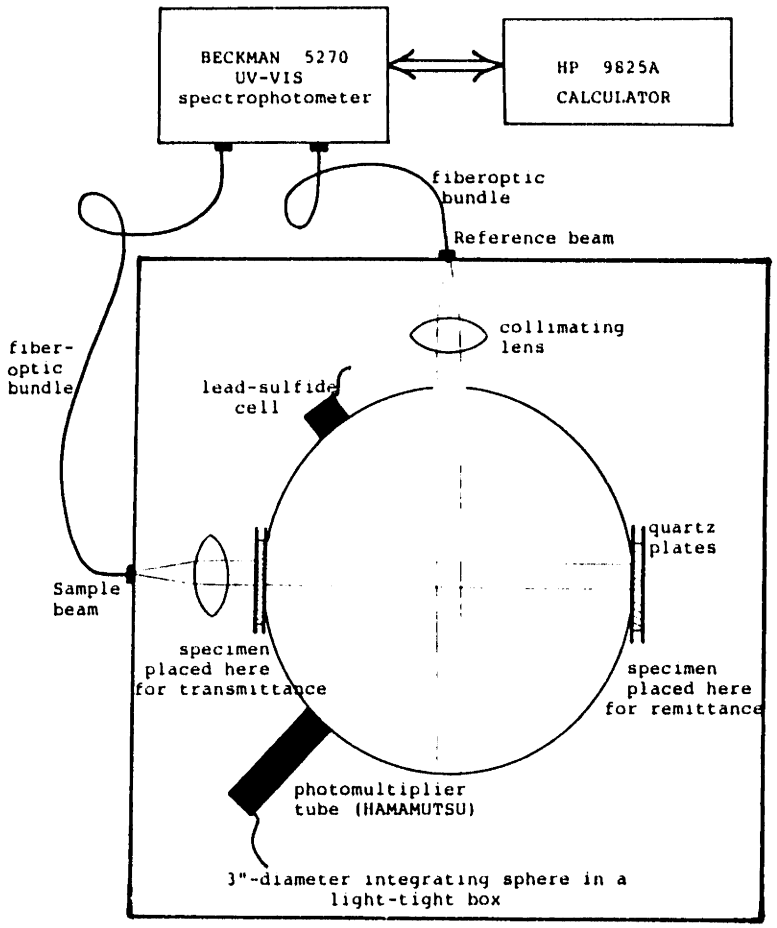

Figure III.1 Integrating sphere/spectrophotometer apparatus. Light from a conventional spectrophotometer is conducted to the integrating sphere via fiberoptic bundles and detected using either a lead sulfide cell (infrared) or a photomultiplier tube (UV and visible). Tissue transmittance is measured by placing the tissue in the path of the sample beam where light enters the integrating sphere on the left, and by covering the exit hole with a plate coated with barium sulfate. Remittance is measured by placing the specimen in the path of the sample beam where light exits the integrating sphere.

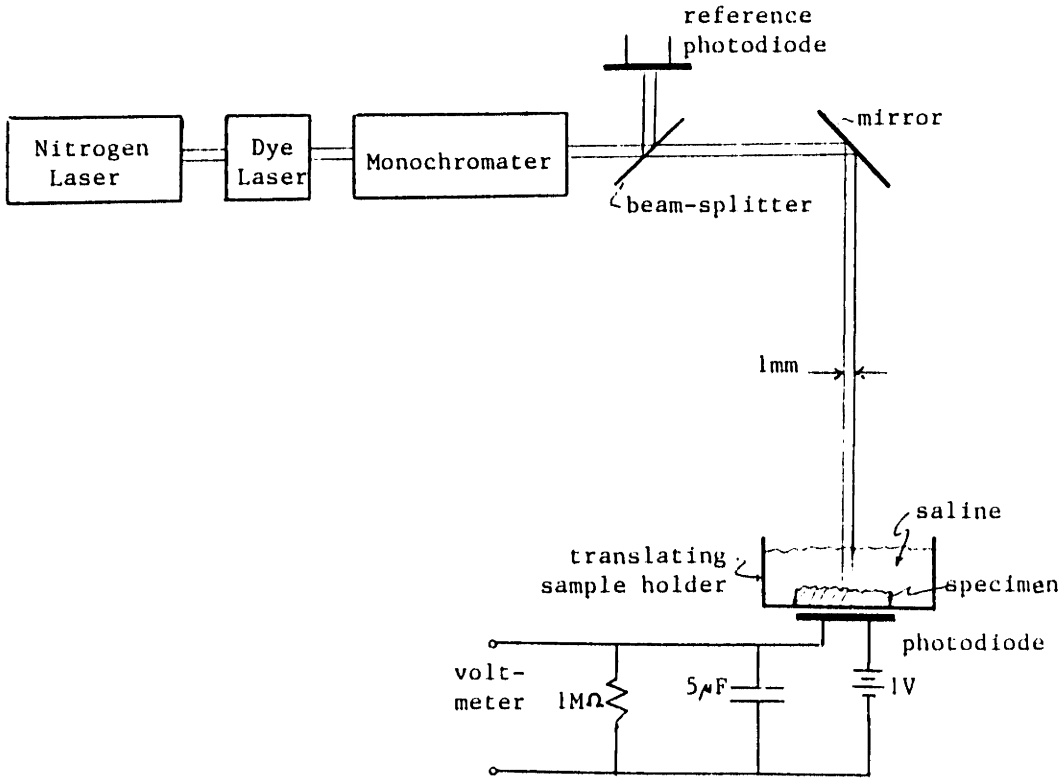

Figure III.2 Laser-based spectrophotometer. This spectrophotometer permits multiple measurements on areas as small as 1-mm diameter with transmittance $\geq 10^{-3}$%. The tissue is immersed in normal saline to approximate the in vivo optical environment and to eliminate optical artifact from index mismatching at surfaces.

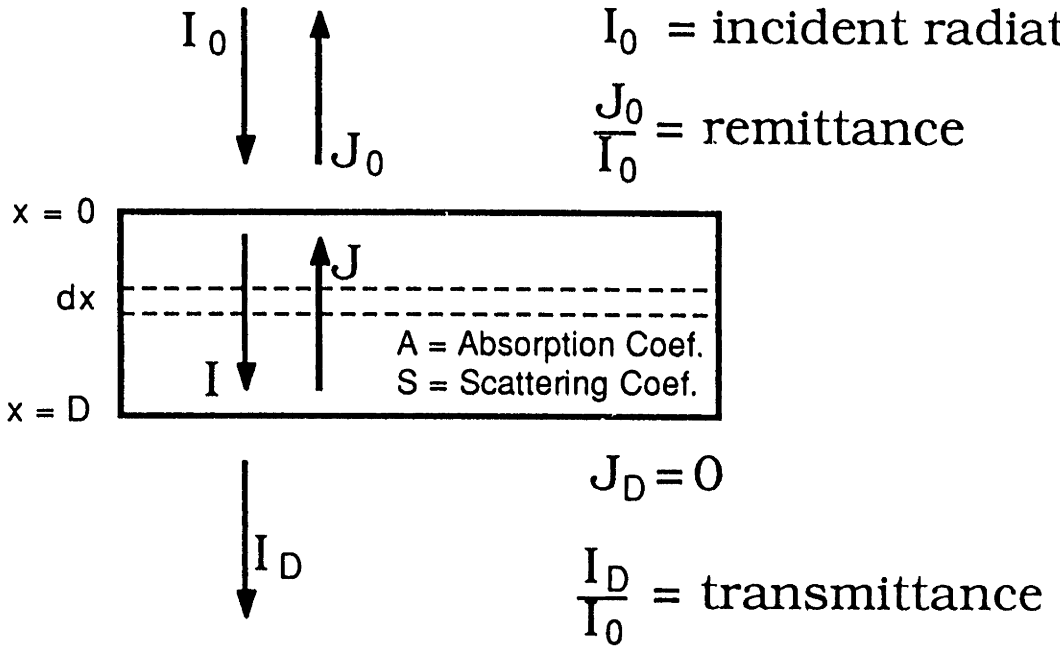

$$\frac{dI}{dx} = -SI - AI + SJ$$

$$\frac{dJ}{dx} = -SI - AJ + SI$$

Figure III.3 The Kubelka-Munk model. Light is assumed to be propagating diffusely through tissue where I_o is the incident light, J_o is the remitted light, I_D is the transmitted light, and D is the specimen thickness. By considering a differential element, dx, it is possible to describe the change in I and J with the differential equations shown.

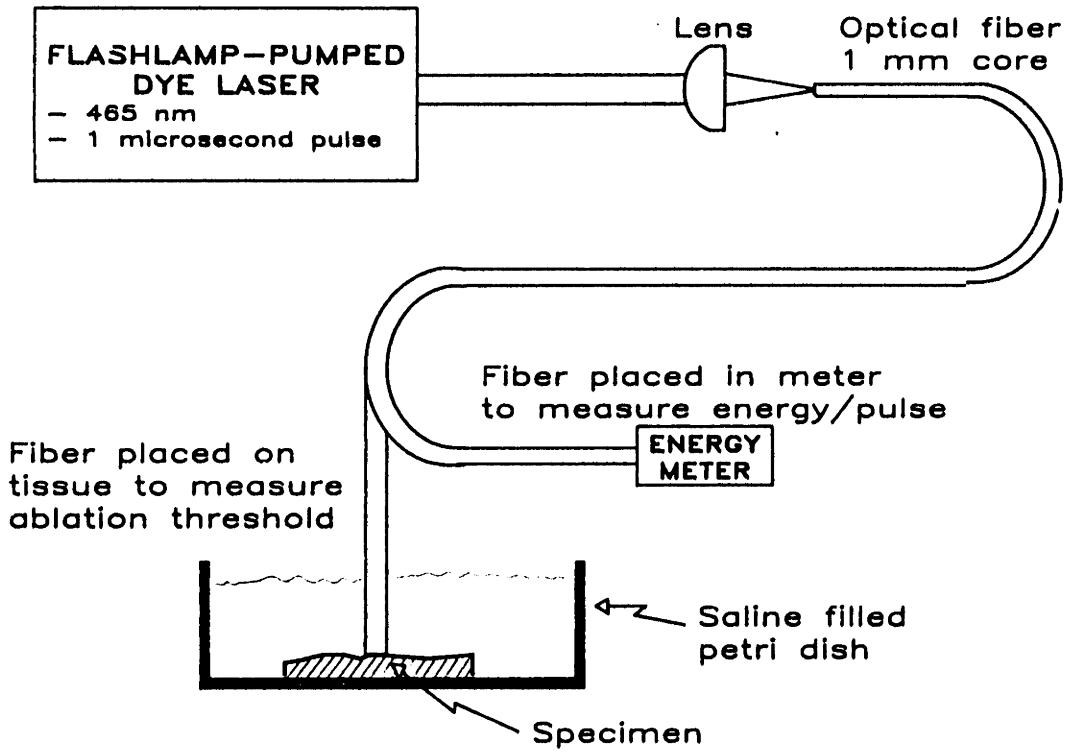

Figure III.4 Experimental setup for measuring the threshold fluence for ablation. Radiation from the flashlamp pumped dye laser is coupled into an optical fiber with a core diameter of 320, 650 or 1000 μm. The output end of the fiber is abutted against the tissue, which is submerged under saline to simulate the <u>in vivo</u> optical environment. The threshold energy is determined by gradually increasing the energy/pulse until there is an observable ablative effect on the tissue.

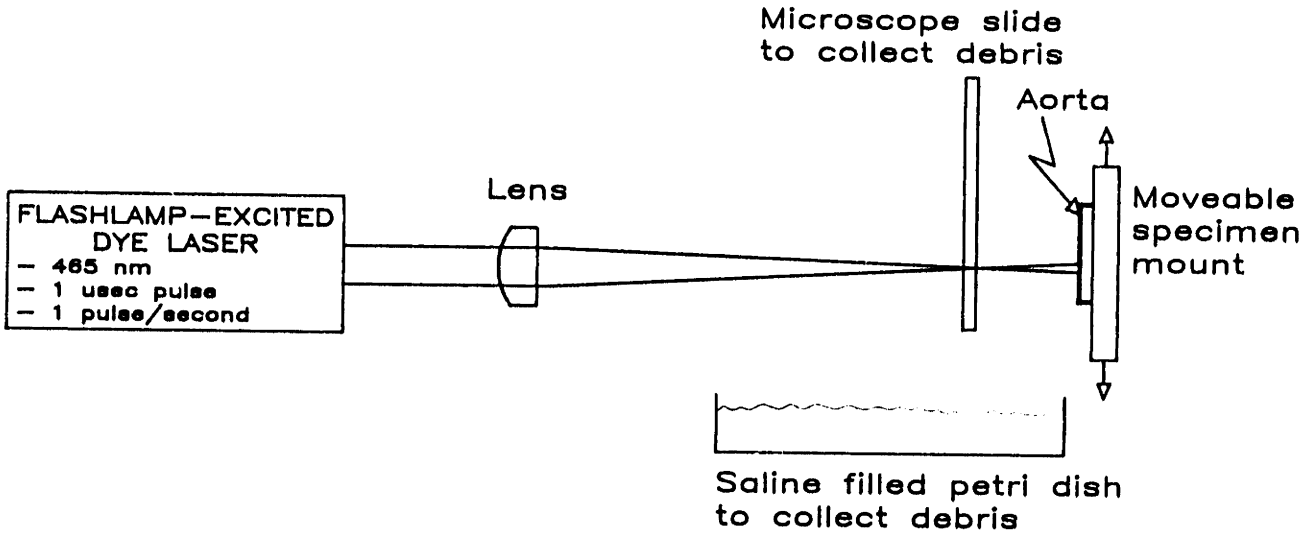

Figure III.5 Experimental setup for studying ablation of large areas of tissue in air.

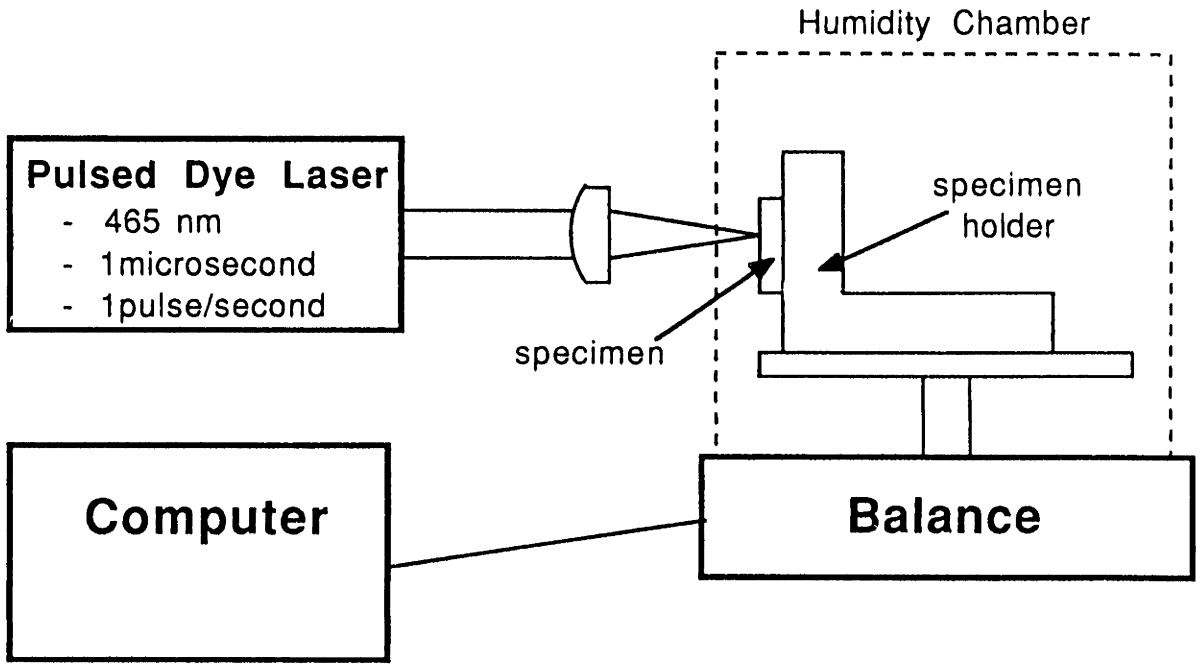

Figure III.6 Experimental method of measuring the mass of tissue ablated. Tissue is mounted vertically on a balance such that ablation products will land off the balance. The tissue and balance are contained within a chamber which eliminates air currents and maintains a high level of humidity to avoid mass loss from evaporation. Laser radiation enters through a hole in the chamber and the tissue mass is recorded automatically before, during and after ablation at 2 Hz by a microcomputer.

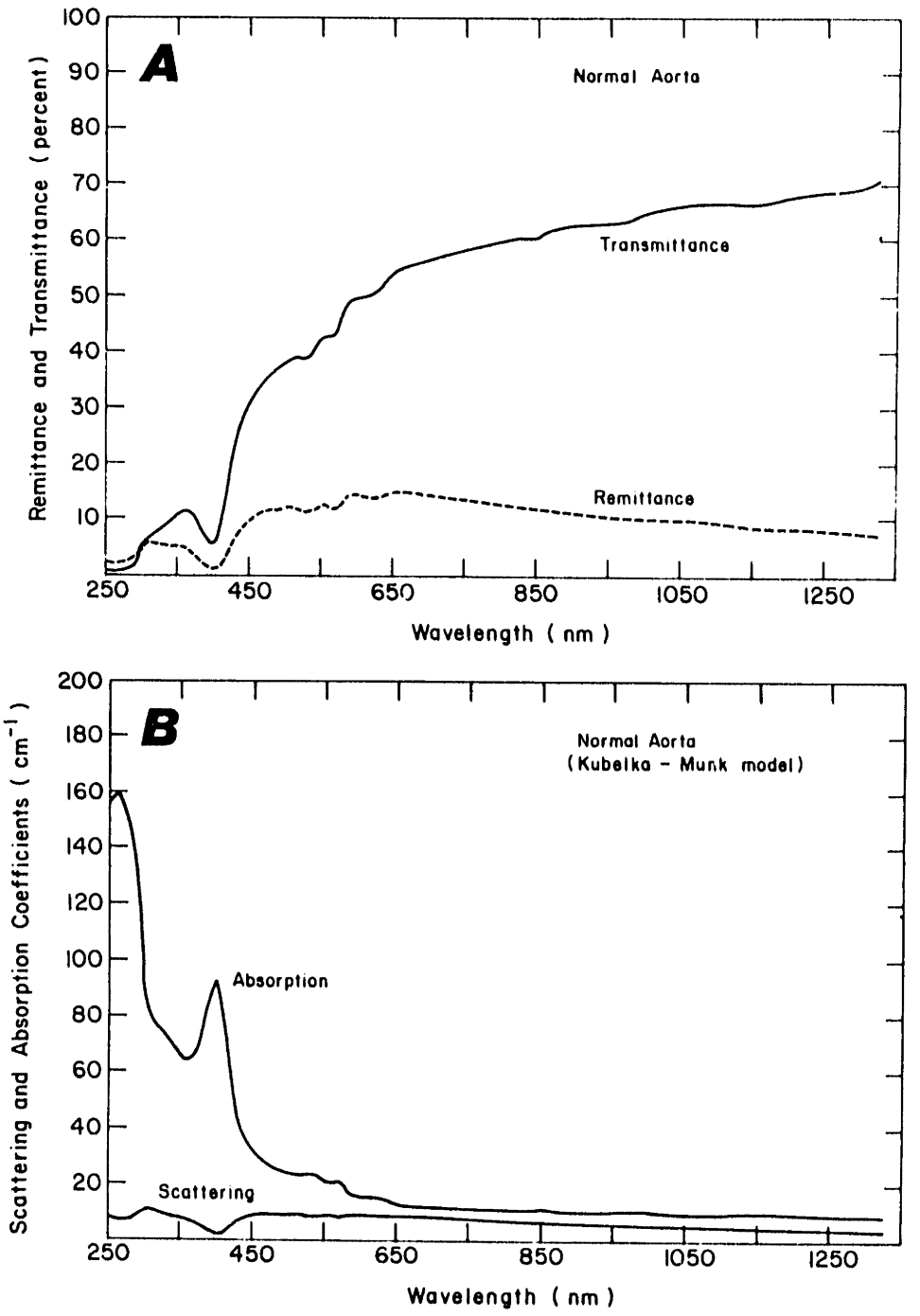

Figure IV.1 A and B Integrating sphere measurements for a typical specimen of normal cadaver aotic intima, 310 microns thick. A) Remittance and transmittance measured with the integrating sphere and B) Calculated KM absorption and scattering coefficients. Note the absorption peaks corresponding to known tissue chromophores (hemoglobin at 550-570, 530-550 and 390-420 nm, aromatic amino acids and DNA at 250-290 nm).

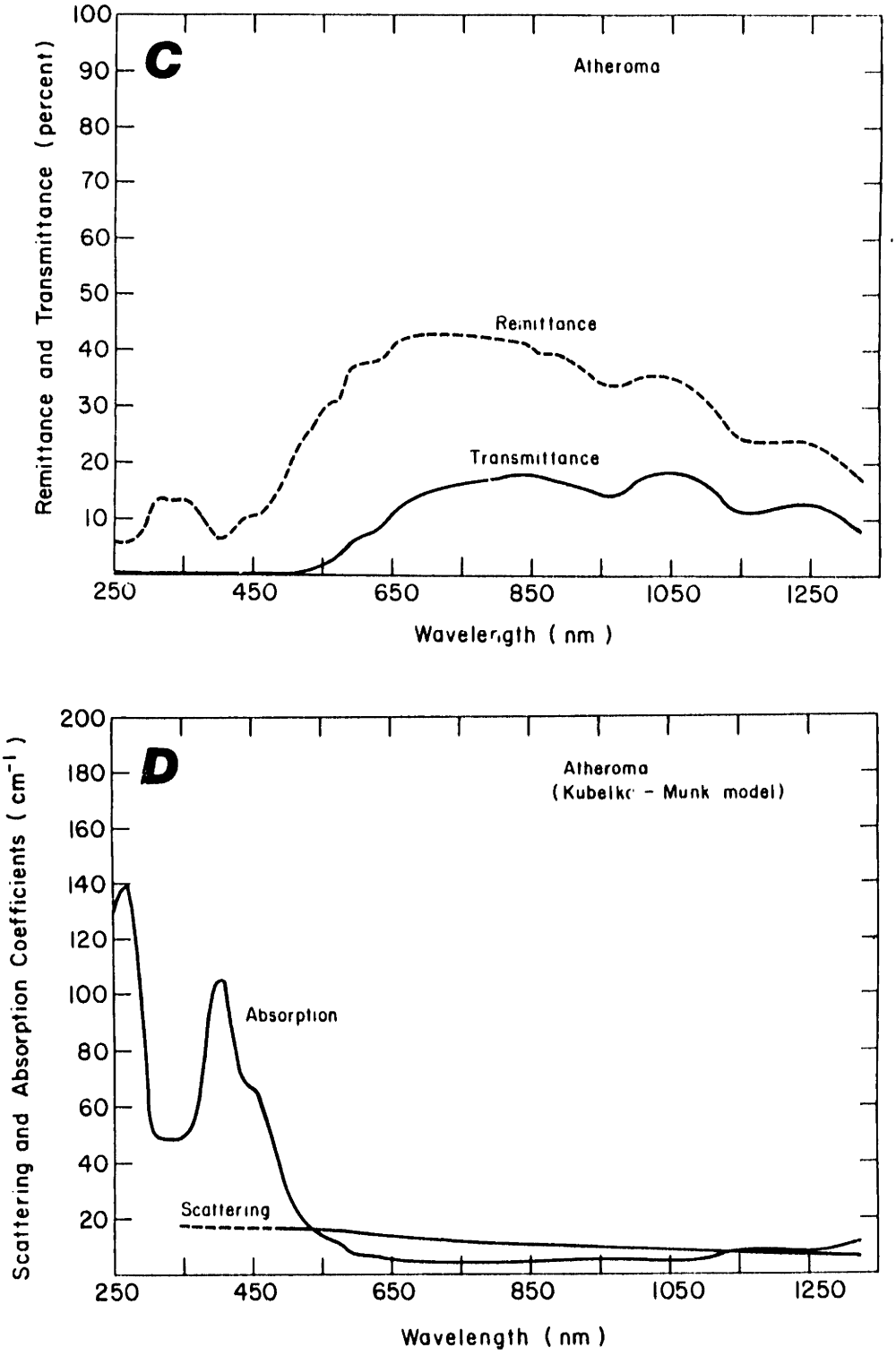

Figure IV.1 C and D Integrating sphere measurements for a typical atheroma, 1.5-mm thick. C) Remittance and transmittance data and D) Calculated KM absorption and scattering coefficients. Note the extra absorbance for atheroma (relative to normal tissue, Figure IV.1B) at about 470 nm.

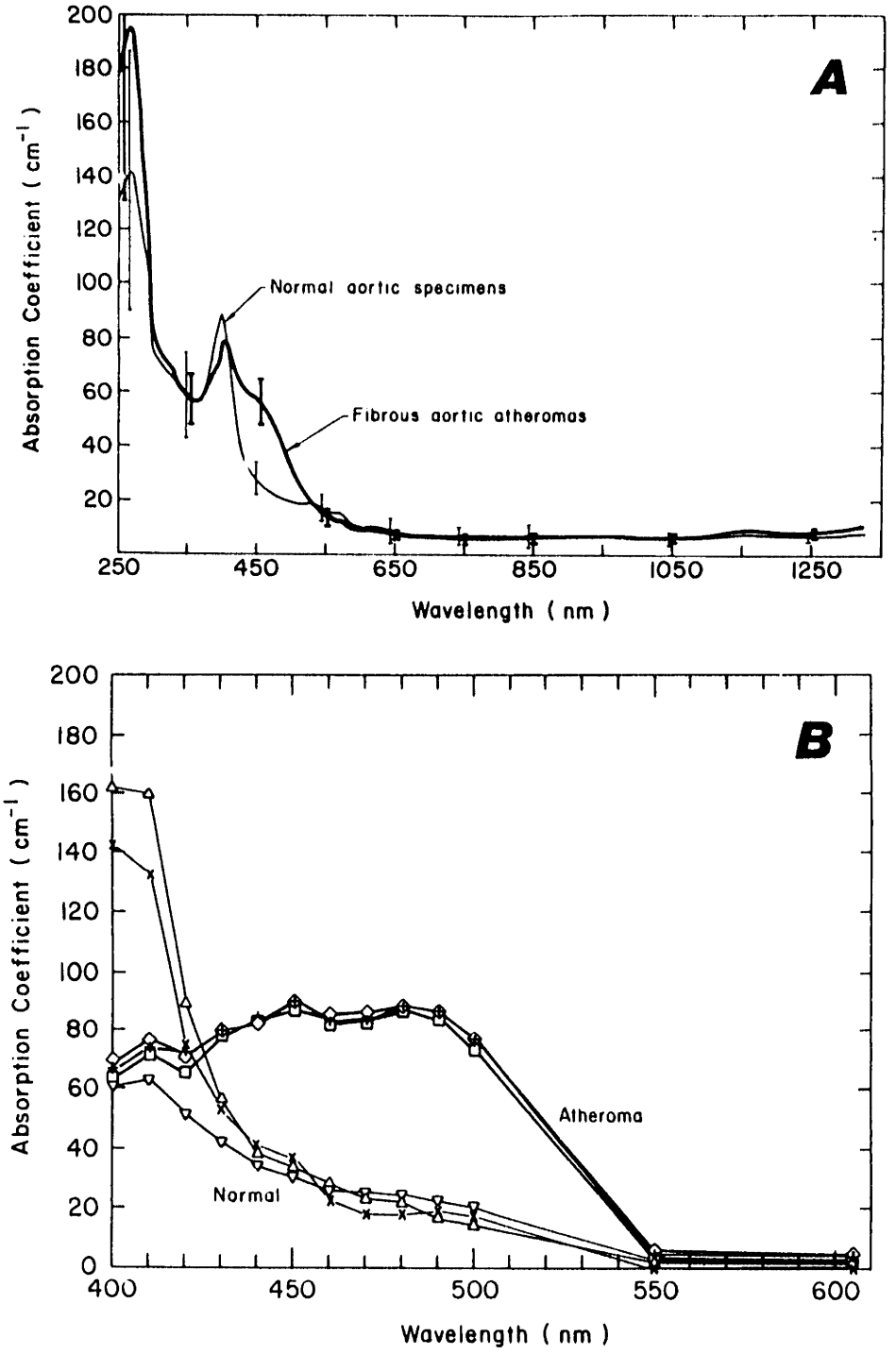

Figure IV.2 Comparison of absorption coefficients for atheromatous and normal aortic specimens. (A) The average KM absorption coefficients for seven normal specimens (thin line) are compared to the average for six fibrous aortic atheromas (thick line). Bars indicate ± 1 standard deviation. (B) The KM absorption coefficients from laser spectrophotometer data for three regions of atheroma (□ ,+ ,◊ , thick lines) and three adjacent normal regions (∇,×,Δ, thin lines) from the same aorta. Note that in the region from 420 to 530 nm the atheroma absorption coefficient is greater than that of normal specimens.

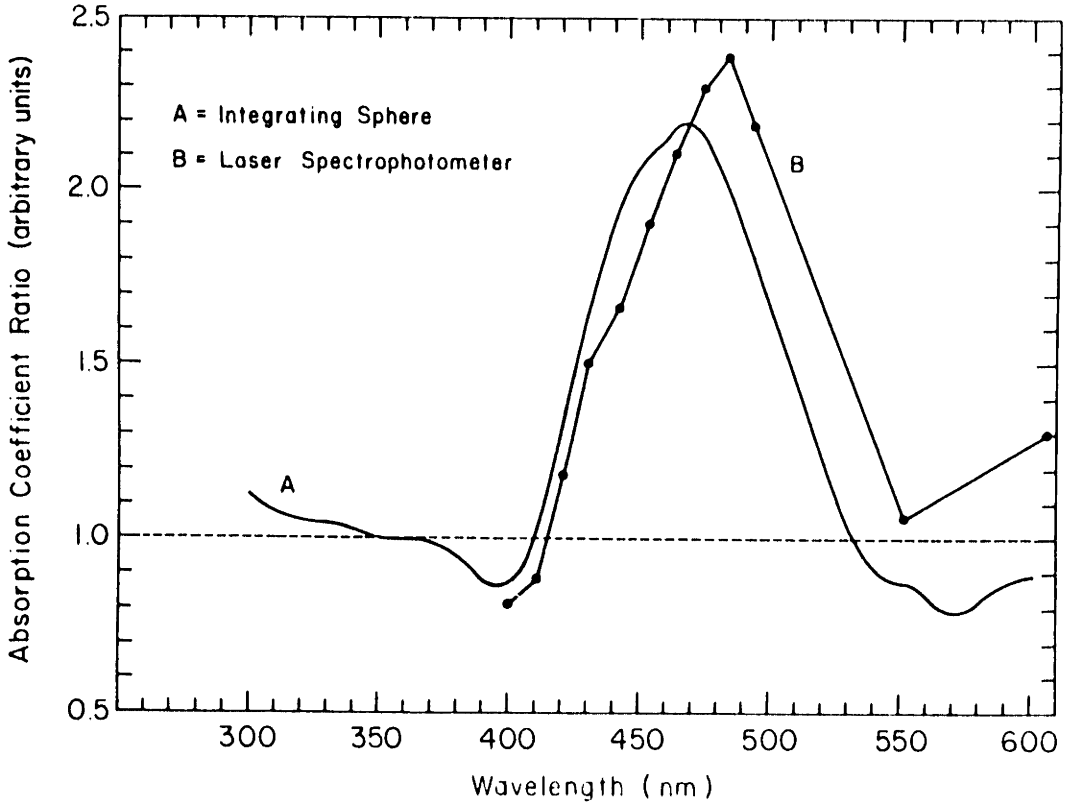

Figure IV.3 The ratio of atheroma to normal absorption coefficients. Note that between 450 and 500 nm the average atheroma absorption is greater than 1.7 times that of normal artery.

Figure IV.4 Histology of a typical atheroma. The four regions marked in the figure are A) a fibrous cap overlying B) variable amounts of irregularly deposited grumous material that appears to consist of extracellular lipids, cellular debris and scattered dystrophic calcifications with underlying C) dense hyalinized collagen bundles with diminished amounts of elastic tissue and smooth muscle cells, and a layer D) of relatively normal underlying media and adventitia.

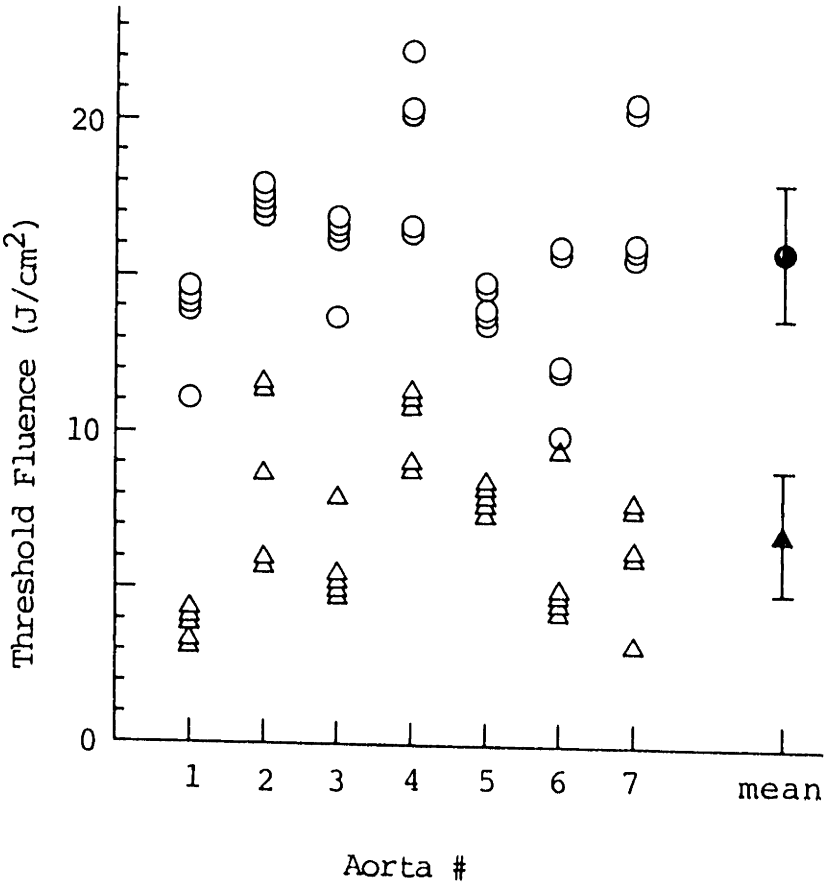

Figure IV.5 Threshold fluences for ablation of atheromatous and normal regions on 7 human aortas. Note that for each individual, normal aorta (circles) required 2-3 times more energy per unit area for ablation than atheromas (triangles). Bars on the solid symbols for the means indicate ± 1 standard deviation.

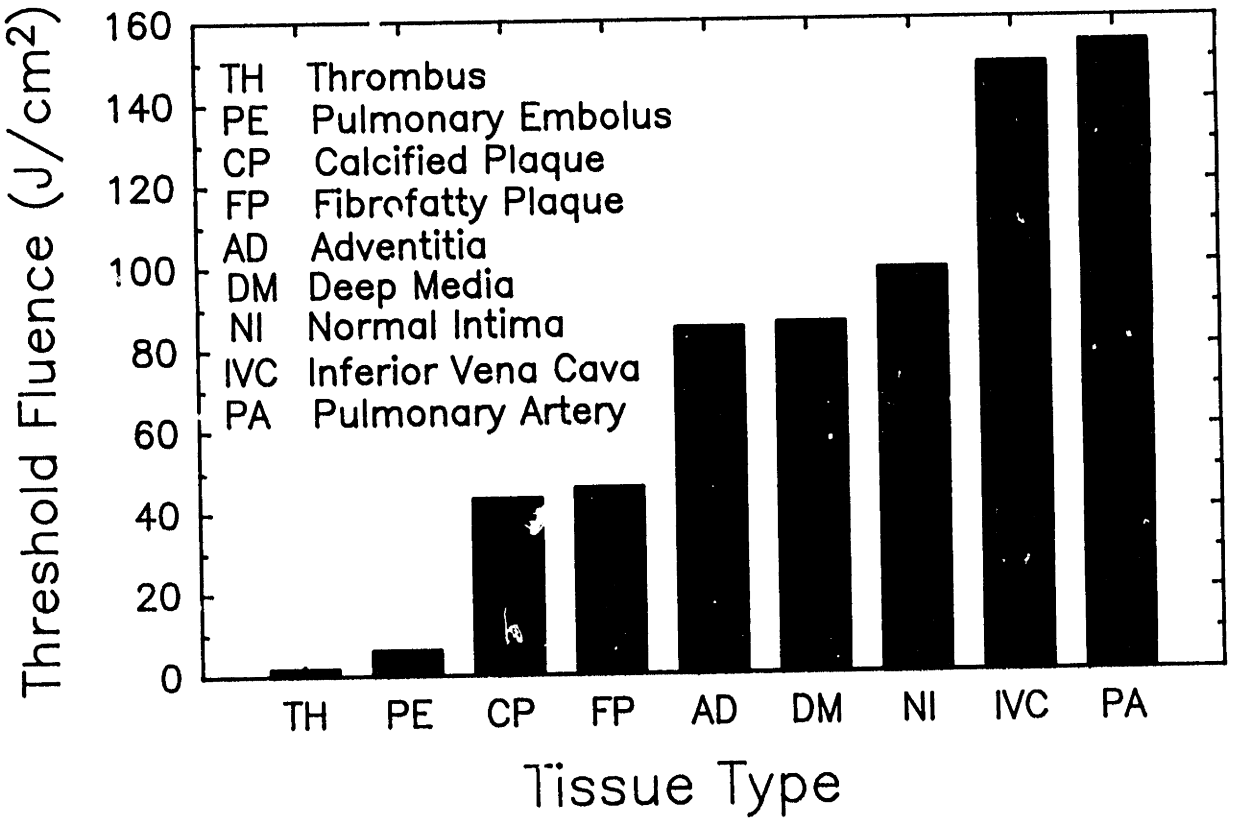

Figure IV.6 Ablation threshold fluences for 482 nm radiation delivered to cardiovascular tissues via a 320 micron core diameter quartz fiber. Note that the normal tissues, adventitia, media, normal intima, inferior vena cava and pulmonary artery all have significantly higher ablation thresholds than the diseased tissue, fresh thrombus, pulmonary embolus, calcified plaque and fibrofatty plaque.

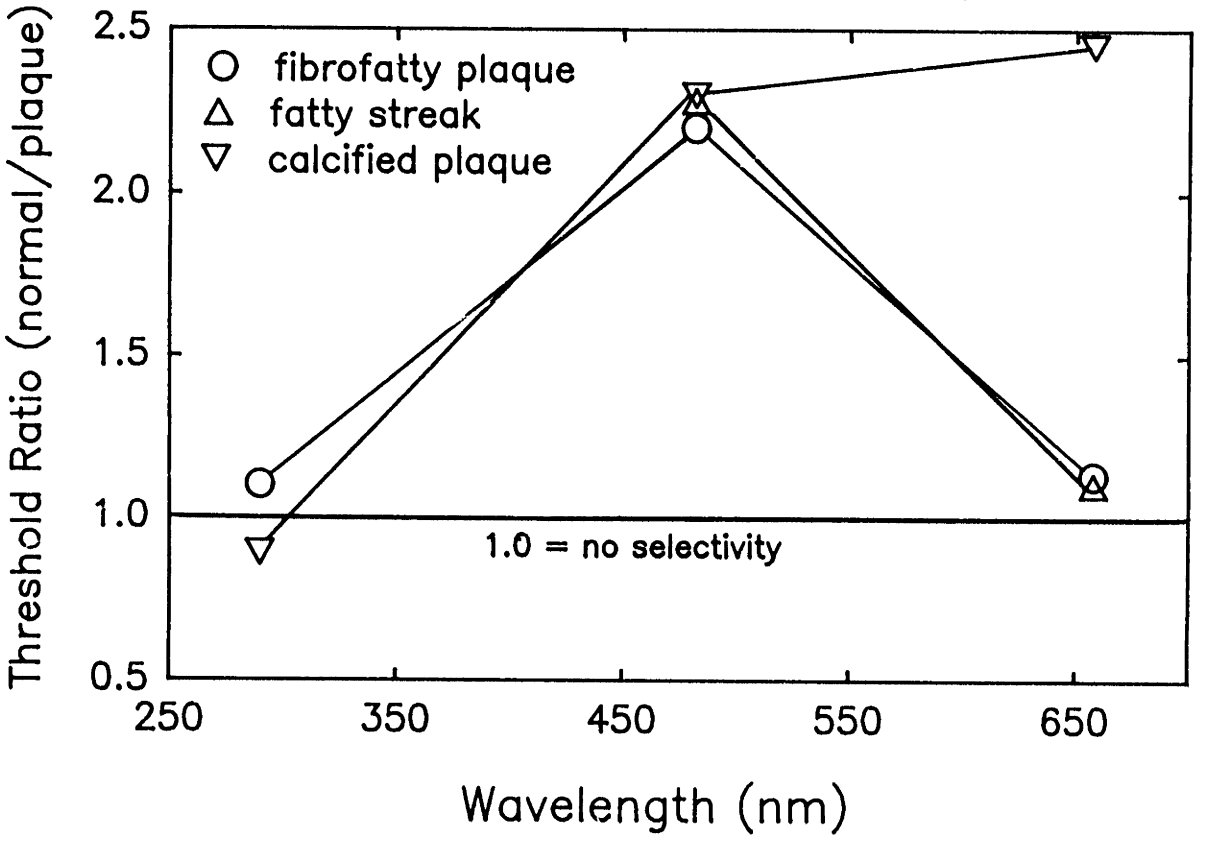

Figure IV.7 Effect of wavelength on selectivity. The normal artery to plaque ratio of ablation threshold fluences is plotted as a function of wavelength for fibrofatty plaque, fatty streaks and calcified plaque for the data in Tables IV.4 and IV.5. At 290 nm, in the ultraviolet, there is no selectivity. At 482 nm, where there is two-fold preferential absorption, there is a two-fold difference in thresholds making selective ablation possible. At 658 nm there is still selectivity for calcified plaque suggesting that selective ablation of calcified plaque is not based on preferential absorption.

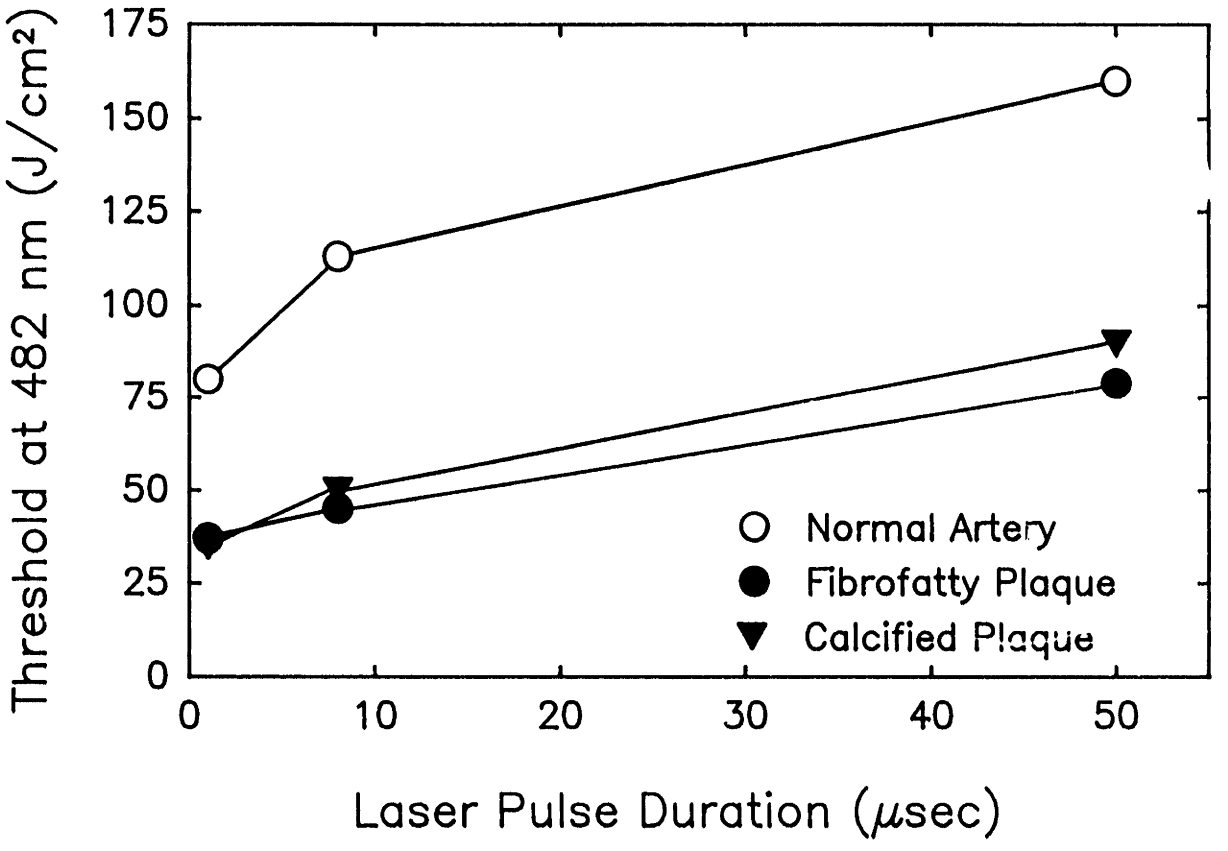

Figure IV.8 Effect of pulse duration on threshold fluence. Ablation thresholds were measured under saline at 482 nm with a 320-μm-diameter fiber as shown in Figure III.4 (data shown in Table IV.6). For these pulses, which are all shorter than the thermal relaxation time of the tissue ($\tau_R \approx 40$ msec), one would not expect the fluence to vary at all with pulse duration. Nevertheless, there is a slight, two-fold increase in threshold fluence over the 50-fold range of pulse duration.

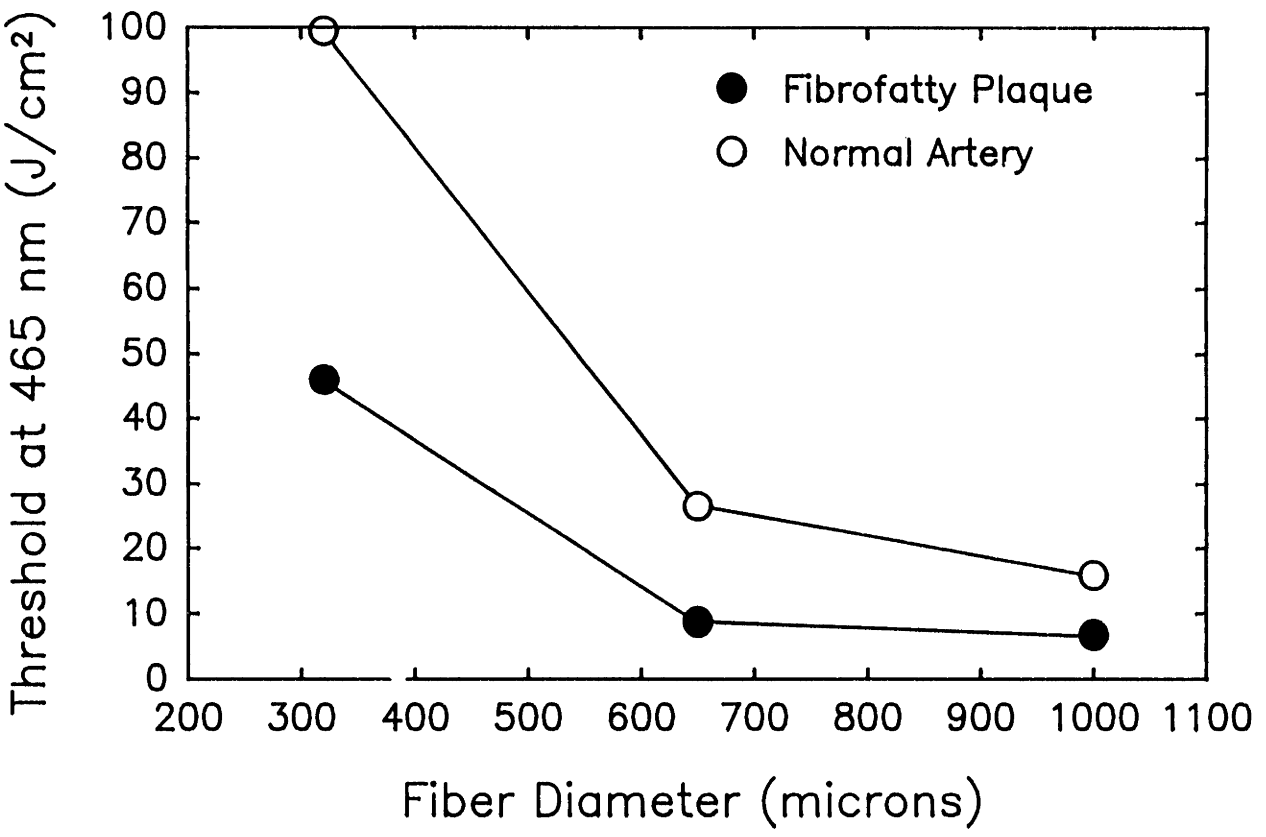

Figure IV.9 Effect of fiber diameter on ablation threshold. Threshold measurements were made under saline with 1-μsec-pulse durations of 465-482 nm radiation delivered by fibers with core diameters of 320, 650 and 1000 μm as shown in Figure III.4 (data are shown in Table IV.3). The measured threshold fluence increases considerably in small diameter fibers.

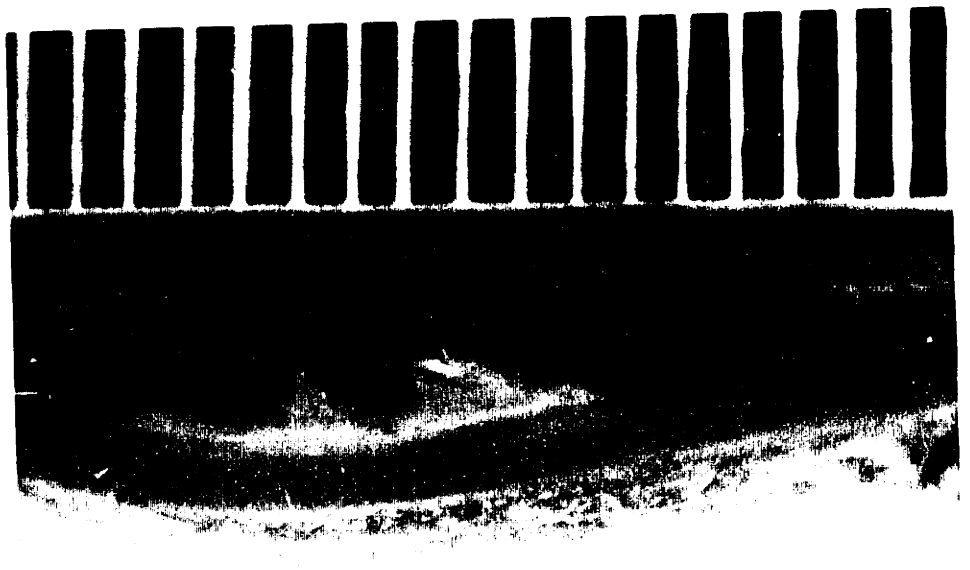

Figure IV.10 A cross-sectional view of selective ablation. Four sites on human aorta were irradiated with ten pulses of 465 nm laser radiation at 18 J/cm^2 per pulse with a 1 μsec pulse width. The two craters in the atheroma (left) are 1-1.5 mm deep, while the two irradiated areas of normal aorta show only roughening of the surface with minimal ablation. The black material is india ink used to mark the irradiated sites. No char was present. The scale indicates mm.

Figure IV.11 Histology of a crater in atheromatous aorta made by ablation with ten pulses of 465 nm radiation at 18 J/cm^2 per pulse and 1 μsec pulse width. The crater edges are irregular suggesting a tearing/shearing ablative process. There is little evidence of thermal injury at this magnification but at higher power (not shown) one can appreciate 2-100 μm of histologic alteration lining the crater. The black material is india ink and the debris in the crater is an artifact of preparation. (Hematoxylin and eosin stain; bar = 1 mm.)

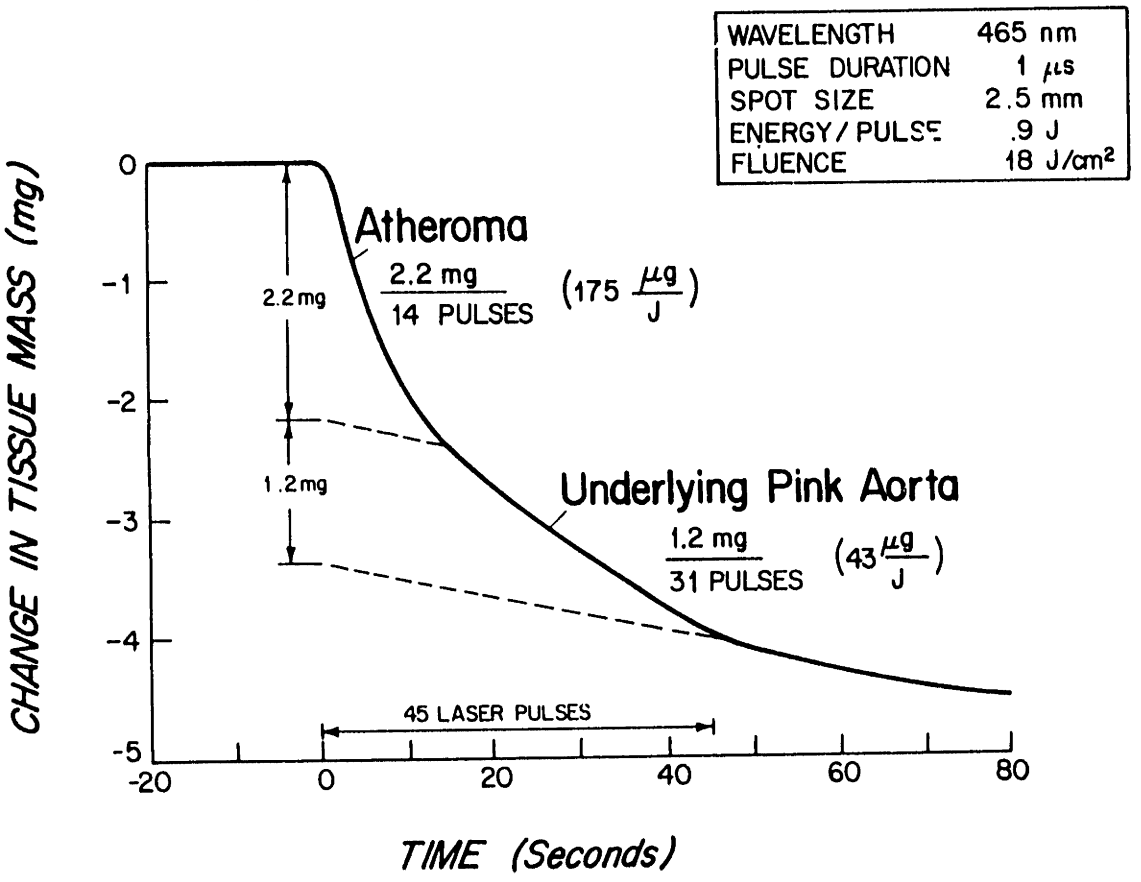

Figure IV.12A Measurement of ablation efficiency in air. The mass of a specimen mounted on an electronic balance is plotted versus time for the period before, during and after irradiation with 465 nm radiation at a fluence of 18 J/cm^2 (as shown in Figure III.6) in order to measure the ablation efficiency (mass of tissue ablated per unit of incident energy). A) Note the slight mass loss due to evaporation before the start of irradiation, the rapid loss of mass during the period of irradiation and the significant rate of mass loss post irradiation due to evaporation. During irradiation, 3.3 mg of plaque were ablated compared to 0.66 mg of normal, a five-fold difference in ablation efficiencies.

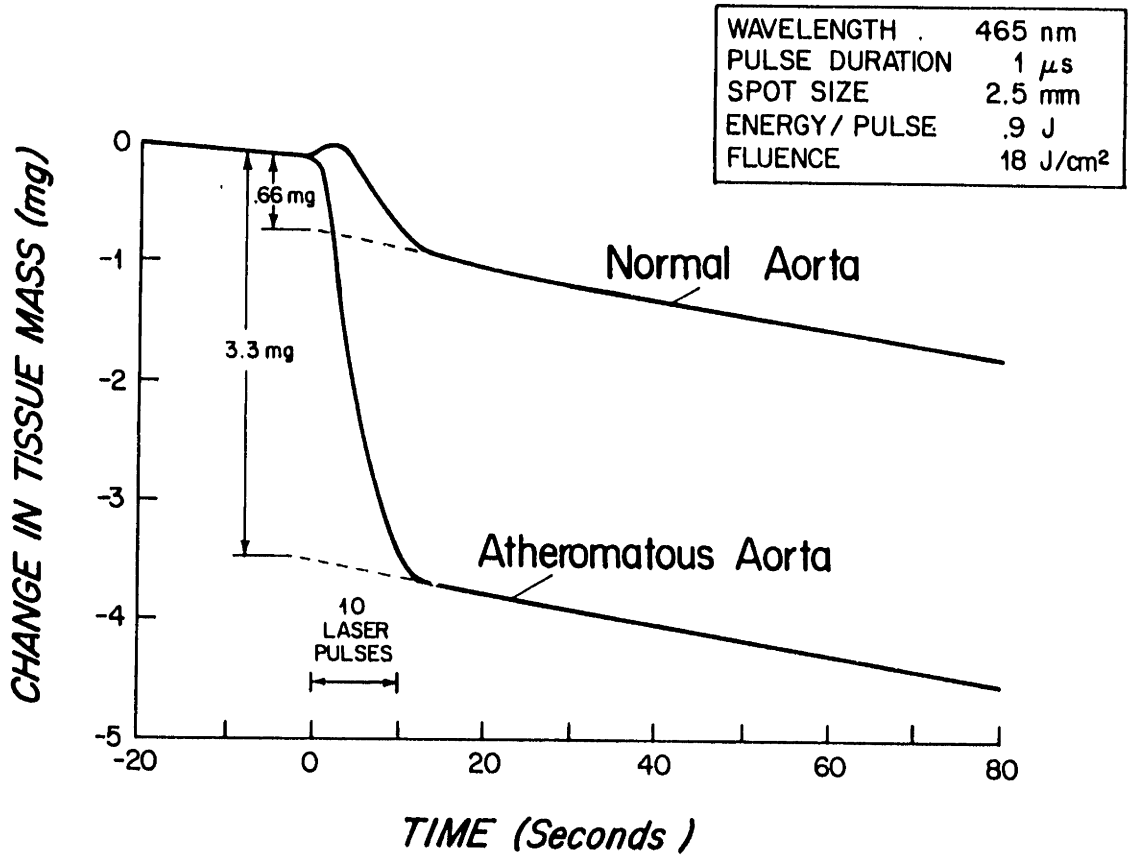

Figure IV.12B Measurement of ablation efficiency in air (continued). B) A specimen of plaque is irradiated with 45 laser pulses where, after 14 pulses, the underlying normal aorta was reached and the ablation efficiency diminished by a factor of 4.

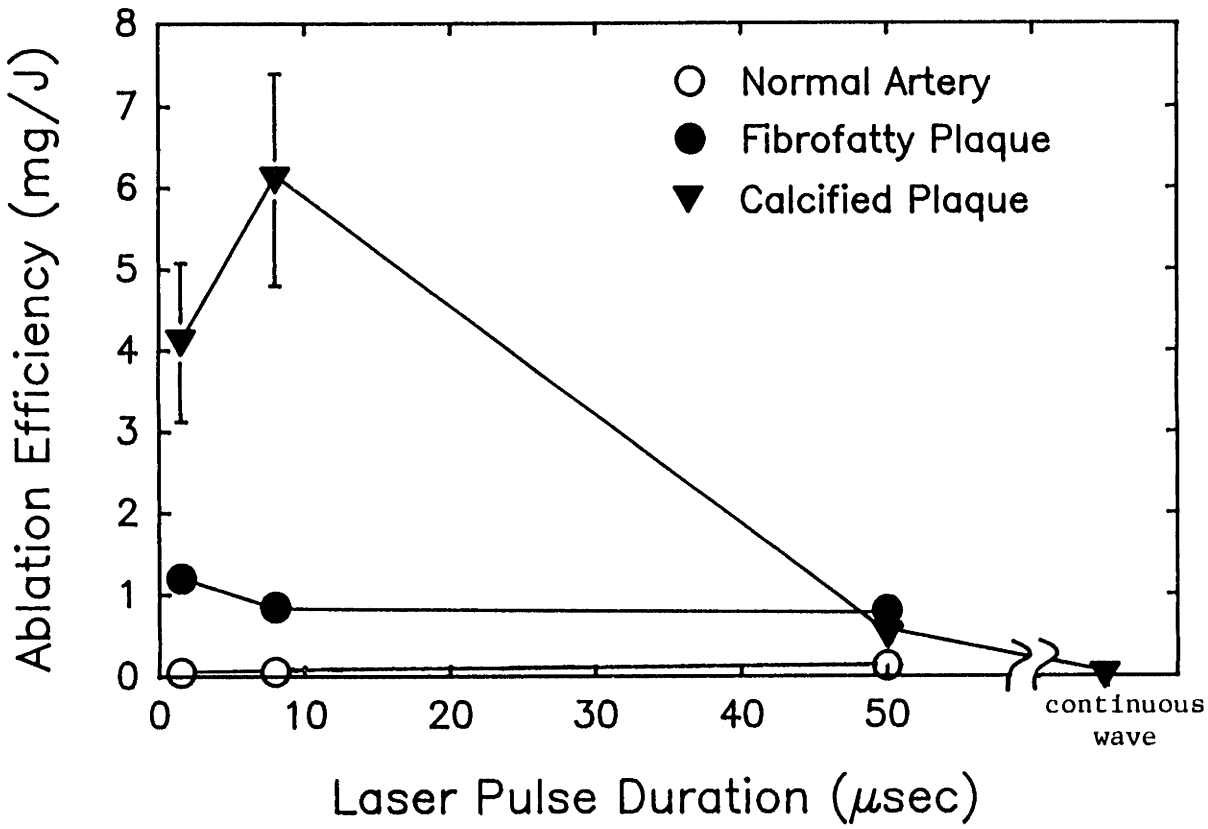

Figure IV.13 Ablation efficiency under saline and the effect of pulse duration. Measurements were made with 482 nm radiation delivered via 320 micron core fibers to normal artery, fibrofatty plaque and calcified plaque submerged in a saline bath (see Table IV.8). For each pulse duration evaluated all tissues were irradiated at a fluence that was approximately equal to the threshold fluence for ablating normal artery with a 320 μm diameter fiber (since this would be the optimal fluence for selective ablation). Note that the ablation efficiencies for ablation of fibrofatty and calcified plaque are significantly greater than that of normal artery and also greater than 1/(latent heat of vaporization of water) = 0.4 mg/J.

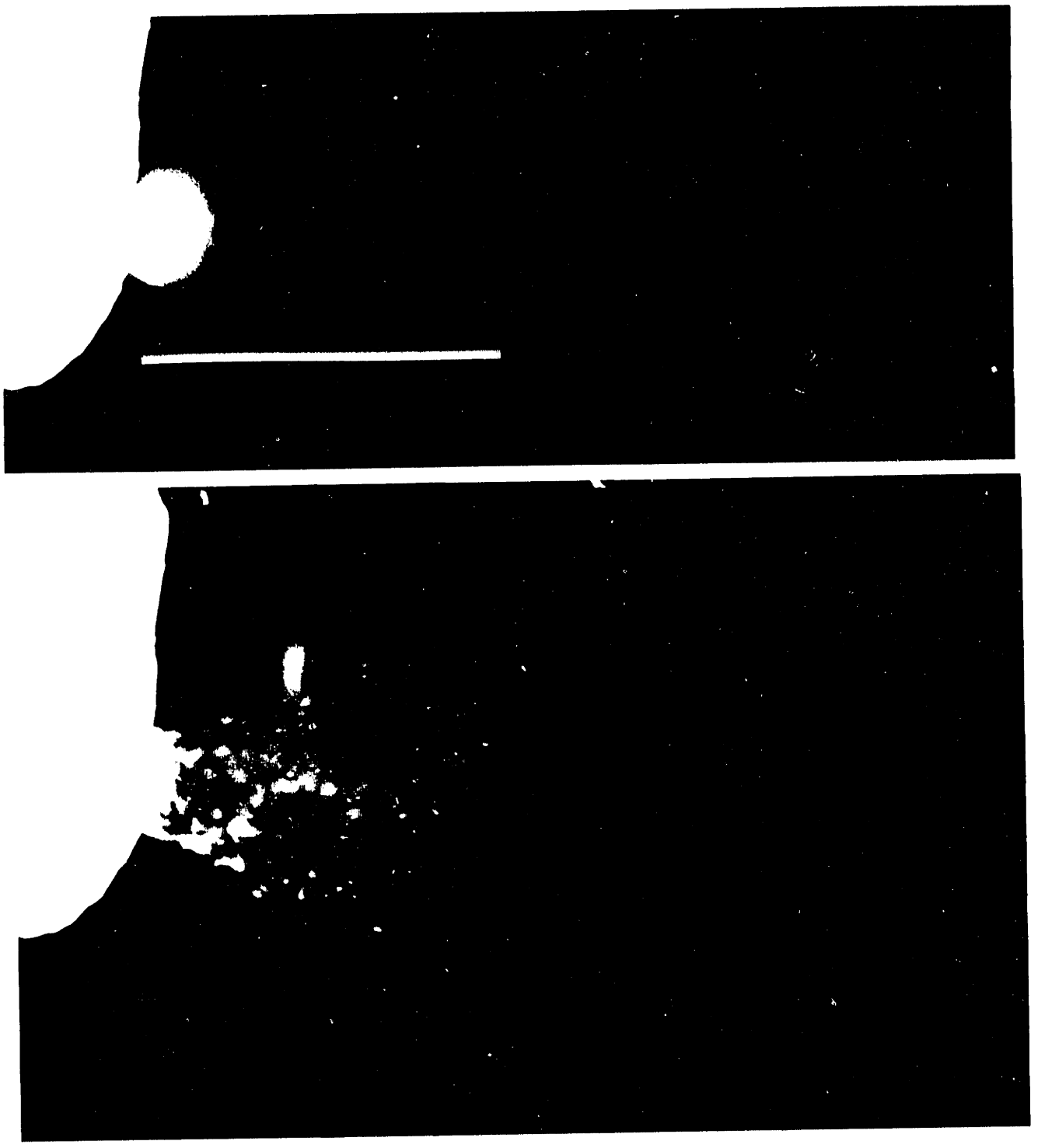

Figure IV.14 High speed flash photography. Photos show soft plaque ablation by 1μsec pulses of 465 nm laser radiation at 25 J/cm^2. The camera lens is covered with a filter that excludes the laser radiation and the image is captured by leaving the shutter open, keeping the room dark and exposing the film with a 1 μsec flash at delays of A) 10 μsec, B) 150 μsec, C) 500 μsec and D) 2500 μsec after irradiation. The bar indicates 1 cm.

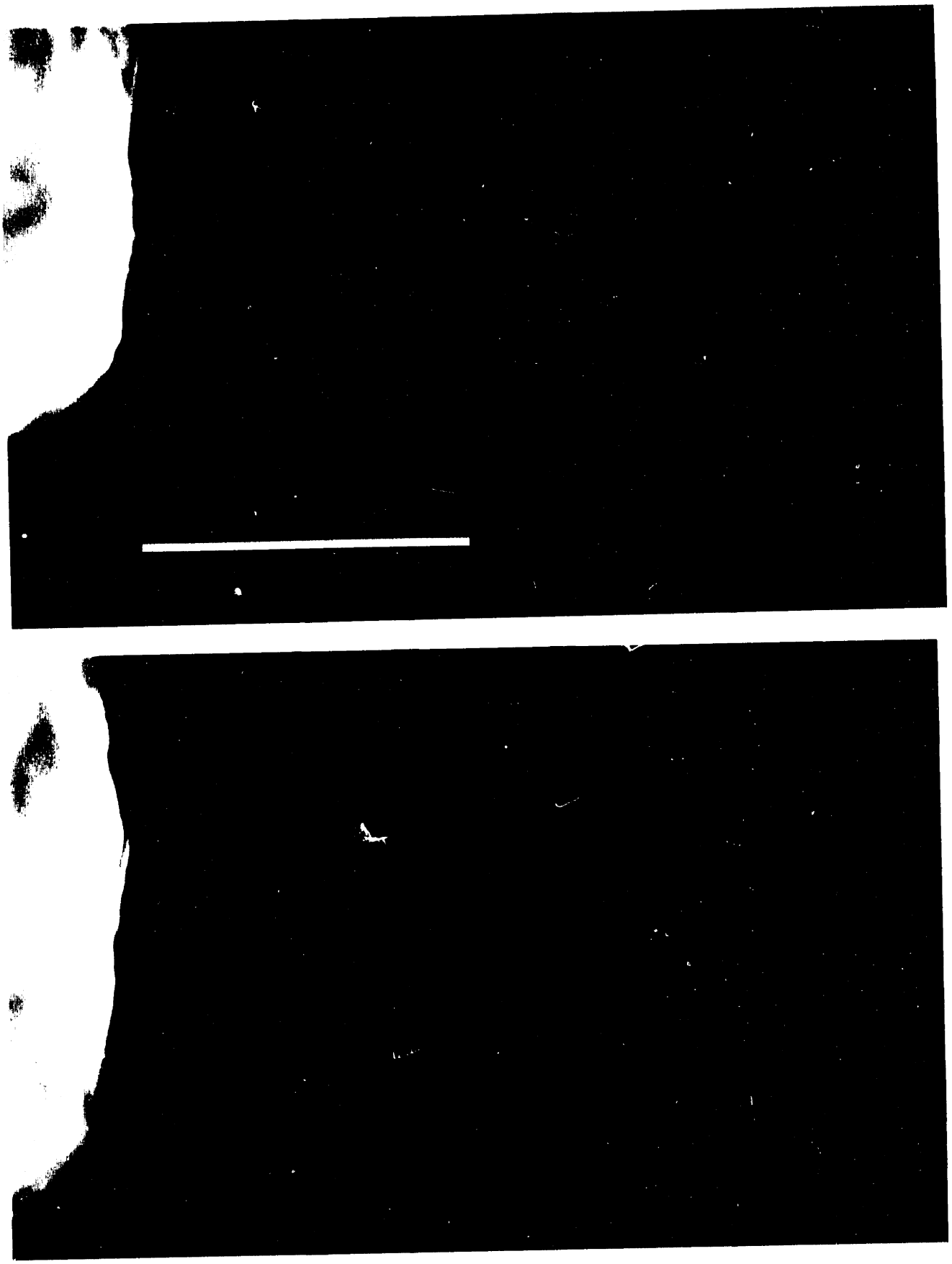

Figure IV.14C & D

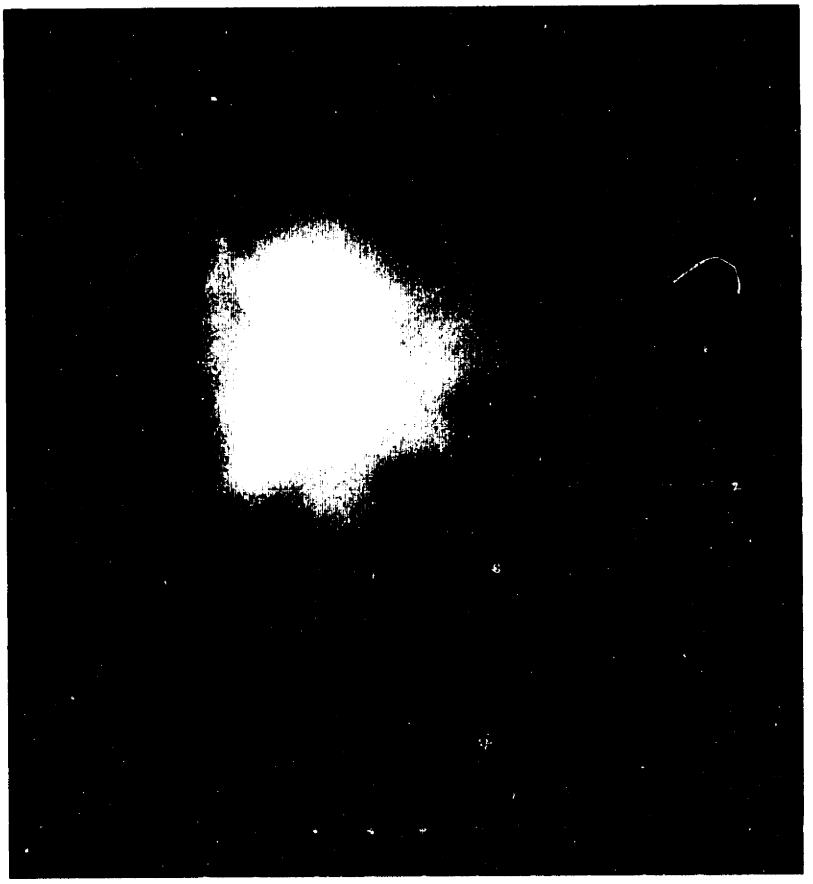

Figure IV.15A Luminescent plume due to irradiation of calcified plaque. The photo shows calcified human arterial plaque irradiated with a single 1 μsec, 100 mJ pulse of 450 nm radiation delivered via a 320 μm core-diameter, optical fiber. The tip of the fiber can barely be seen as a bright spot in the center of the plume. The photograph was taken with a yellow filter to exclude the laser radiation, with the shutter open for several seconds and with the room darkened to allow exposure of the film only by induced luminescence. The scale indicates mm.

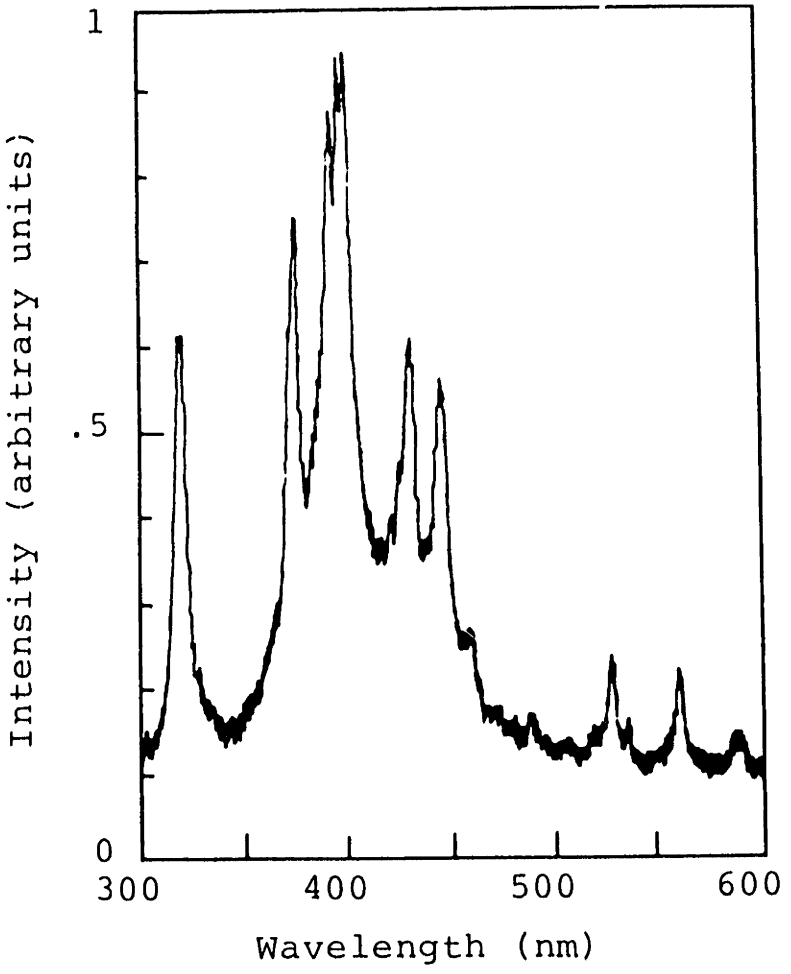

Figure IV.15B Spectrum of laser-induced emission from calcified plaque. This spectra of the calcified plaque ablation plume was taken 0.6 μsec after the start of a 690 nm laser pulse of 0.8 μsec duration. There is a broad continuum from 350 to 500 nm with superimposed emission lines. Emission lines at wavelengths shorter that 400 nm are due to ionized calcium (Ca II) and those lines at longer wavelengths are due to emission from neutral calcium (Ca I). The features indicate the presence of a plasma.

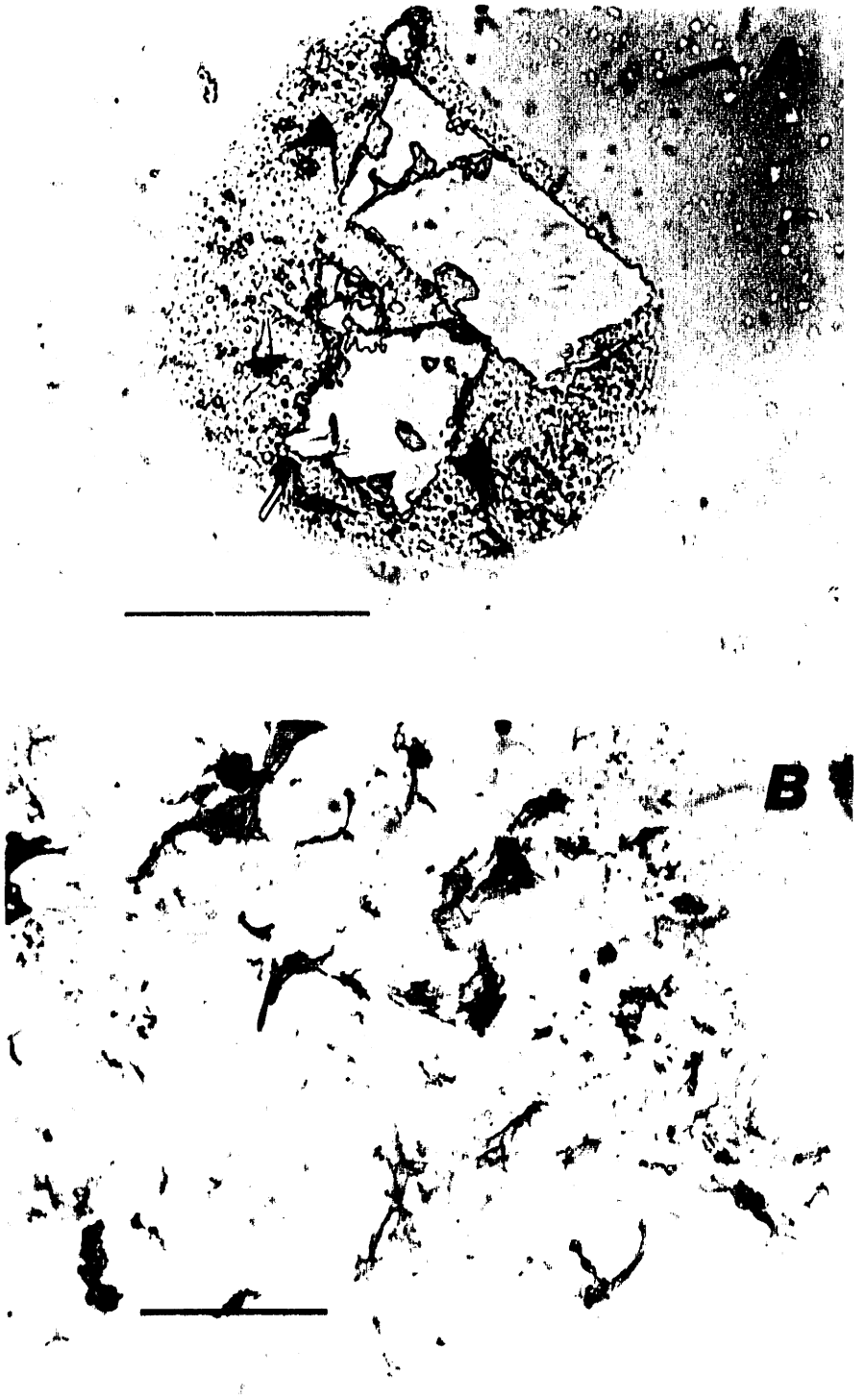

Figure IV.16 Ablation debris. Debris was collected on a microscope slide placed 1 cm in front of an atheroma during irradiation with 1 μsec duration pulses of 465 nm radiation. (A) Intact and shattered cholesterol crystals. (bar = 100 microns) (B) Collagen fragments and small bits of calcific material. (hematoxylin and eosin stain, bar = 200 microns). Note that only a few collagen fragments have the deep staining quality of denatured collagen.

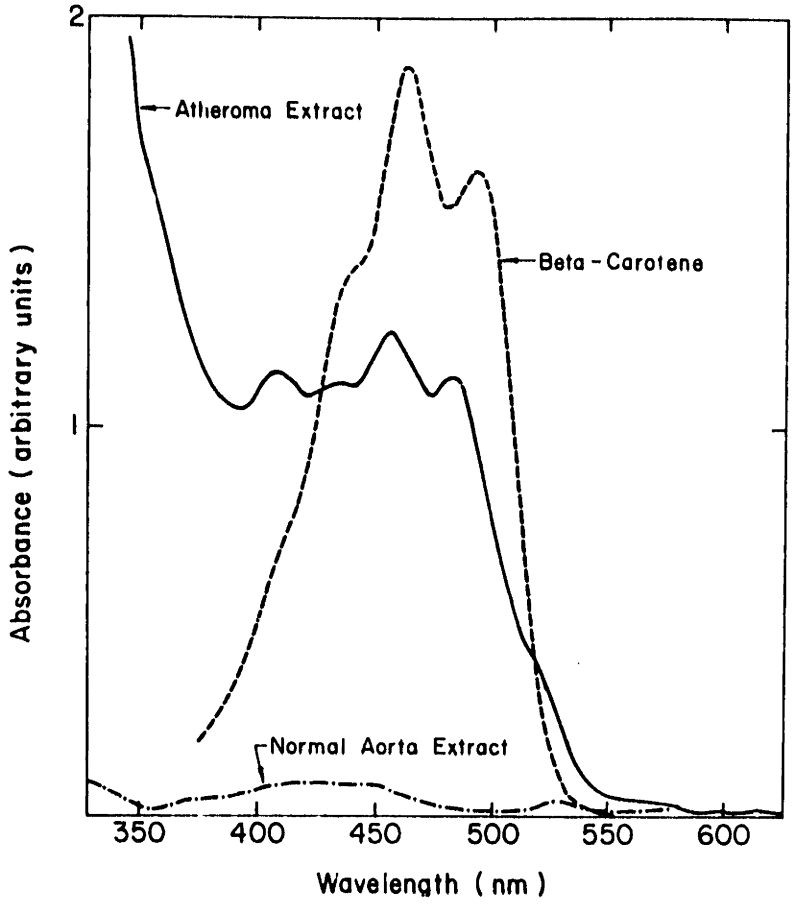

Figure IV.17 Absorption spectra of lipophilic chromophores extracted from atheroma and normal aorta compared to spectra for beta carotene. Chromophores extracted from atheromas absorb in the same waveband where there is preferential absorption in atheromas. No chromophores extracted from normal aorta showed significant absorption in that waveband.

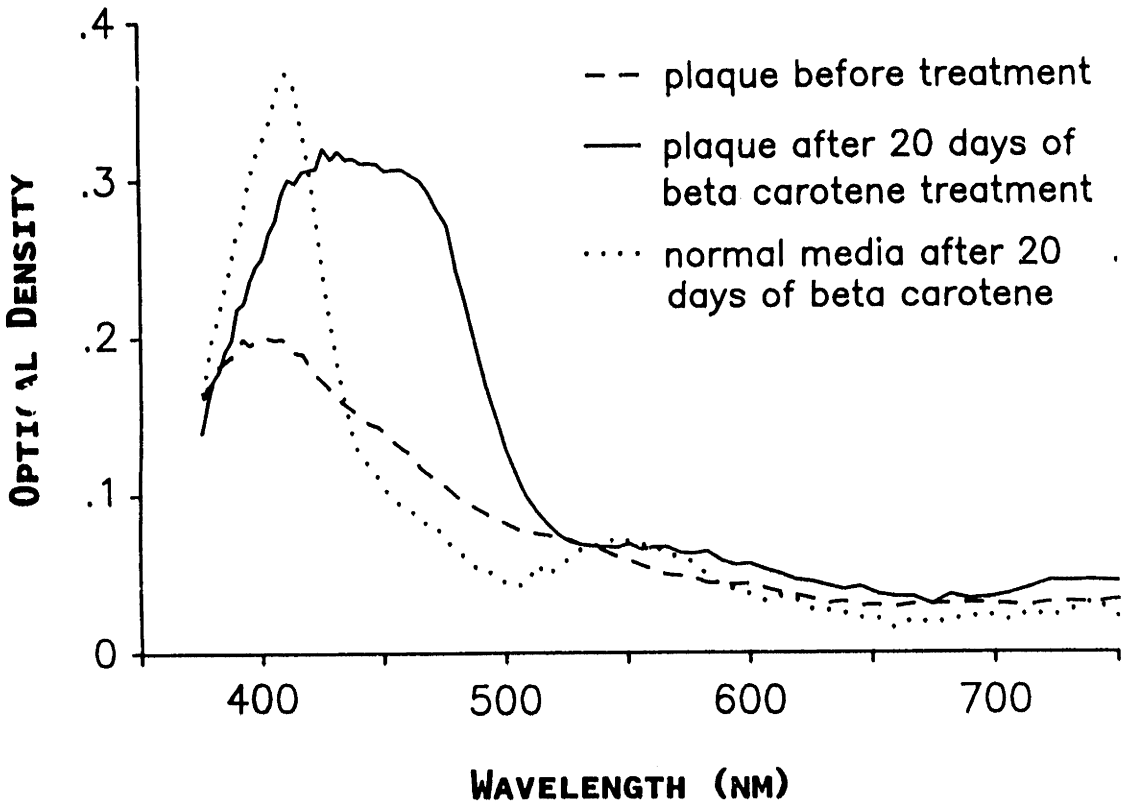

Figure IV.18 Optical density of carotid plaques measured by microspectrophotometry. These spectra are of specimens from the same patient taken before and after beta carotene treatment. Before treatment (dashed line), the plaque spectra consists of a broad peak from 350 to 600 nm which represents a combination of absorption from heme pigments (with peaks at 410 nm and 540 to 600 nm) and carotenoids (with peaks at 430 to 530 nm). After beta carotene treatment, the plaque spectra (solid line) is dominated by a beta carotene-like spectra with a peak at 450 nm. Also after beta carotene treatment normal smooth muscle underlying the plaque (dotted line) shows peaks at 410 nm and 540 to 600 nm consistent with myoglobin absorption.

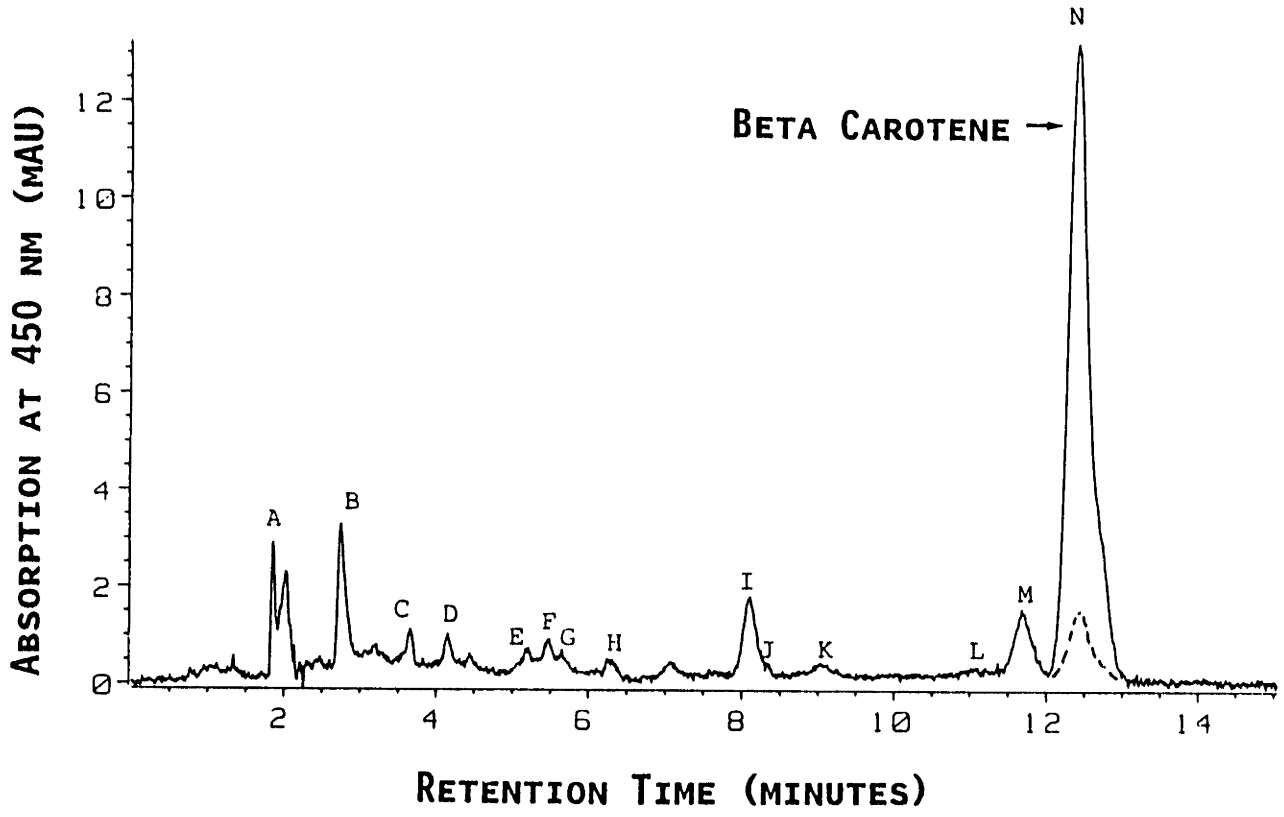

Figure IV.19 A representative HPLC chromatogram and spectra of the separated compounds (A-N). The solid line shows the separation of carotenoids extracted from a single, post beta carotene treatment specimen. There are multiple carotenoid peaks. Beta carotene, eluting at 12.5 minutes, is a single distinct peak. The dashed line indicates the magnitude of the beta carotene peak from a specimen taken from the same patient before beta carotene treatment. The difference in areas of the beta carotene peaks represents the increase in the plaque beta carotene content with oral beta carotene loading. The peaks which have been identified include: I - lycopene, M - alpha carotene, and N - beta carotene.

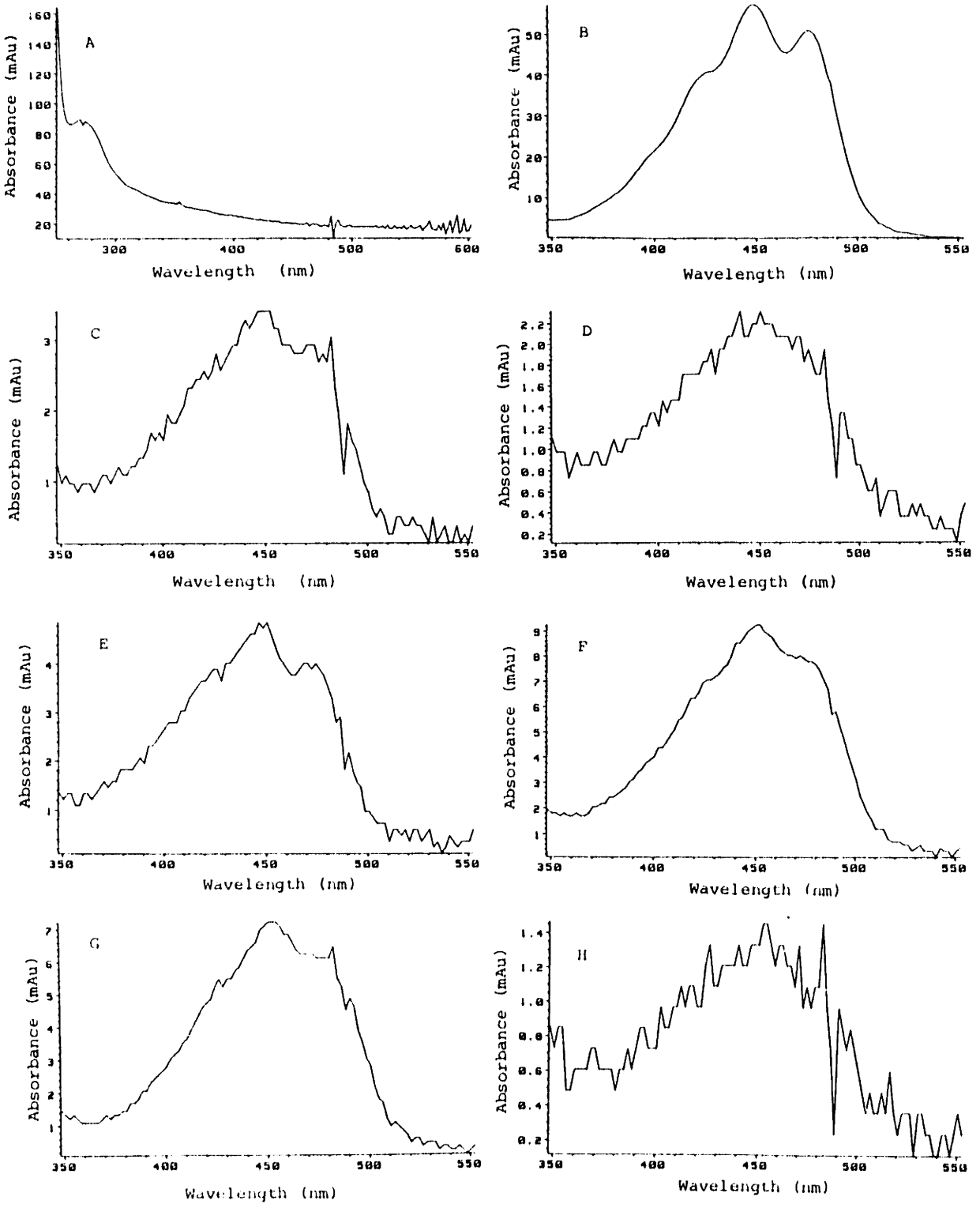

Figure IV.19 (page 2)

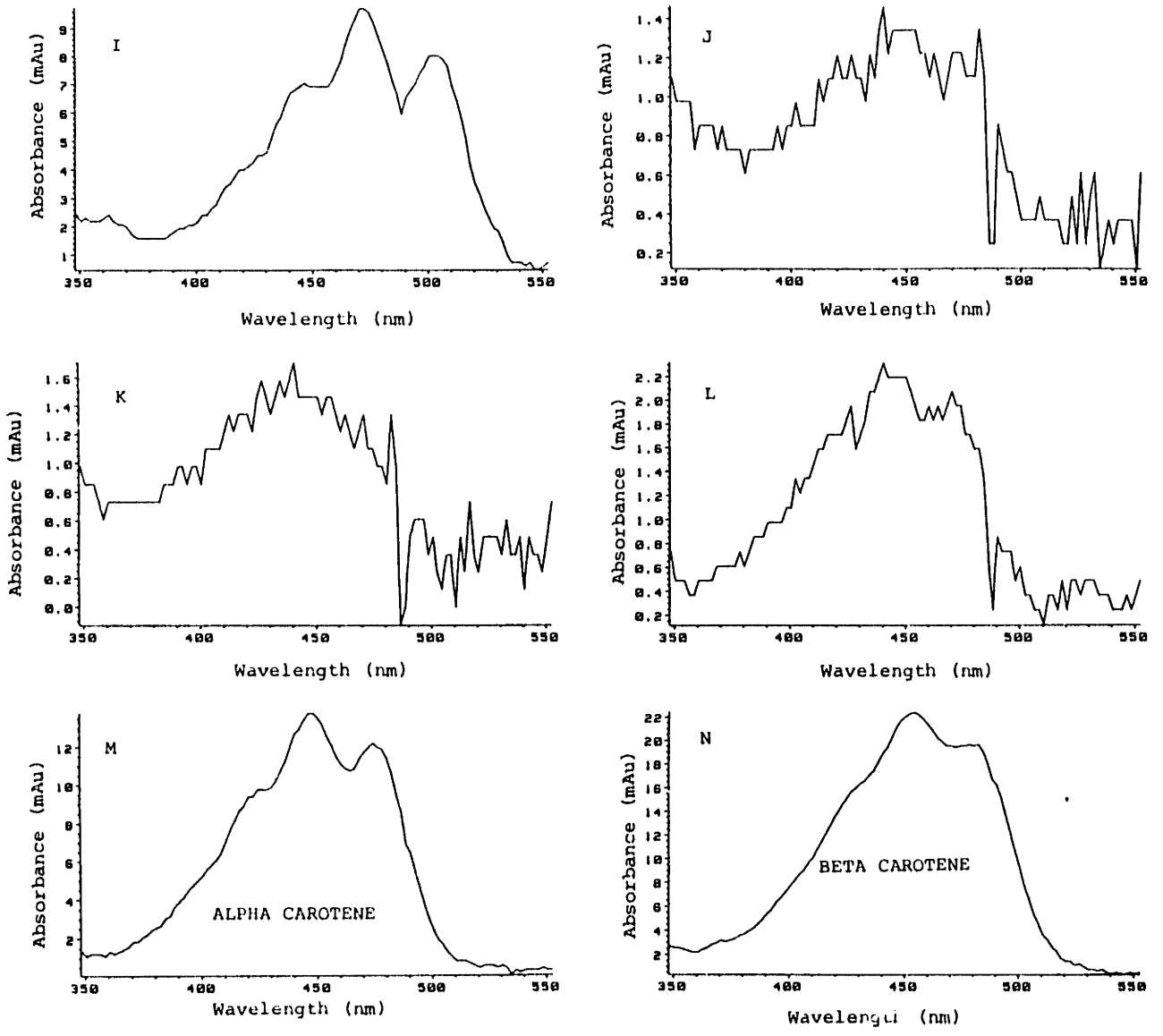

Figure IV.19 (page 3)

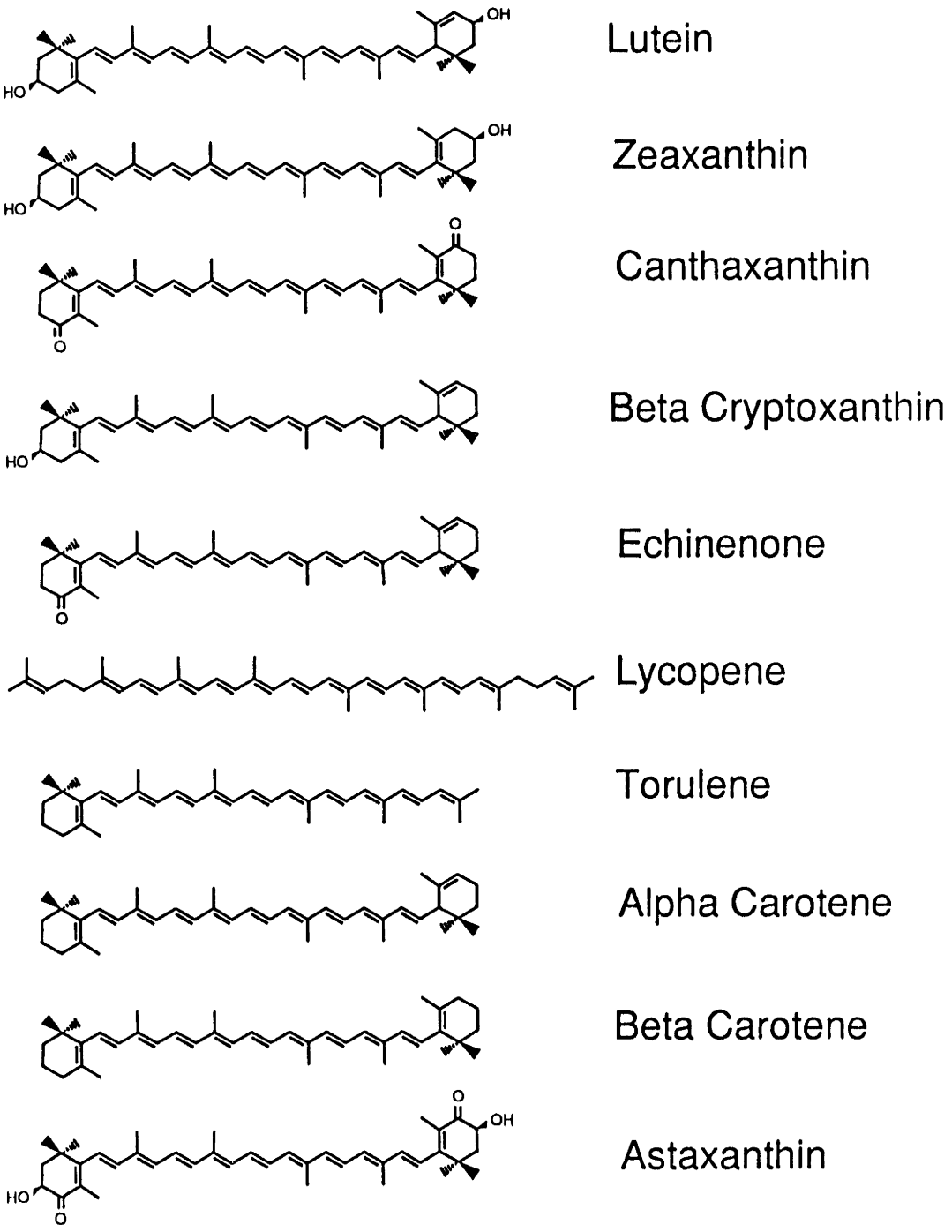

Figure V.1 Molecular structures of common carotenoids. Note the long sequence of alternating double bonds which indicates a continuous covalent bond involving the pi orbitals of carbon atoms along the entire length of the molecule.

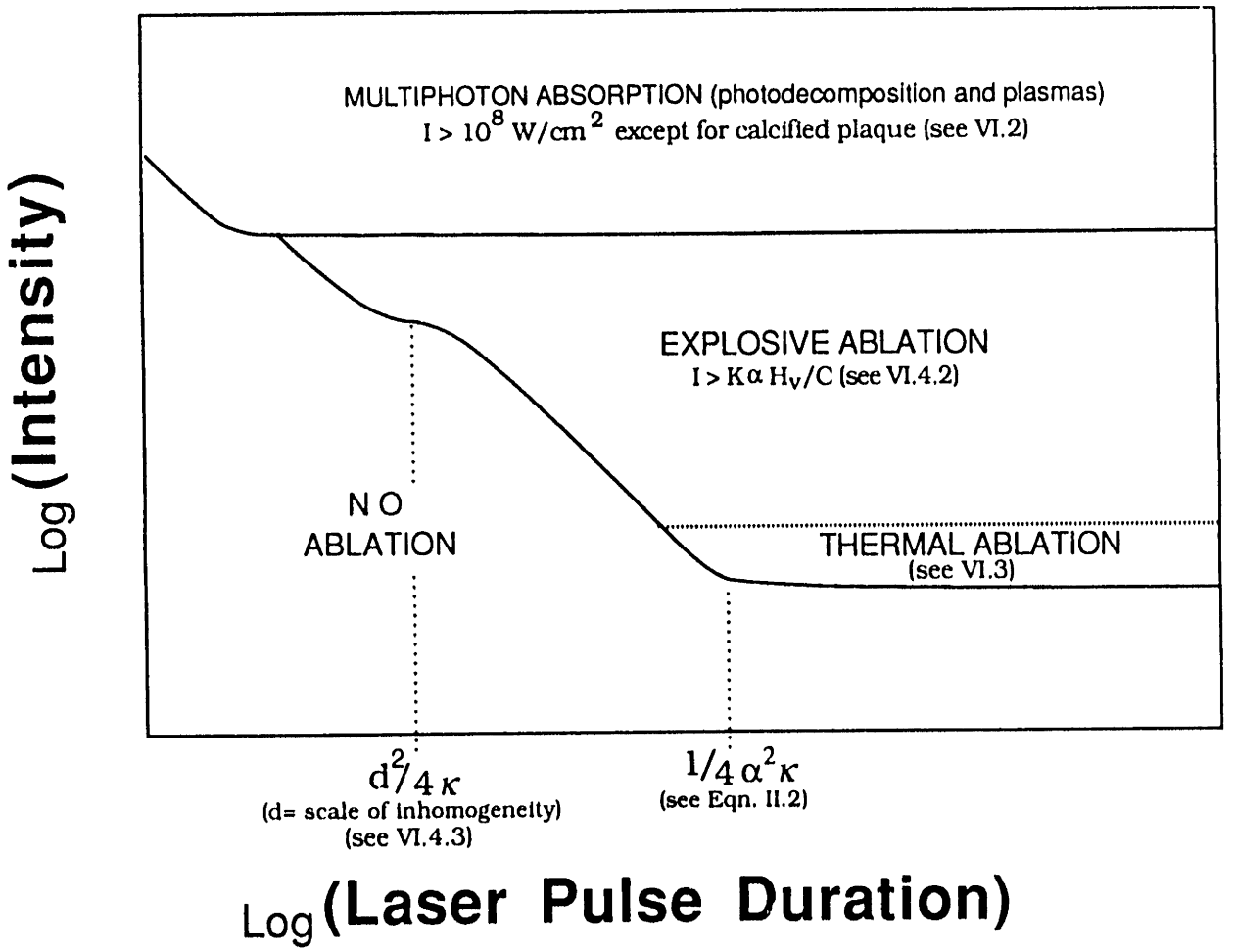

Figure VI.1 Ablation regimes.

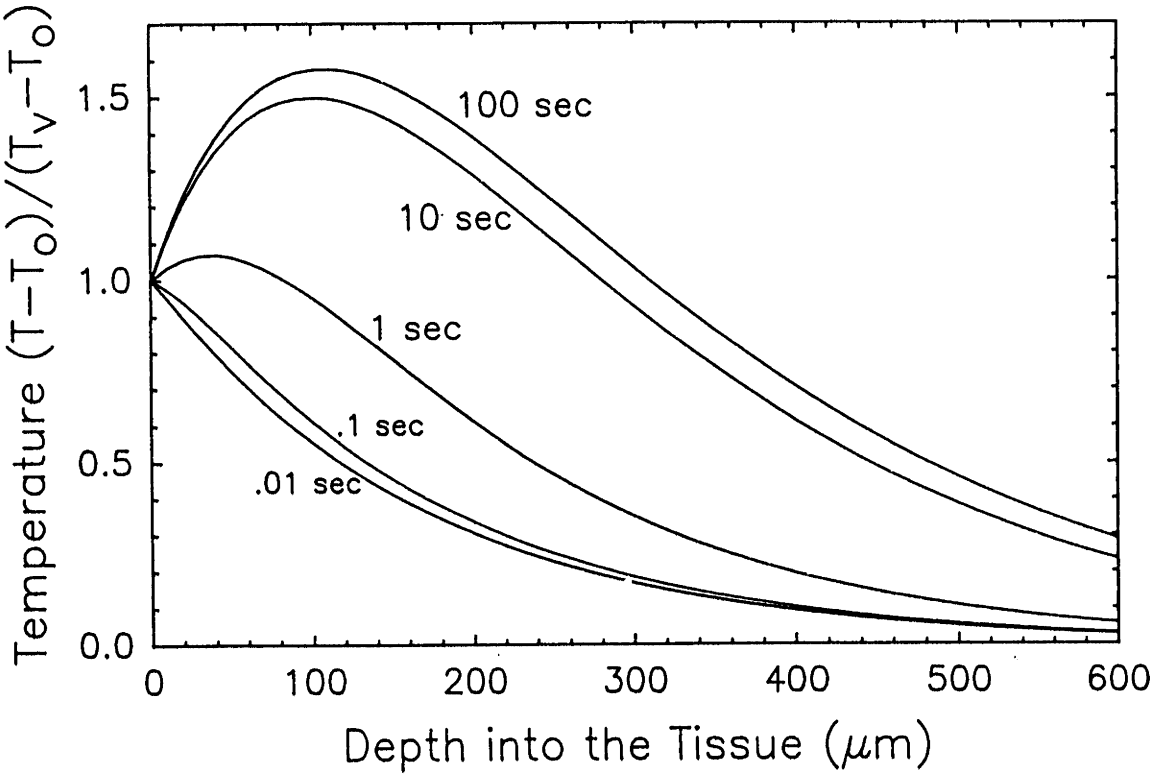

Figure VI.2 Temperature distribution in tissue for low intensity irradiation. Normalized temperature is plotted as a function of depth into plaque for various pulse durations at an intensity typical of an argon ion laser (I_o= 300 W/cm^2, α=60 cm^{-1}, κ = .013 cm^2/sec, ρ = 1 gm/cm^3, C = 4 J/gm^{o}C).

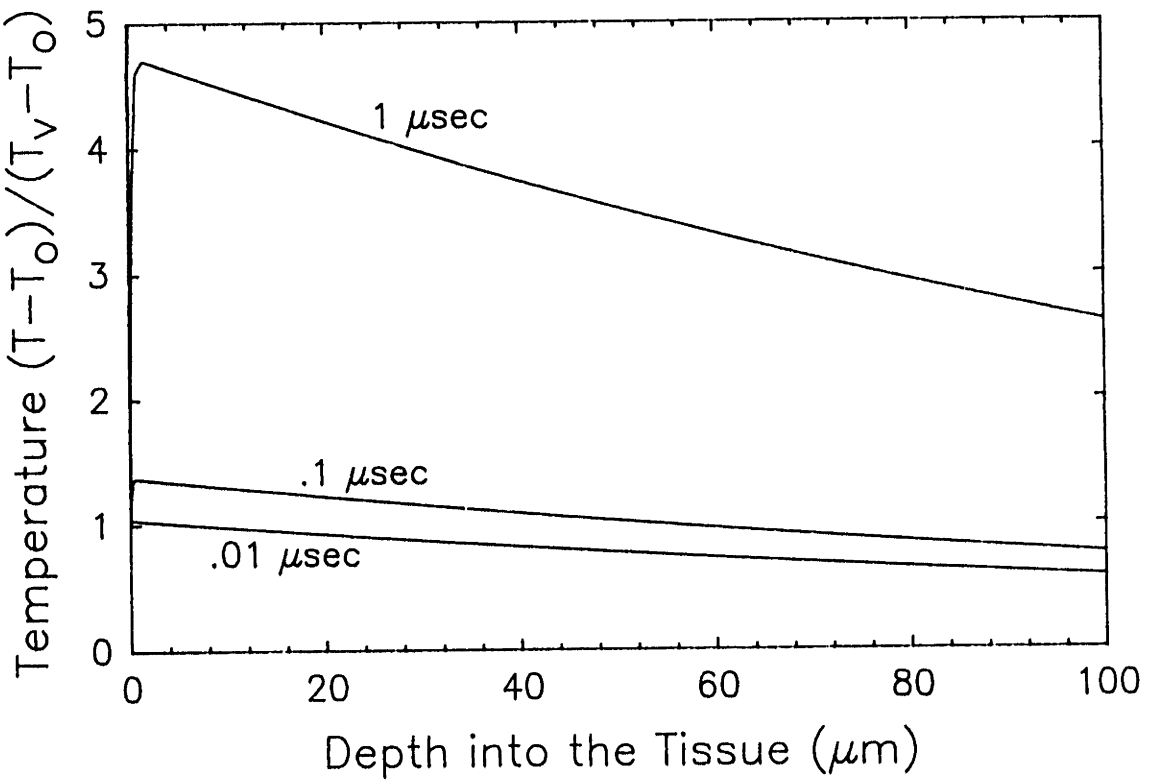

Figure VI.3 Temperature distribution in plaque for high intensity irradiation. Normalized temperature is plotted as a function of depth into plaque for various times post initiation of irradiation by radiation typical of the pulsed dye laser (I_o = 20 MW/cm^2, α=60 cm^{-1}, κ = .013 cm^2/sec, ρ = 1 gm/cm^3, C = 4 J/gm^{o}C). Note the rapid rise in the subsurface temperature reaching nearly 5 times (T_v-T_o) at just 1 μsec.

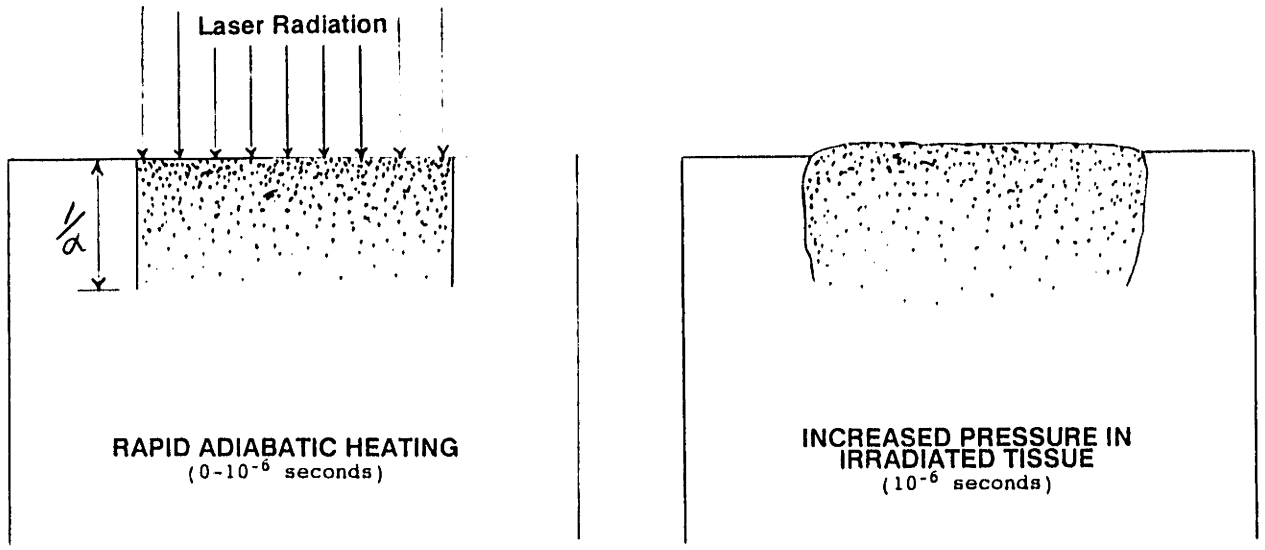

Figure VI.4 Proposed mechanism for plaque ablation at 480 nm with a 1-μsec-pulse duration. The high intensity laser pulse causes A) exponential, adiabatic heating of the tissue during the period of laser irradiation (1μsec) and over a characteristic depth of $\approx 1/\alpha$. The sudden increase in enthalpy of the tissue causes B) superheating of tissue fluid and a large increase in pressure in the volume irradiated. As the presurized tissue expands C), vapor may form at niduses of locally higher absorption within the tissue. The continued expansion D), over the course of hundreds of microseconds to milliseconds causes shearing and liquefaction of the irradiated tissue. The expansion occurs primarily toward the path of least resistance, away from the residual tissue. The residual tissue E), is held together by tensile elements and remains intact. Ablation debris is carried away by convection. The biologic response F), is unknown.

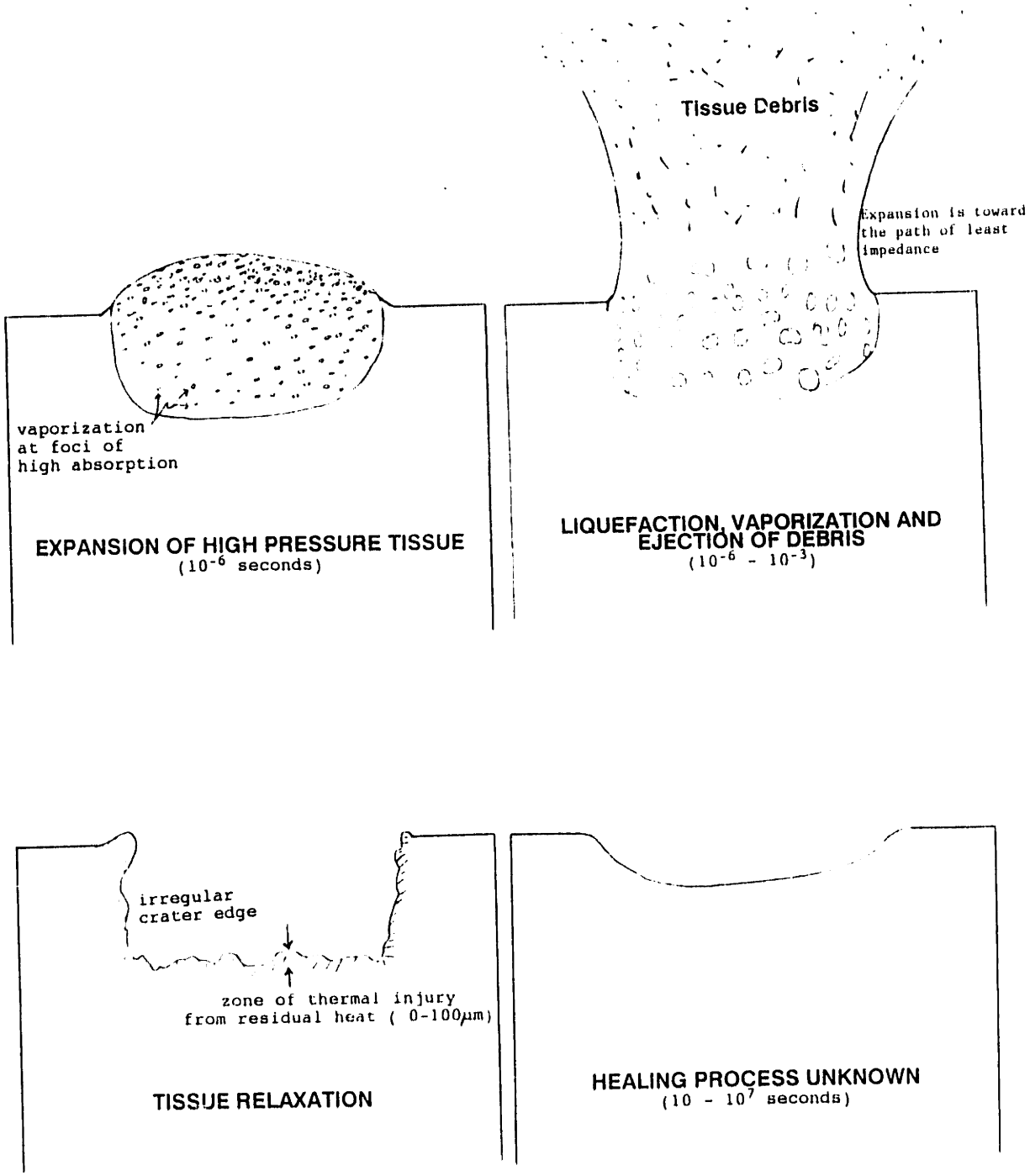

Figure V.9 (page 2)